



University of Oran 2
Institute of Maintenance and Industrial Safety

THESIS

For obtaining the doctoral degree « L.M.D »
In Electromechanics

**Contribution to the Performance Enhancement of a Flat Plate Solar
Thermal Collector**

Publicly presented by:
Mr. SEDDAOUI Ali

In front of the jury consisting of:

Mr. HACHEMI Khalid	Professor	University of Oran 2	President
Mr. NOUREDDINE Rachid	Professor	University of Oran 2	Supervisor
Mr. DAR RAMDANE Mohamed Zouhir	Assistant Professor	University of Oran 2	Co- supervisor
Mr. HASSINI Abdelatif	Professor	University of Oran 2	Examiner
Mr. HAMIDOU Mohamed Kamel	Professor	USTO-MB	Examiner
Mr. BENLEFKI Abdelkrim	Assistant Professor	University of Tissemsilt	Examiner

2023



Université d'Oran 2
Institut de Maintenance et de sécurité Industrielle

THESE

Pour l'obtention du diplôme de Doctorat « L.M.D »
En Electromécanique

**Contribution à l'Amélioration des Performances d'un Capteur
Solaire Thermique Plan**

Présentée et soutenue publiquement par :

Mr. SEDDAOUI Ali

Devant le jury composé de :

Mr. HACHEMI Khalid	Professeur	Université d'Oran 2	Président
Mr. NOUREDDINE Rachid	Professeur	Université d'Oran 2	Directeur de thèse
Mr. DAR RAMDANE Mohamed Zouhir	MCB	Université d'Oran 2	Co-encadreur
Mr. HASSINI Abdelatif	Professeur	Université d'Oran 2	Examineur
Mr. HAMIDOU Mohamed Kamel	Professeur	USTO-MB	Examineur
Mr. BENLEFKI Abdelkrim	MCA	University de Tissemsilt	Examineur

2023

Contribution to the Performance Enhancement of a Flat Plate Solar Thermal Collector

Abstract:

The tremendous demand for hot water for domestic use has led to a dramatical increase in energy consumption required to provide this service. To overcome this challenge, it is mandatory to incorporate renewable energy solutions. The solar power source, which is under development, offers a clean alternative energy. Flat plate solar thermal collectors are generally designed for domestic applications operating in a low and medium temperature range (between 50°C and 100°C) that can provide an effective solution and may reduce electricity and gas consumption. However, these heating systems suffer from heat loss that prevents them to achieve high temperatures and thermal efficiency. Therefore, the aim of this research project is to enhance the thermal performance of a flat plate solar collector using a novel insulation technique. This is can be accomplished by employing vacuum insulation from the front side and opaque thermal insulation (Rockwool) from the back side of a collector. A comparative theoretical study has been carried out for this new insulation technique to identify the best in terms of heat losses, absorber temperatures and efficiency, as an indication of thermal performance. According to the results, the proposed new configuration shows better thermal performance as compared to other configurations. In conclusion, the new configuration presents a promising solution that has the required ability for producing hot water at a low cost and may take place as heating system in various industrial and household activities.

Key words: Renewable energy, Solar thermal system, Flat plate solar thermal collector, Experimental study, Theoretical analysis, Performance enhancement.

المساهمة في تحسين أداء المجمع الحراري الشمسي ذو اللوح المسطح

الملخص:

يؤدي الطلب المتزايد على الماء الساخن للاستخدام المنزلي إلى زيادة معتبرة في استهلاك الطاقة المطلوبة لتقديم هذه الخدمة. لمواجهة هذا التحدي، من الضروري دمج حلول الطاقة المتجددة. يوفر مصدر الطاقة الشمسية، الذي هو قيد التطوير، طاقة بديلة نظيفة. تم تصميم المجمعات الحرارية الشمسية ذات الألواح المسطحة بشكل عام للتطبيقات المنزلية التي تعمل في نطاق درجات حرارة منخفضة ومتوسطة (بين 50 و100 درجة مئوية) والتي يمكن أن تكون حلاً فعالاً وقد تقلل من استهلاك الكهرباء والغاز. لكن، هذه الأنظمة الحرارية تعاني من ضياعان في الحرارة الذي يمنعها من تحقيق درجات حرارة عالية وفعالية حرارية. من هذا المنطلق، فإن الهدف من هذا المشروع البحثي هو تحسين الأداء الحراري للمجمع الشمسي المسطح باستخدام تقنية العزل المبتكرة. حيث يمكن تحقيق ذلك من خلال استخدام العزل الفراغي الأمامي والعزل الحراري المعتم (الصوف الصخري) الخلفي للمجمع. كما تم إجراء مقارنة نظرية لتقنية العزل الجديدة هذه لتحديد الأفضل من حيث فقد الحرارة ودرجات حرارة لوح الامتصاص والفعالية، كمؤشر على الأداء الحراري. وفقاً للنتائج، يُظهر التكوين الجديد المقترح أداءً حراريًا أفضل مقارنة بالتكوينات الأخرى. في الختام، يقدم التكوين الجديد حلاً واعدًا لديه القدرة المطلوبة لإنتاج الماء الساخن بتكلفة منخفضة ويمكن أن يُدمج كنظام تدفئة في مختلف الأنشطة الصناعية والمنزلية.

كلمات مفتاحية: الطاقة المتجددة، النظام الحراري الشمسي، المجمع الحراري الشمسي ذو اللوح المسطح، الدراسة التجريبية، التحليل النظري، تحسين الأداء.

Acknowledgements

In the beginning, I would like to pay my undivided gratitude to almighty Allah for providing me the opportunity to be on this planet and take a part in the advancement of the human race with my best capability. Thereafter, I am highly indebted to my parents for their constant encouragement and support in all stages of my life. My words fall short to thank them.

Sincere gratitude to the members of the doctoral committee of the Institute of Maintenance and Industrial Safety, who taught me the basic foundations of scientific research. I would like to express my deep thanks and sincere indebtedness to Prof. NOUREDDINE Rachid for supervising this research and for his efforts to put the research work on the right path. I would also like to acknowledge the considerable amount of help and support provided by my co-supervisor Dr. DAR RAMDANE Mohamed Zouhir to complete this thesis.

Warm thanks to my family for their presence in difficult times and the encouragement, and to all my colleagues; the PhD students, who welcomed me cordially from first day and helped me adapt to the scientific research environment.

Contents

Acknowledgements.....	i
Contents.....	ii
List of Figures.....	v
List of Tables.....	vii
Nomenclature.....	viii
Introduction.....	13
Chapter 1: Flat Plate Solar Water Collectors.....	15
1.1 Renewable Energies in Algeria.....	16
1.2 Solar Energy in Algeria.....	17
1.3 Solar Thermal Collectors.....	19
1.3.1 Solar Thermal Collectors Types.....	19
1.4 Flat Plate Solar Collector.....	21
1.4.1 Typical Flat Plate Solar Collector Main Components.....	22
1.4.2 Typical Flat Plate Solar Collector Operating Principle.....	29
1.5 Passive and Active Fluid Circulation in Thermal Solar Collector.....	29
1.5.1 Passive Fluid Circulation (Thermosyphon Circulation).....	29
1.5.2 Active Fluid Circulation (Forced Circulation).....	30
1.6 Comparison Between Passive and Active Fluid Circulation Solar Collector.....	31
1.6.1 Collector Price.....	31
1.6.2 Collector Installation.....	31
1.6.3 Collector Reliability.....	31
1.6.4 Collector Flexibility.....	32
1.6.5 Collector Application.....	32
1.6.6 Collector Performance.....	32
1.7 Parameters Characterising the Operation Mode.....	32
1.7.1 External Parameters.....	32
1.7.2 Internal Parameters.....	33
1.8 Orientation and Inclination of Flat Plate Solar Collector.....	34
1.9 Heat Loss in Flat Plate Solar Collector.....	34
1.9.1 Heat Conduction.....	34
1.9.2 Heat Convection.....	35
1.9.3 Heat Radiation.....	36
1.10 Application.....	41
1.11 Conclusion.....	55
Chapter 2: Literature Review.....	56
2.1 History and Utilisation of Solar Heating Systems.....	57
2.2 Performance Enhancement Techniques.....	58
2.2.1 Geometrical and Material Modifications.....	59
Transparent cover.....	59
Multi-channels absorber and heat pipes.....	60

2.2.2	Heat Transfer Fluids	61
	Porous medium	61
	Nanofluids	61
2.2.3	Selective Coatings.....	62
2.2.4	Spacing and Insulation.....	63
	Transparent Insulation Materials.....	63
	Gas insert.....	64
	Vacuum insulation	64
2.3	Conclusion.....	66
Chapter 3: Theoretical Model and Computational Algorithm		67
3.1	Heat Transfer in Collector.....	68
3.2	Collector Heat Losses Evaluation	69
3.2.1	Top Heat Loss Coefficient	71
	a) Heat loss between the absorber plate and the front cover.....	71
	b) Heat loss between the front cover and ambient	74
3.2.2	Back Heat Loss Coefficient	77
	a) Heat loss between the absorber plate and the back cover.....	77
	b) Heat loss between the back cover and ambient.....	78
3.2.3	Overall Heat Loss Coefficient.....	78
3.3	Heat Transfer from Sheets to Tubes.....	78
3.3.1	Absorber plate temperature distribution.....	78
3.3.2	Collector Efficiency Factor	81
3.4	Fluid Temperature Distribution in Flow Direction.....	84
3.4.1	Collector Heat Removal Factor.....	86
3.5	Computational Programming Methodology.....	87
3.5.1	Calculation Programme Principle	87
3.5.2	Calculation Programme Steps.....	88
3.5.3	Calculation Programme Organigram.....	90
3.6	Conclusion.....	92
Chapter 4: Experiments Carried Out on Flat Plate Solar Water Collector.		93
4.1	Site Characteristics.....	94
4.2	Measurement Station Features	94
4.3	Experimental Heating System Description.....	95
4.3.1	Heating System Components	96
4.4	Instruments of Measurement.....	97
4.4.1	Measurement of Temperature	97
4.4.2	Measurement of Solar Irradiation	97
4.4.3	Data Acquisition	98
4.5	Instruments Accuracy	99
4.5.1	Accuracy of pyranometers	99
4.5.2	Accuracy of Thermocouples	100
4.5.3	Thermocouple Calibration	100
4.6	Experiment Procedure.....	100
4.6.1	Experiment Schematic Diagram.....	100
4.6.2	Procedure of the Experimental Work.....	102
4.6.3	Recommendations Before Starting Tests	102
4.7	Conclusion.....	103

Chapter 5: Results and discussions.....	104
5.1 Experimental Results and Model Validation.....	105
5.1.1 Solar Radiation Measurement.....	105
5.1.2 Temperatures Measurement.....	106
5.1.3 Model Validation.....	107
5.2 Contribution to Collector Performance Enhancement.....	109
5.2.1 Specifications of New Configuration.....	109
5.2.2 Insulation Technique Effect.....	110
5.2.3 Selective Coating Effect.....	112
5.2.4 Optimum Number of Riser Tubes.....	115
5.3 Cost Evaluation.....	117
5.3.1 Collector Parts Cost.....	118
5.3.2 Collectors Cost Comparison.....	119
5.4 Conclusion.....	121
Conclusion.....	122
Bibliography.....	124

List of Figures

Figure 1.1 Fossil fuel damages.....	16
Figure 1.2 Algeria's renewable energy potential (Islam et al., 2013).....	17
Figure 1.3 Algeria location Map with mean annual irradiation (Stambouli & Koinuma, 2012).....	18
Figure 1.4 Various types of solar collectors: (a) flat plate, (b) evacuated tube (c) Linear Fresnel (d) parabolic trough, (e) parabolic dish and (f) Heliostat field.....	20
Figure 1.5 Flat plate solar thermal devices.....	22
Figure 1.6 Main components of a typical flat plate solar collector.....	23
Figure 1.7 Schematic diagram of piping system fixation models: a) pipe lower bond model, b) pipe side bond model and c) pipe upper bond model.....	26
Figure 1.8 Basic forms of piping system: a) serpentine configuration, b) unidirectional parallel pipes configuration and c) parallel pipes configuration.....	26
Figure 1.9 Operating principle of a typical flat plate solar collector.....	29
Figure 1.10 Flat plate solar collector using passive fluid circulation mode.....	30
Figure 1.11 Flat plate solar collector using active fluid circulation mode.....	31
Figure 2.1 Prototype of the primely solar water collector (Fortuin & Stryi-Hipp, 2013).	58
Figure 2.2 The most used performance enhancement techniques in flat plate solar collectors	59
Figure 3.1 Equivalent thermal-circuit diagram for a flat plate solar collector.....	70
Figure 3.2 The heat transfer from sheet to tube.....	79
Figure 3.3 The equivalent thermal-circuit diagram of heat transfer from the sheet to the fluid inside tube.....	81
Figure 3.4 The energy flow through fluid.....	84
Figure 3.5 Calculation programme organigram.....	91
Figure 4.1 Location of URAER (Gairaa & Bakelli, 2013b).....	94
Figure 4.2 Photograph of the experimented flat plate thermal solar collector.....	95
Figure 4.3 Photograph of the thermocouple used for measurement.....	97
Figure 4.4 Photograph of the pyranometers used for measurement.....	98
Figure 4.5 Photograph of the data logger and the computer.....	99
Figure 4.6 Schematic diagram of the experiment.....	101
Figure 5.1 Evolution of diffused, direct and global solar irradiation as a function of local time during 22 nd May.....	105

Figure 5.2 Evolution of absorber plate temperature, ambient air temperature and inlet fluid temperature as a function of local time during 22 nd May.....	106
Figure 5.3 Evolution of measured and calculated absorber plate temperatures as a function of local time during 22 nd May.	108
Figure 5.4 Isometric view of the proposed VFPSC.....	110
Figure 5.5 Evolution of absorber plate temperature of FPSC, ETSC and VFPSC as a function of local time.	110
Figure 5.6 Evolution of overall heat loss of FPSC, ETSC and VFPSC as a function of local time.....	111
Figure 5.7 Evolution of thermal efficiency of FPSC, ETSC and VFPSC as a function of local time.	112
Figure 5.8 Absorber plate temperature of FPSC, ETSC and VFPSC for different absorber emissivity.....	113
Figure 5.9 Overall heat loss of FPSC, ETSC and VFPSC for different absorber emissivity.	113
Figure 5.10 Thermal efficiency of FPSC, ETSC and VFPSC for different values of absorber emissivity.....	114
Figure 5.11 Inlet manifold and riser tubes connected in parallel.	115
Figure 5.12 Outlet fluid (dashed line) and absorber plate (continuous line) temperatures of FPSC, ETSC and VFPSC as a function of the tubes number.....	116
Figure 5.13 Thermal efficiency of FPSC, ETSC and VFPSC as a function of the tubes number.....	117
Figure 5.14 Thermal efficiency and total collector cost of FPSC, ETSC and new VFPSC using absorber emissivity of 0,05.....	119
Figure 5.15 Thermal efficiency and total collector cost of FPSC, ETSC and new VFPSC using absorber emissivity of 0,95.....	120

List of Tables

Table 1.1 Solar potential in Algeria.....	18
Table 1.2 Types of Solar Thermal Collectors with their salient features.....	21
Table 1.3 Various types of top transparent cover used and their main features.....	24
Table 1.4 Various types of absorber plate.....	25
Table 1.5 Product names and optical properties of commercially available absorber coatings.....	25
Table 1.6 Summary of nanofluids with their properties.....	27
Table 1.7 Characteristics of the most commonly used insulators materials.....	28
Table 1.8 Typical temperature ranges of industrial processes.....	54
Table 3.1 Selected correlations of Nusselt number used for the natural convection calculation in a closed cavity.....	72
Table 3.2 Selected correlations for the external natural convection calculation on the top cover.....	75
Table 3.3 Selected equations for equivalent sky temperature calculation.....	76
Table 3.4 formulae of F' and F for various configurations of collector.....	83
Table 5.1 Characteristics of the examined flat plate solar collector.....	107
Table 5.2 Main components prices and total cost of solar collectors.....	121

Nomenclature

Nomenclature

A	total collector area (m^2)
A_g	top cover area (m^2)
A_{mw}	mean wall area (m^2)
C_f	fluid specific heat (J/kg K)
d	tube inside diameter (m)
D	tube outside diameter (m)
e_{is}	back insulator thickness (m)
e_p	absorber plate thickness (m)
e_{tb}	tube thickness (m)
F	sheet efficiency factor
F'	collector efficiency factor
F_R	heat removal factor
g	gravitational constant (m/s^2)
G^*	global solar radiation (W/m^2)
h_{1c}	convection heat transfer coefficient between absorber and front cover ($\text{W/m}^2 \text{K}$)
h_w	wind convection coefficient ($\text{W/m}^2 \text{K}$)
h_{3c}	convection heat transfer coefficient between absorber and back side ($\text{W/m}^2 \text{K}$)
h_{4c}	convection heat transfer coefficient between back side and ambient ($\text{W/m}^2 \text{K}$)

h_{1r}	radiation heat transfer coefficient between absorber and front cover ($W/m^2 K$)
h_{2r}	radiation heat transfer coefficient between front cover and sky ($W/m^2 K$)
h_{3r}	radiation heat transfer coefficient between absorber and back side ($W/m^2 K$)
h_{4r}	radiation heat transfer coefficient between back side and ambient ($W/m^2 K$)
h_f	film heat transfer coefficient ($W/m^2 K$)
K_g	fluid thermal conductivity ($W/m K$)
L_g	spacing between absorber and top cover (m)
L_{tb}	tube length (m)
\dot{m}_f	fluid mass flow rate (kg/s)
n	number of tubes
N_u	Nusselt number
Q_{ab}	absorbed energy rate (W/m^2)
Q_p	energy heat loss (W/m^2)
$Q_{p_{back-3}}$	energy heat loss between absorber plate and back cover (W/m^2)
$Q_{p_{back-4}}$	energy heat loss between back cover and ambient (W/m^2)
$Q_{p_{top}}$	energy heat loss through the front side (W/m^2)
$Q_{p_{top-1}}$	energy heat loss between absorber plate and front cover (W/m^2)
$Q_{p_{top-2}}$	energy heat loss between front cover and ambient (W/m^2)
Q_u	useful energy rate (W/m^2)
R_1	thermal resistance between absorber and front cover ($m^2 K/ W$)

R_2	thermal resistance between front cover and ambient ($m^2 K/ W$)
R_3	thermal resistance between absorber and back cover ($m^2 K/ W$)
R_4	thermal resistance between back cover and ambient ($m^2 K/ W$)
Ra	Rayleigh number
T_a	ambient temperature (K)
T_c	cover temperature (K)
T_{fi}	inlet water temperature (K)
T_{fo}	outlet water temperature (K)
T_i	actual value of measured temperature (K)
\hat{T}_i	actual value of calculated temperature (K)
\bar{T}	average value of measured temperature (K)
T_p	absorber plate temperature (K)
T_{sky}	sky temperature (K)
U_b	back heat loss coefficient ($W/m^2 K$)
U_L	overall heat loss coefficient ($W/m^2 K$)
U_t	top heat loss coefficient ($W/m^2 K$)
v_{wind}	wind speed (m/s)
W	absorber sheet width (m)
<i>Greek symbols</i>	
ε_c	cover emissivity

ε_p	absorber emissivity
η_{th}	thermal efficiency
λ_{is}	back insulator thermal conductivity (W/m K)
λ_p	absorber plate thermal conductivity (W/m K)
λ_t	tube thermal conductivity (W/m K)
σ	Stefan–Boltzmann constant (W/m ² K ⁴)
$(\tau\alpha)_c$	absorptance-transmittance product
β'	volumetric coefficient of expansion (K ⁻¹)
ϑ_a	kinematic viscosity (m ² /s)

Introduction

Over the recent few decades, there has been a change towards renewable energy resources to overcome fossil fuel deficiency and catastrophic environmental issues. The target is to minimise the fossil fuels dependency which mitigate climate change problems and, consequently, protect the environment. The effectiveness and dispatchability of energy generation from renewable sources can be enhanced exploiting solar power technologies. Specifically, thermal solar systems can be deployed to bridge the mismatch between solar energy supply and demand. Solar energy is one of the most promising and available energy sources all over the world that can be integrated into numerous applications in the form of thermal energy and electrical energy.

In recent years solar energy has been strongly promoted as a viable energy source. One of the simplest and most direct applications of this energy is the conversion of solar radiation into heat. The domestic sector can lessen its impact on the environment by the installation of solar thermal devices such as flat plate collectors for heating water. Although it should be said that some of these collectors have been in service for the last 40-50 years without any real significant change in their design and operational principles.

A typical flat plate collector consists of an absorber in an insulated box together with transparent cover sheets (glazing). The absorber is usually made of a metal sheet of high thermal conductivity, such as copper or aluminium, with integrated or attached tubes. Its surface is coated with a black paint or with a special selective material to maximise radiant energy absorption while minimising radiant energy emission. The insulated box reduces heat losses from the back side of the collector. However, heat loss is inherent in this type of collector, especially from the front side, which reduces its thermal performance. Therefore, the research aim in this thesis is concerned with the enhancements of the performance, energy conversion and thermal efficiency of the flat plate solar collector by improving the quality of insolation. The use of vacuum environment inside the front gap between absorber sheet and transparent glass is a means of enhancing the heat transfer. This technique requires a change in the collector design that offers the appropriate resistance to force caused by difference between the internal and external pressure.

In order to achieve these objectives, an experiment on a thermal solar collector available at the Applied Research Unit in Renewable Energies Ghardaïa is performed. A calculation model using MATLAB programming language is implemented to simulate the thermal behaviour of the flat plate solar water collector based on an iterative calculation. Finally, the validation of computational results with experimental data is carried out and an investigation of some collector parameters that effect the thermal performance is discussed.

This thesis is presented in five main chapters to show the findings of the research work conducted on the studied topic.

- The first chapter presents a concise introduction to the subject matter that focuses on solar energy. In addition, this chapter emphasizes on providing general details on solar thermal collectors, classifications according to the forms and the temperature levels of each type. Moreover, the working principle of flat plate solar collector and the internal and external parameters that can influence its performance. From this, the incentive for carrying out this work has been defined, which identifies key area to be reviewed in the second chapter.

- The second chapter presents a literature review on flat plate solar collectors including the previous work in this area. A summarise of the enhancement techniques that significantly influence the thermal performance of flat plate solar collector.

- The third chapter is divided in two parts; the first part presents the theoretical model that includes the governing equations and heat transfer equations. The second part is devoted to the computational program that used for the prediction of thermal performance of the investigated collectors.

- The fourth chapter is devoted to carry out outdoor experiment on the investigated flat plate solar water collector using the various appropriate measuring devices. This chapter provides also a detailed description of each component that has been used in the experimental setup.

- The last chapter consists of the results and discussion which includes the validation of the developed calculation program by comparing the results obtained with the experimental results. A comparison between the ameliorated vacuum flat plate collector and the conventional flat plate collectors is also discussed.

A general conclusion relating to this work is presented.

Chapter 1: Flat Plate Solar Water Collectors

Solar energy is one of the most serviceable sources of renewable energy that is abundantly available throughout the regions of Algeria. One of the systems that applies the solar power to heat fluid is solar thermal collector. The current chapter focuses on a special type of non-concentrating collector; commonly known, the flat plate thermal solar collector. This chapter also includes the main components, the operating principle and parameters characterising the operation mode of a typical flat plate solar collector. Furthermore, the orientation, inclination and heat transfer modes in this collector are briefly introduced.

1.1 Renewable Energies in Algeria

Fossil fuels resources such as hydrocarbons (liquid hydrocarbon and natural gas) and coal, which are non-renewable resources, provide the major part of total energy used. However, the extraction, production and exploitation of fossil fuels causes very serious threats to the environment, human health, ecosystem quality, energy resources...etc (see Figure 1.1). In contrast, the renewable energies are energies that can be provided by inexhaustible and naturally replenished resources, such as sunlight, wind, heat of earth, water or even plants. Besides, these sources are clean and friendly to the both environment and human, with little or no harmful consequences.

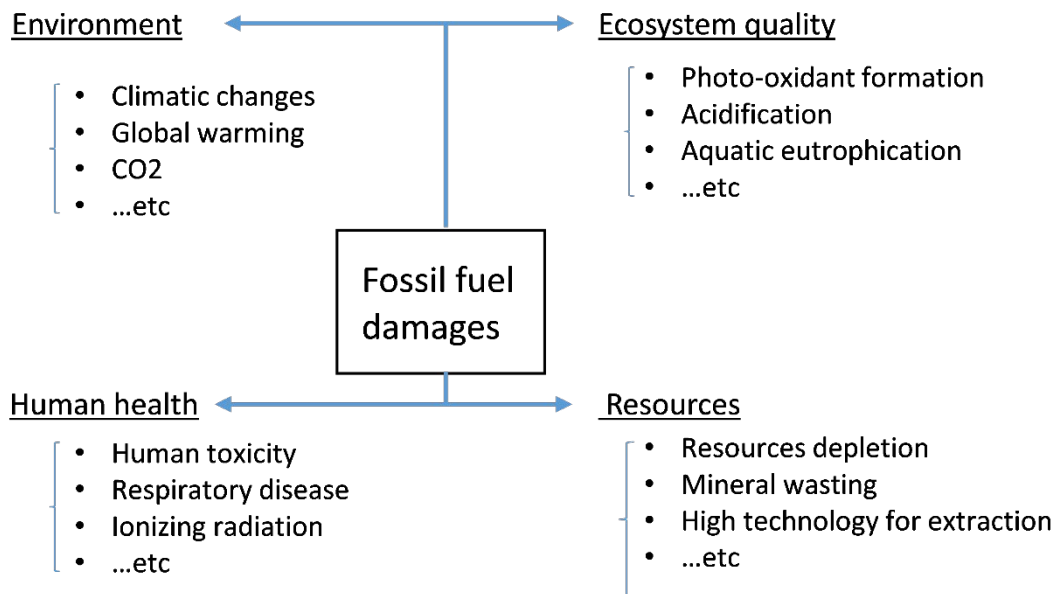


Figure 1.1 Fossil fuel damages.

As part of the national policy for energy transition and the development of renewable energies, Algeria has adopted an ambitious program to develop its renewable energy strategy and energy efficiency [1]. The vision of the Algerian government is based on a strategy that focuses on the development of alternative clean energies such as solar power, wind power, geothermal, biomass...etc, and thus reduce the dependency on fossil fuels (see Figure 1.2). The proposed renewable energy program consists of installing about 22,000 MW by 2030 for the national commercialisation, while maintaining the export option as a strategic objective. This program was launched in February 2011, revised in May 2015 and placed as a national priority in February 2016 [2].

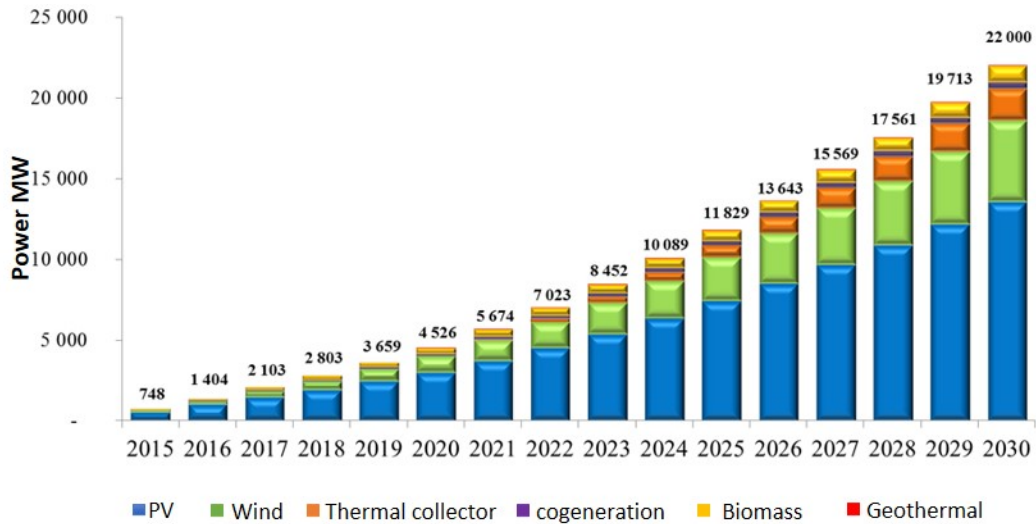


Figure 1.2 Algeria's renewable energy potential [1].

Algeria's energy efficiency is expected to play an important role in the national energy context characterised by the explosive growth in consumption driven, in particular, by the domestic sector through the construction of new houses and buildings, and the recovery of the industrial sector. Therefore, the main goal of the government is to provide the same energy services, but using as much renewable resources as possible.

In fact, it must be recognised that energy saving is, nowadays, an essential integrant of any coherent energy policy, including energy saving, energy control and rational energy consumption. Consequently, fighting against the waste of energy has become one of the main goals of government, but with the participation of citizens [3].

1.2 Solar Energy in Algeria

Solar energy is the cleanest and most abundant renewable energy source available throughout the world, which is inexhaustible and is obtained from the electromagnetic radiation coming from the sun. Solar devices can harness this power for a diversity of use in an entirely sustainable and free manner, including the generation of electrical energy and thermal energy for both domestic and industrial use.

Algeria, which is located in the Sunbelt, has a high potential of solar power. Moreover, it is the largest county in Africa with area of 2,381,741 km² and the tenth largest one in the world. The Sahara part of the country consists of an enormous portion with about 86% of the total area. This desert region is hot year around and is considered to be among the areas with the highest average solar irradiation globally, see Figure 1.3 [4].

Table (1.1) presents the potential of solar power in Algeria. The county receives mean solar energy estimated of about 2100 (hour/m²/year) and average sunshine duration around 3000 (hour/year) annually [5]. These given statistics indicates, considering the solar energy point of view, that this county is blessed by high potential of solar power which makes it more suitable for solar applications, particularly thermal solar systems.

Table 1.1 Solar potential in Algeria.

	Coastal area	Inner area	Desert area
Surface (%)	4	10	86
Average of the insolation (hour/year)	2650	3000	3500
Average energy received (hour/m ² /year)	1700	1900	2650

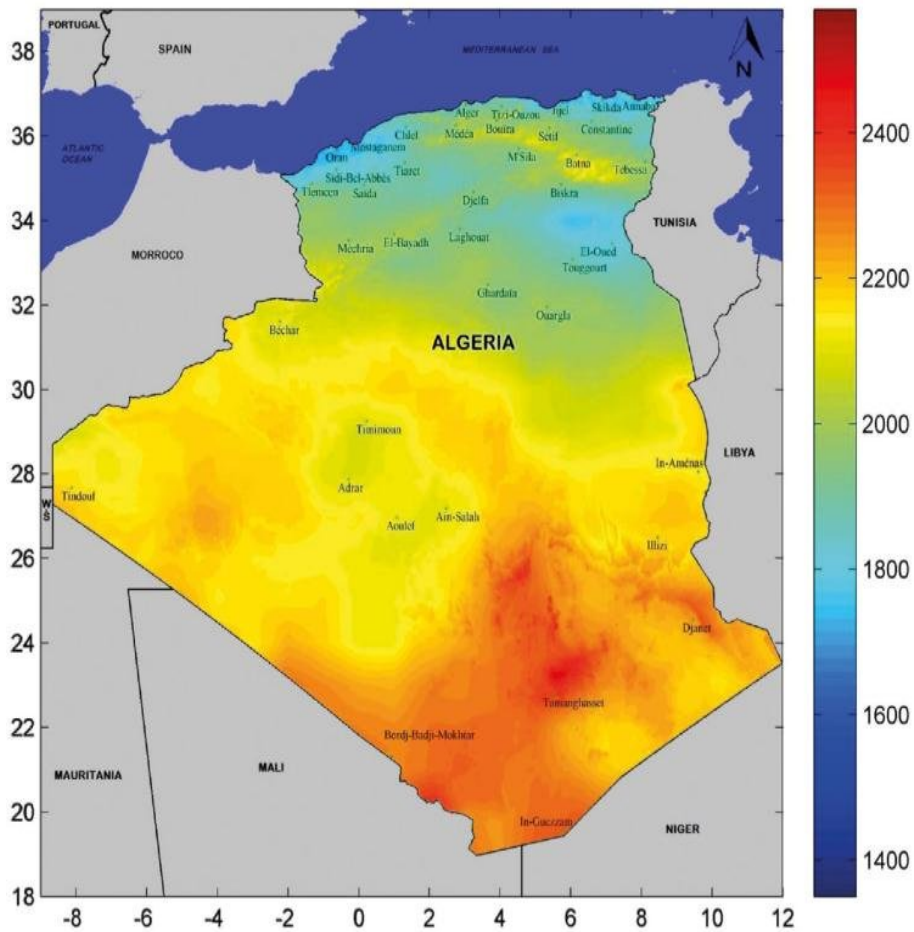


Figure 1.3 Algeria location Map with mean annual irradiation [5].

1.3 Solar Thermal Collectors

Solar energy technology can offer unlimited potential of power for both domestic and industrial energy needs. Solar energy can be converted through three processes (chemical, electrical and thermal) as follows:

- **Chemical process** through photosynthesis, which maintains life on earth by producing food and converting CO₂ to O₂.
- **Electrical process**, using photovoltaic systems to convert electromagnetic radiation to electrical power.
- **Thermal process**, using solar thermal systems to absorb electromagnetic radiation and then produce heat energy.

Solar thermal collectors are defined as a special kind of heat exchangers that convert solar irradiation into heat energy through a heat transfer fluid (e.g., water, air, oil, nanoparticle...etc) for useful applications such as supplying heat energy to domestic systems or/and industrial systems.

1.3.1 Solar Thermal Collectors Types

There are fundamentally two types of solar thermal collectors; namely, non-concentrating collectors and concentrating collectors (using sun tracking system). A non-concentrating thermal collector has the same area for absorbing and for receiving solar irradiation. However, a concentrating thermal collector typically has concave reflecting surfaces to intercept and concentrate the solar irradiation to a specific area, thereby multiplying the radiation flux. Figure 1.4 illustrates various types of solar collectors.

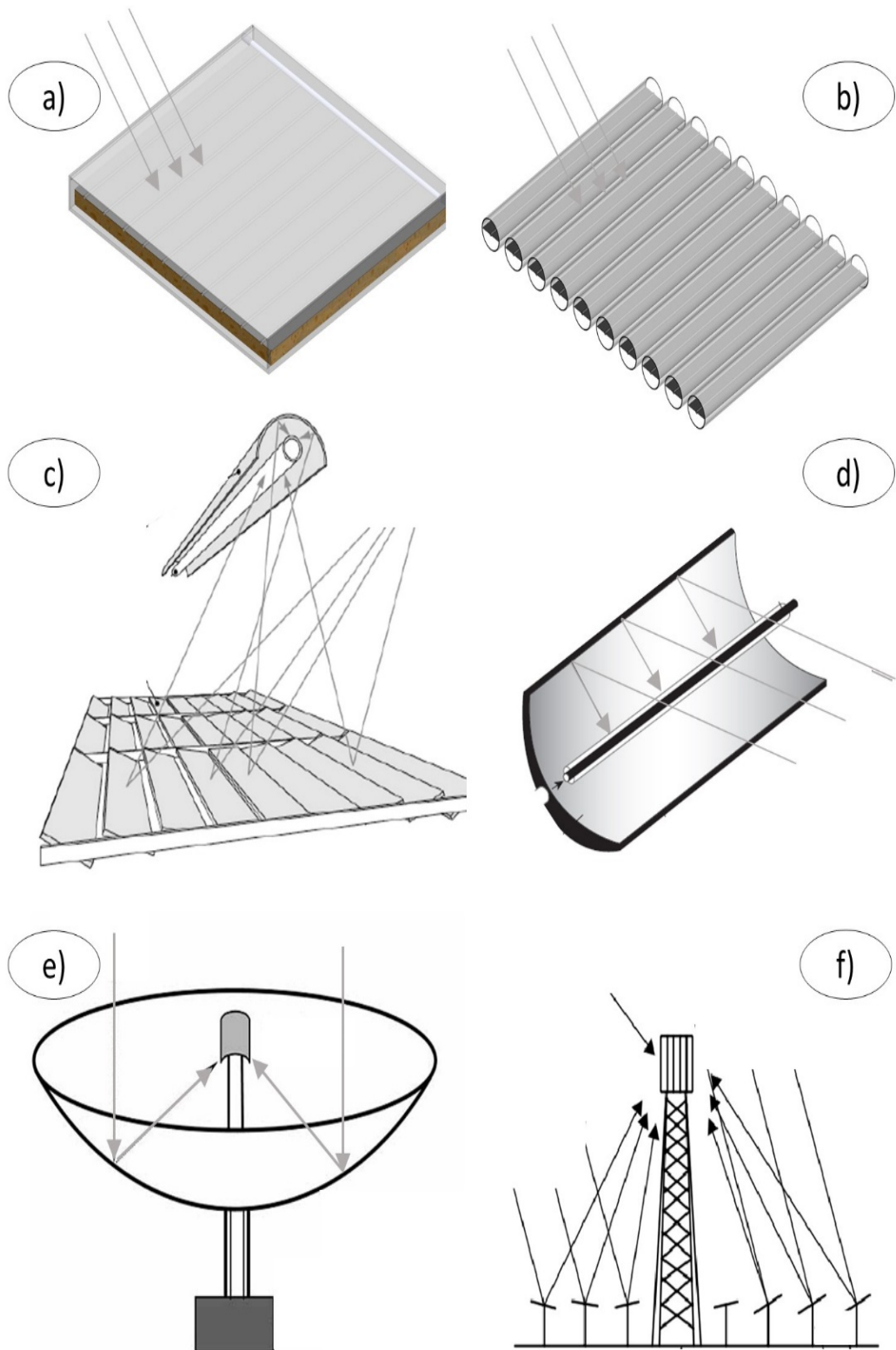


Figure 1.4 Various types of solar collectors: (a) flat plate, (b) evacuated tube (c) Linear Fresnel (d) parabolic trough, (e) parabolic dish and (f) Heliostat field.

Thermal solar collector can be classified according to temperature level (low temperature [50°C-100°C], medium temperature [100°C-300°C] and high temperature [$>300^{\circ}\text{C}$]) or/and absorber/receiver geometry. The following Table (1.2) outlines types of solar thermal collectors with their salient features.

Table 1.2 Types of Solar Thermal Collectors with their salient features.

Motion	Collector Type	Absorber Type	Concentration Ratio	Temperature Range [°C]	
Stationary	Flat plate collector (FPC)	Flat	-	30 to 80	
	Evacuated tube collector (ETC)	Flat	-	50 to 200	
Sun-tracking system	One-axis tracking	Linear Fresnel reflector (LFR)	Tubular	$10 \leq C \leq 40$	60 to 250
		Parabolic trough collector (PTC)	Tubular	$15 \leq C \leq 45$	60 to 300
	Two-axes tracking	Parabolic dish reflector (PDR)	Point	$100 \leq C \leq 1000$	100 to 500
		Heliostat field collector (HFC)	Point	$100 \leq C \leq 1500$	150 to 2000

1.4 Flat Plate Solar Collector

Flat plate solar collectors are heating systems that collect solar energy using high conductive metal sheets in flat geometry, which can absorb as much both direct and diffuse solar radiation as possible, and convert it into thermal energy (generally low-grade energy), and then transfer this energy to a heat transfer fluid as water, oil, air...etc. This kind of heating devices are the most commonly used for solar-powered domestic hot water systems. For the reasons that the general idea behind this technology is pretty simple in terms of manufacturing, installation,

reliability and budget. In addition, they do not require a sun-tracking system, which means little maintenance and more reliable, see Figure 1.5.

The flat plate solar thermal devices can be used for several applications in a low to medium temperature range ($<150^{\circ}\text{C}$), for instance, building heating systems, air conditioning, and industrial process heat. In general, the hot water available from these devices can probably be used for all domestic needs. However, in case of low thermal performance or insufficient solar energy is available (e.g., cloudy sky, winter period, night period...etc.), then an auxiliary energy source should be integrated.



Figure 1.5 Flat plate solar thermal devices.

1.4.1 Typical Flat Plate Solar Collector Main Components

A flat plate collector generally consists of the following components:

Top transparent cover, flat absorber plate, risers and head pipes, back insulation and enclosure box (see Figure 1.6).

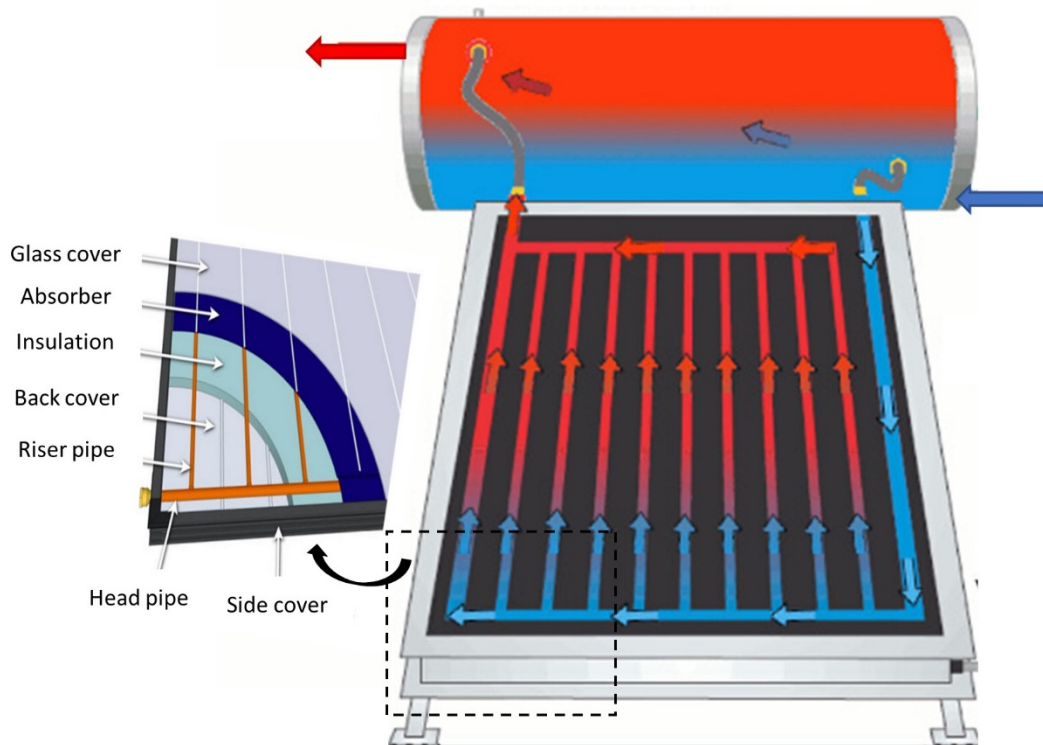


Figure 1.6 Main components of a typical flat plate solar collector.

Top transparent cover

Since the top cover of a flat plate collector must be transparent to allow sunlight to pass through, glass is the most widely used material. The transparent cover should have high transmittance and additional required features such as good resistance to mechanical loads (shock, hail, rain, snow...etc) and thermal loads (heat insulation, high temperatures level... etc.).

In some cases, especially when flat plate collectors are installed on the roofs of houses or facades of buildings, transparent plastic materials are used. Because they are lighter, cheaper, safer and easier to set up, but its service life and characteristics are less than that of glass materials.

The main characteristics of top cover are:

- Coefficient of transmittance.
- Coefficient of reflectance.
- Coefficient of absorptance.
- Coefficient of emittance.

The coefficient of transmittance (τ) is essentially determined by the structure of the transparent material (thickness, number (single, double or triple...), quality of manufacturing...etc) and the nature of the filling gas between the absorber and the top cover. The characteristics of various materials that can be used as a transparent cover are given in the Table (1.3).

Table 1.3 Various types of top transparent cover used and their main features.

Material	Thickness (mm)	Transmittance	Refractive Index	Density (Kg/m³)
Float glass (normal window glass)	3.9	0.83	1.463	2230
Low-iron glass	3.2	0.90	1.58	1150
Perspex	3.1	0.82	1.49	1190
Polyvinyl fluoride	0.1	0.92	1.46	1390
Polycasa CAST PMMA	/	0.93	1.492	1190

Absorber plate

The main role of an absorber plate is to collect solar irradiation and convert it into heat energy. It is usually painted black (or coated with a selective surface) to absorb maximum irradiation.

The absorber is chosen according to the following characteristics:

- High thermal conductivity.
- Low density.
- Absorb as much solar radiation as possible.
- Transmit the heat produced to the working fluid with a minimum of losses.
- Good corrosion resistance.

The choice of absorber material has a great influence on the thermal performance of solar collector. Copper, aluminium and steel are the most commonly used materials, due to their high

thermal conductivities. The characteristics of various materials that can be used as an absorber plate are given in the Table (1.4).

Table 1.4 Various types of absorber plate.

Material	Thermal Conductivity (W/m/K)	Specific Heat Capacity (J/kg/k)	Density (Kg/m³)
Copper	385	3850	8930
Aluminium 1050-O	231	900	2705
Iron, Fe	76.2	4400	7870
AISI 1012 Steel	51.9	4720	7870

Selective coating

In order to reduce radiation heat losses, the absorber plates should be coated with a selective layer. The surface selectivity of the absorber plate is very important; it is characterised by high absorptivity in the visible and low emission in the infrared radiation. Table 1.5 represents characteristics of several materials that can be applied as an absorber coating. The selective coating is chosen according to the following coefficients:

- Absorptivity coefficient (optimal: 1).
- Emissivity coefficient (optimal: 0).

Table 1.5 Product names and optical properties of commercially available absorber coatings.

Product name	Absorptivity	Emissivity	Deposition method
Black paint	0.95	0.95	Painting
Thurmalox 250	0.96	0.65	Painting
CuO (TT)	0.91±0.02	0.51±0.01	Electrodeposition
ThermProtect	0.945	0.33	Physical vapor deposition
AS	0.95	0.16	Electroplating
TiNOX energy	0.95±0.02	0.04±0.02	Physical vapor deposition

Piping system

The piping system of a solar collector is a substantial element that ensures the transport of the fluid passing through it. The most important physical and thermal properties of the tubes are the same as those of the absorber plate (see Table 1.4). The way of fixing the tubes in the absorber plate has a direct effect on the quality of the heat transferred to the working fluid. As shown in Figure 1.7, there are three common ways to fix the tubes (pipe lower bond model, pipe side bond model and pipe upper bond model).

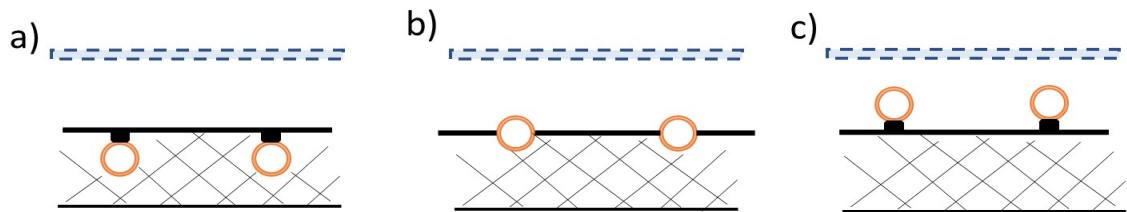


Figure 1.7 Schematic diagram of piping system fixation models: a) pipe lower bond model, b) pipe side bond model and c) pipe upper bond model.

Piping system can also be distinguished by the different forms, as presented in Figure 1.8:

- Serpentine configuration.
- Unidirectional parallel pipes configuration.
- Parallel pipes configuration.

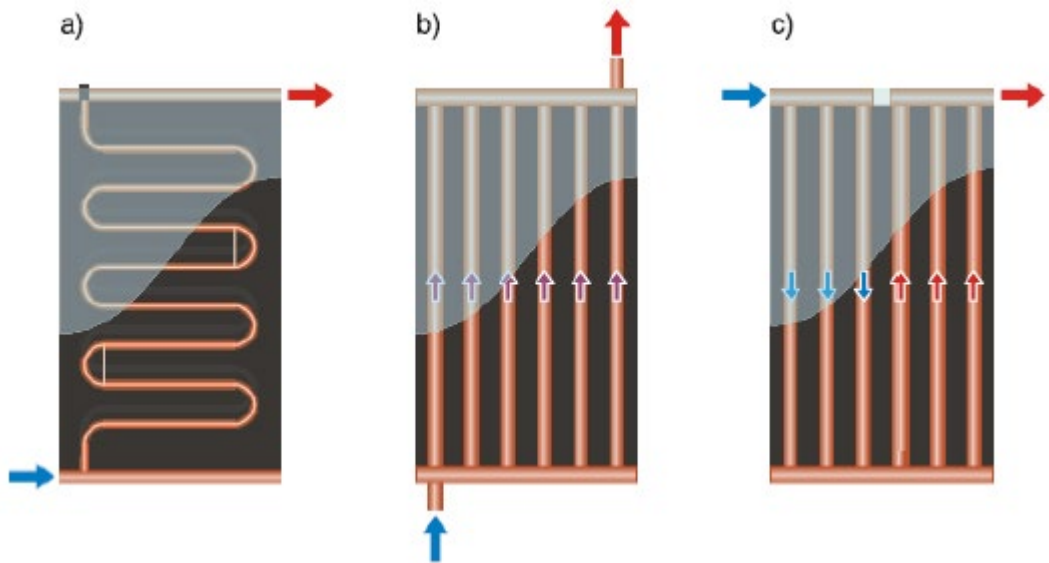


Figure 1.8 Basic forms of piping system: a) serpentine configuration, b) unidirectional parallel pipes configuration and c) parallel pipes configuration.

Working fluid

The main aim of the working fluid is to absorb heat energy coming from the tubes and transfer it to the fluid inside the storage tank. The heat transfer fluid is an important component of flat plate heating systems. Thus, it is crucial to choose an appropriate working fluid for an effective heating system. The working fluid should be selected based on the following factors:

- High thermal conductivity.
- High specific heat capacity.
- Low thermal expansion coefficient.
- Low viscosity.
- Anti-corrosive properties.

Water is one of the usual options as a working fluid due to its accessibility and acceptable thermal properties. However, under certain harsh circumstances, one disadvantage of water is that it freezes, which may deteriorate the collector's piping system. In addition, the selection of the working fluid depends on the application and collector temperature level as well. There are many methods to enhance the thermal properties of heat transfer fluid. One of the most efficient ways is to add nano-sized particles of high thermal conductivity into the heat transfer fluid to ameliorate the overall conductivity of the working fluid. With the advancements in nanotechnology, a new combination of fluids become available, called as nanofluids which consists of a nano sized particles suspended in a base fluid. Table 1.6 summarises some nanofluids with their properties.

Table 1.6 Summary of nanofluids with their properties.

	Particle	Base-fluid	Average particle size (nm)	Thermal conductivity enhancement
Metallic nanofluids	Cu	Water	100	78%
	Cu	Ethylene glycol	10	40%
	Au	Water	10–20	21%
	Fe	Ethylene glycol	10	18%
	Ag	Water	60–80	17%

Non-metallic nanofluids	Al ₂ O ₃	Water	13	30%
	TiO ₂	Water	15	30%
	Al ₂ O ₃	Water	68	21%
	CuO	Water	50	17%
	SiC	Water	26	16%

Back insulation material

The solar collector needs to be well thermally insulated using appropriate materials. The latter must have properties that are required in order to reduce conduction, convection and radiation thermal losses. For an optimal choice of an insulating material, the following parameters should be considered:

- Low thermal conductivity.
- Low density.
- Good resistance to high temperature level.
- Good resistance to humidity.

The characteristics of the most commonly used insulators materials are listed in Table 1.7.

Table 1.7 Characteristics of the most commonly used insulators materials.

Insulating material	Thermal conductivity (W/m/K)	Density (Kg/m³)	Relative moisture absorption
Mineral wool	0.045	24	Very high
Expanded polystyrene 15	0.04	15	Medium
Expanded polystyrene 30	0.037	30	Medium
Extruded polystyrene	0.27	32	Medium
Polyurethane foam	0.018	36	Low
Phenolic foam	0.027	32	Low
Cellular foam	0.41	125	Low

Casing box

The casing box is a non-functional element, that carry out all the flat plate collector elements and also acts as protection enclosure against climatic conditions. Usually, it is made of wood or PVC-aluminium.

1.4.2 Typical Flat Plate Solar Collector Operating Principle

The solar radiation arrives the front transparent cover, in which a part of this radiation reflected to the environment, and the other part passes through it to reach the absorber plate. The latter heats up and transfers the heat to the working fluid circulating into the piping system, see Figure 1.9. Contemporaneously, the absorber plate emits radiation (mainly in the infrared) which is reflected by the top cover, this is the principle of the greenhouse effect. The majority of the energy absorbed must be transmitted to the transfer heat fluid, therefore thermal losses to the surrounding environment must be minimised. The circulation of the working fluid can be naturally occurring (the thermophone effect) or using a pump (forced circulation).

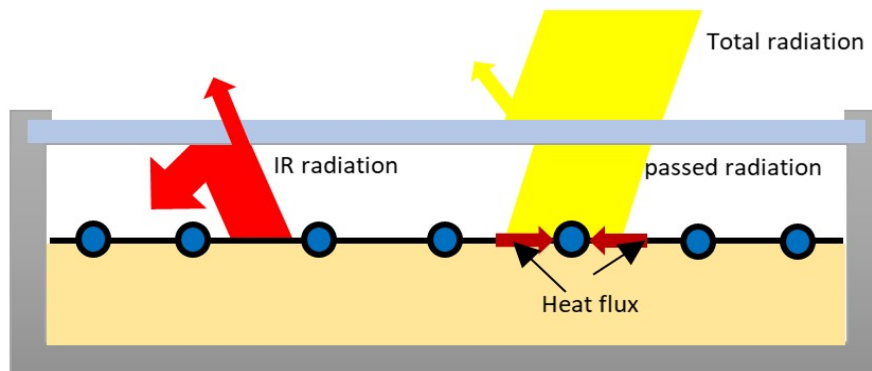


Figure 1.9 Operating principle of a typical flat plate solar collector.

1.5 Passive and Active Fluid Circulation in Thermal Solar Collector

Depending on the fluid circulation mode, two main types are distinguished as follows:

1.5.1 Passive Fluid Circulation (Thermosyphon Circulation)

As the solar radiation heats up the absorber plate and then tubes, the temperature of the heat transfer fluid increases, while its density decreases. According to the principle of gravitation, the hot fluid rises in the circuit and is replaced by cold fluid, which is relatively heavier, coming from the storage tank (thermosyphon effect). To ensure the circulation of the

working fluid in this mode of circulation, the storage tank must be positioned higher than the solar collector panel with a predefined distance, see Figure 1.10.

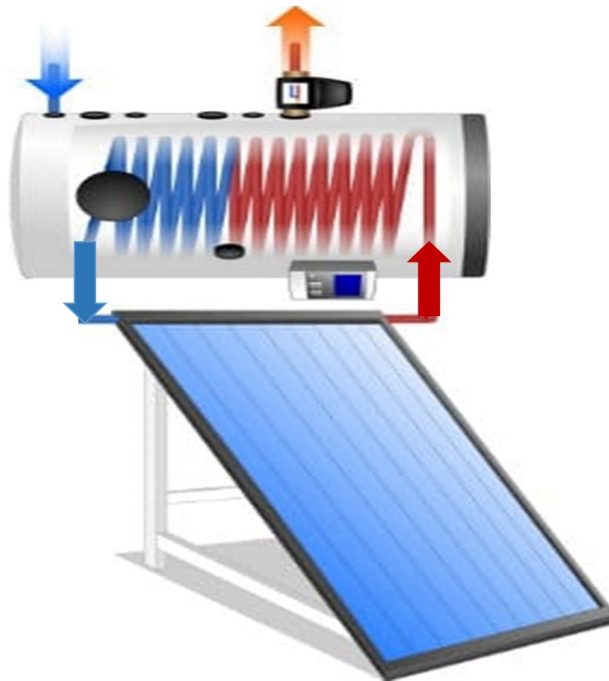


Figure 1.10 Flat plate solar collector using passive fluid circulation mode.

1.5.2 Active Fluid Circulation (Forced Circulation)

Contrary to thermosiphon fluid circulation, forced mode requires a pump to generate fluid circulation, see Figure 1.11. Thus, the storage tank can be fixed at any position, which is one of the advantages of forced circulation mode.

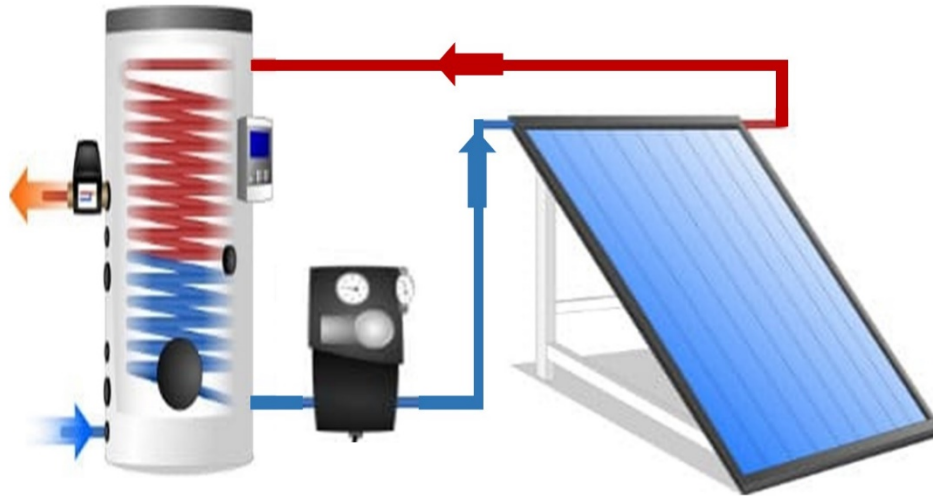


Figure 1.11 Flat plate solar collector using active fluid circulation mode.

1.6 Comparison Between Passive and Active Fluid Circulation Solar Collector

1.6.1 Collector Price

- Advantage for the passive fluid circulation.

A solar collector that adopts thermosiphon fluid circulation does not need a pump or a regulating system, thus it requires low maintenance and is less expensive.

1.6.2 Collector Installation

- Advantage for the passive fluid circulation.

The installation of a passive fluid circulation solar collector is easier than an active fluid circulation solar collector. For the reasons that the passive fluid circulation requires no regulator, pump or electrical network, and therefore less effort to install it.

1.6.3 Collector Reliability

- Advantage for the passive fluid circulation.

The regulation system and the pump of the active fluid circulation solar collector are the most parts that causes the failure. Without these non-robust elements, the passive circulation solar collector has minimal maintenance level, and significantly improves the duration of its life cycle.

1.6.4 Collector Flexibility

- Advantage for the active fluid circulation.

The flexibility of the installation is the strong point of the active fluid circulation solar collector compared to the passive fluid circulation solar collector, as the storage tank can be positioned almost anywhere (near or far from the solar collector), particularly below the solar collector.

1.6.5 Collector Application

- Advantage for the active fluid circulation.

In most cases, the passive fluid circulation solar collector can only be used individually, however the active fluid circulation solar collector is generally used for domestic or industrial use, and can be applied in several implementations.

1.6.6 Collector Performance

- Advantage for the active fluid circulation.

The active fluid circulation solar collector benefits from the pump and regulation system to control the heat transfer fluid circulation, especially when the solar radiation is very low, the thermal losses of the heating system for both the solar collector and storage tank are very large.

1.7 Parameters Characterising the Operation Mode

The parameters characterising the operation mode of a flat plate solar collector can be classified into two categories as follows:

1.7.1 External Parameters

The main external parameters that can directly affect the thermal performance of a flat plate solar collector are:

Sun parameters:

- Intensity of irradiation.
- Duration of insolation.
- Position of sun.

Environment parameters:

- Ambient temperature.
- Wind speed.

- Humidity.
- Weather conditions.

Geographical parameters:

- Altitude of the location.
- Latitude of the location.
- Longitude of the location.

1.7.2 Internal Parameters

Geometric parameters:

- Thickness, length and width of components (cover, absorber, insulator...etc).
- Diameters of tubes.
- Distance between cover and absorber plate.
- Distance between tubes.
- Shape of absorber plat.
- Piping system fixation model and form.

Material parameters:

- Thermal conductivity.
- Density.
- Transmittance.
- Absorptance.
- Emittance.

Operational parameters:

- Mass flow rate.
- Inlet fluid temperature.
- Working fluid features.

1.8 Orientation and Inclination of Flat Plate Solar Collector

The solar collector absorbs maximum solar energy when the radiation hits its surface perpendicularly. Therefore, making sure that the solar collector faces the right orientation and has the appropriate inclination will produce the maximum power as it is exposed to the highest radiation intensity for the largest period of time.

A flat plate solar collector, which is a non-tracking system, should be oriented geographically to maximise the amount of daily and seasonal solar power that they receive. In the northern hemisphere, the optimum orientation for a flat plate solar collector is that the face of the absorber should be directed towards the South Pole. By the same reason, if the solar collector is located in the southern hemisphere, the face of the absorber should instead be directed towards the North Pole.

The inclination of a solar collector is much as important as collector orientation. There is a general rule for optimal annual energy production is to fix the solar collector inclination equal to the geographical latitude. The closer a solar collector is located to the equator the more the solar collector is inclined to approach the horizontal line. The closer the solar collector is to the poles, the more its inclination towards the equator.

1.9 Heat Transfer Modes in Solar Collector

Heat transfer appears when there is a difference in temperature between two objects. The heat energy passes from the hot object to the cold object until the system attains a thermal equilibrium. The thermal losses in flat plate solar collector can take place by the three main modes of heat transfer process; namely, conduction, convection and radiation.

1.9.1 Heat Conduction

Heat transfer by conduction occurs when heat energy is exchanged between atoms of a substance without the transfer of these atoms. In flat plate solar collector, the heat loss by conduction takes place at the level of the insulation of the rear side and also the top cover, as it may exist between the absorber plate and the top cove when the distance between them is very close. Fourier 's law is used to determine the heat conduction rate. The equation (1.1) presents this relationship as follows:

$$Q_{cond} = -KA \left(\frac{dT}{dx} \right) \quad (1.1)$$

Where, K is the thermal conductivity, A is the surface area, $\frac{dT}{dx}$ is the temperature gradient

1.9.2 Heat Convection

Heat convection refers to the transfer of heat from one place to another due to the movement of fluids (liquids or gases). The heat transfer rate by convection is defined by using Newton's law which is expressed in equation (1.2) as follows:

$$Q_{conv} = hA(T_w - T_f) \quad (1.2)$$

Here, h the heat transfer coefficient by convection.

Heat convection transfer occurs through two primary mechanisms; natural convection and forced convection.

Natural Convection:

Natural convection is the process of heat transfer where fluid motion is caused by density differences within a fluid due to temperature gradients. As a fluid near a heated surface warms up, it becomes less dense and rises, displacing cooler fluid which then moves towards the heat source to be heated and rise again. This creates a continuous circulation pattern, transferring heat away from the surface.

Characteristics:

No external influence (such as a pump or fan) is required to induce fluid motion.

Driven by buoyancy forces due to temperature differences within the fluid.

Forced Convection:

Forced convection is the process of heat transfer where fluid motion is induced by an external force such as a pump, fan, compressor, etc. The external force creates fluid movement, which in turn enhances the heat transfer rate between the fluid and the heated or cooled surface.

Characteristics:

Fluid motion is caused by an external device or mechanism (e.g., a fan blowing air over a radiator).

Heat transfer rates are generally higher compared to natural convection, especially at higher flow velocities.

In both natural and forced convection, the rate of heat transfer is influenced by various factors including the temperature difference between the fluid and the surface, the properties of the fluid (such as viscosity and thermal conductivity), and the flow characteristics (velocity and

turbulence). Understanding these mechanisms is crucial in fields such as thermal engineering, where optimizing heat transfer processes is essential for efficiency and performance.

1.9.3 Heat Radiation

The heat transfer by radiation can be described by the process of emissions from the material in a non-opaque medium such as solid, liquid or gas, and also vacuum space, in the form of electromagnetic waves. This mode of heat transfer can have a significant influence on the thermal performance of the flat plate solar collector if the absorber plate does not have a low emissivity (selective coating). The heat flux from the radiation can be determined from the Stefan-Boltzmann law. The mathematical representation of this law is simplified, when surface A is very less compared to B, as shown in the following equation (1.3):

$$Q_{rad} = \sigma \varepsilon A (T_A^4 - T_B^4) \quad (1.3)$$

Where, σ is the Stefan-Boltzmann constant, ε is the body emissivity coefficient and T_A and T_B are temperature of surfaces A and B (where $A \ll B$), respectively.

1.10 Dimensionless Numbers Used in Heat Transfer

Dimensionless numbers in heat transfer are used to characterise and analyse the behaviour of heat transfer processes without being dependent on specific units of measurement. They provide valuable insights into the relative importance of various physical phenomena involved in heat transfer. Some important dimensionless numbers in heat transfer include:

1.10.1 Reynolds Number (Re):

The Reynolds number is a dimensionless quantity used to predict flow patterns in fluids. It is defined as the ratio of inertial forces to viscous forces within a fluid flow. Mathematically, it's expressed as:

$$Re = \frac{\rho v L}{\mu} \quad (1.4)$$

Where:

ρ is the density of the fluid, v is the velocity of the fluid, L is the characteristic length and μ is the dynamic viscosity of the fluid.

a) Natural Convection:

In natural convection, fluid motion arises due to buoyancy forces resulting from temperature differences within the fluid. The Reynolds number in natural convection is defined based on the characteristic length scale of the flow (such as the height or diameter of the object) and the velocity induced by buoyancy forces.

b) Forced Convection:

In forced convection, fluid motion is driven by an external means such as a pump or a fan, creating a flow with a characteristic velocity that is much higher and controlled than in natural convection. The Reynolds number in forced convection is defined based on the flow velocity induced by the external force and the characteristic length of the flow.

In both cases, the Reynolds number helps characterise the type of flow regime:

Low Reynolds Number (< 2000): Laminar flow dominates, characterised by smooth and orderly fluid motion.

Intermediate Reynolds Number (2000 - 4000): Transitional flow regime, where laminar and turbulent flow characteristics may coexist.

High Reynolds Number (> 4000): Turbulent flow regime, characterised by chaotic and irregular fluid motion.

Therefore, whether in natural convection or forced convection, the Reynolds number is a fundamental parameter used to determine the flow regime and predict heat transfer characteristics, although the interpretation and relevance of the Reynolds number may vary depending on the dominant mode of convection (natural or forced).

1.10.2 Prandtl Number (Pr):

The Prandtl number is a dimensionless number used to characterise the relative importance of momentum diffusivity to thermal diffusivity in a fluid. It's defined as the ratio of momentum diffusivity (kinematic viscosity) to thermal diffusivity. Mathematically, it's expressed as:

$$Pr = \frac{C_p \mu}{K} \quad (1.5)$$

Where:

C_p is the specific heat capacity of the fluid at constant pressure and K is the thermal conductivity of the fluid.

The Prandtl number value varies depending on the type of fluid and the conditions under which heat transfer occurs.

a) Natural Convection:

In natural convection, fluid motion is driven by buoyancy forces due to density variations caused by temperature gradients in the fluid. The Prandtl number helps to determine how quickly heat is transferred relative to momentum transfer within the fluid. It influences the boundary layer thickness and the rate of convective heat transfer from a heated surface to the surrounding fluid.

b) Forced Convection:

In forced convection, fluid motion is driven by external means such as pumps or fans. The Prandtl number remains crucial here as well, influencing the heat transfer characteristics of the fluid. For liquids and gases commonly encountered in engineering applications, the Prandtl number typically ranges from 0.7 to 1000, depending on the fluid.

In summary, whether in natural convection or forced convection, the Prandtl number plays a fundamental role in characterising the heat transfer properties of the fluid involved.

1.10.3 Nusselt Number (Nu)

The Nusselt number is a dimensionless number used to characterise the convective heat transfer coefficient. It's defined as the ratio of convective heat transfer to conductive heat transfer across a boundary layer. The value of Nu depends on the flow regime (e.g., laminar, turbulent) and geometry of the system. Mathematically, it's expressed as:

$$Nu = \frac{hL}{K} \quad (1.6)$$

Where:

h is the convective heat transfer coefficient.

a) Natural Convection:

In natural convection, fluid motion is driven by buoyancy forces due to density differences caused by temperature variations within the fluid. The Nusselt number in natural convection is often determined using empirical correlations that relate Nusselt number (Nu) to the Rayleigh number (Ra) and Prandtl number (Pr).

b) Forced Convection:

In forced convection, the fluid motion is caused by an external source such as a pump or fan. The Nusselt number (Nu) in forced convection is typically determined using empirical correlations that relate Nusselt number (Nu) to the Reynolds number (Re) and Prandtl number (Pr) of the flow. These correlations are specific to different geometries (like cylinders and flat plates) and flow conditions.

In both cases, the Nusselt number provides a dimensionless measure of the convective heat transfer rate from a surface. It is used extensively in heat transfer analysis and engineering to predict heat transfer coefficients and thereby the rate of heat transfer between a solid surface and a fluid.

1.10.4 Grashof Number (Gr):

The Grashof number is a dimensionless number used to predict the onset of natural convection in fluids. It's defined as the ratio of buoyancy forces to viscous forces within the fluid. Mathematically, it's expressed as:

$$Gr = \frac{g\beta'(T_s - T_\infty)L^3}{\nu^2} \quad (1.7)$$

Where:

g is the acceleration due to gravity, β' is the coefficient of volume expansion, T_s is the surface temperature, T_∞ is the bulk temperature and ν is the kinematic viscosity of the fluid.

a) Natural Convection:

In natural convection, fluid motion arises due to density differences caused by temperature gradients (buoyancy forces). The Grashof number quantifies the relative importance of these buoyancy forces compared to viscous forces. It helps predict whether natural convection currents will dominate the heat transfer process.

b) Forced Convection:

In forced convection, fluid motion is induced by an external means such as a pump or a fan, rather than by buoyancy forces. The driving force here is primarily the pressure gradient created by the external means. Therefore, the Grashof number is not typically used in forced convection scenarios because buoyancy forces are negligible compared to the forces driving the flow.

In summary, the Grashof number is calculated and used in the context of natural convection to assess the relative significance of buoyancy forces compared to viscous forces. In forced convection, where buoyancy forces are minimal compared to the externally induced flow, other dimensionless numbers such as Reynolds number (Re) and Nusselt number (Nu) are more commonly used to characterise the flow and heat transfer processes.

1.10.5 Rayleigh Number (Ra):

The Rayleigh number (Ra) is another dimensionless parameter that is typically used in the context of natural convection, similar to the Grashof number (Gr). The Rayleigh number is defined as the product of the Grashof number (Gr), which describes the relationship between buoyancy and viscosity within a fluid, and the Prandtl number (Pr), which describes the relationship between momentum diffusivity and thermal diffusivity. The Rayleigh number is a critical parameter in determining whether convection currents will form in a fluid medium. When the Rayleigh number exceeds a critical value specific to the system, convection becomes the dominant mode of heat transfer. Mathematically, it's expressed as:

$$Ra = \frac{g\beta'(T_s - T_\infty)L^3}{\nu\alpha} \quad (1.8)$$

Where:

α is the thermal diffusivity of the fluid.

a) *Natural Convection:*

In natural convection, similar to the Grashof number, the Rayleigh number characterises the relative importance of buoyancy forces compared to viscous forces in a fluid flow. It is particularly useful in predicting the onset of natural convection and the behaviour of fluid flows driven by temperature differences (buoyancy effects).

b) *Forced Convection:*

In forced convection, where fluid motion is driven externally by a pump, fan, or other means, buoyancy forces are typically negligible compared to the forces driving the flow. Therefore, the Rayleigh number is not commonly used in forced convection scenarios because it pertains specifically to the buoyancy driven flows that characterise natural convection.

In summary, the Rayleigh number is calculated and used primarily in the context of natural convection to assess the relative magnitude of buoyancy forces compared to viscous forces within the fluid. It helps determine whether natural convection currents will occur and how they

will affect heat transfer processes. In forced convection, other dimensionless numbers such as Reynolds number (Re) and Nusselt number (Nu) are typically used to characterise the flow and heat transfer characteristics due to the dominance of externally driven forces over buoyancy effects.

These dimensionless numbers play a crucial role in heat transfer analysis, aiding engineers and researchers in designing and optimising heat transfer systems and processes.

1.11 Fins Theory

The theory of fins in heat transfer is a fundamental aspect of thermodynamics and heat transfer engineering. Fins are extended surfaces attached to a body that enhance the rate of heat transfer from the surface of the body to the surrounding fluid (usually air or a liquid). They are commonly used in various engineering applications such as heat exchangers, cooling electronic devices, radiators, and thermal engines [6].

The primary purpose of fins is to increase the surface area available for heat transfer, thereby improving the overall efficiency of heat exchange. By increasing the surface area, fins allow for greater contact between the surface and the surrounding fluid, facilitating faster heat dissipation. There are many engineering applications of fin such as cooling of engine heads, radiators, condenser coils of refrigerators, electric generators, electric power transformers, etc. Various types of fins are used for different applications. Some configurations of fins are given in Figure 1.12.

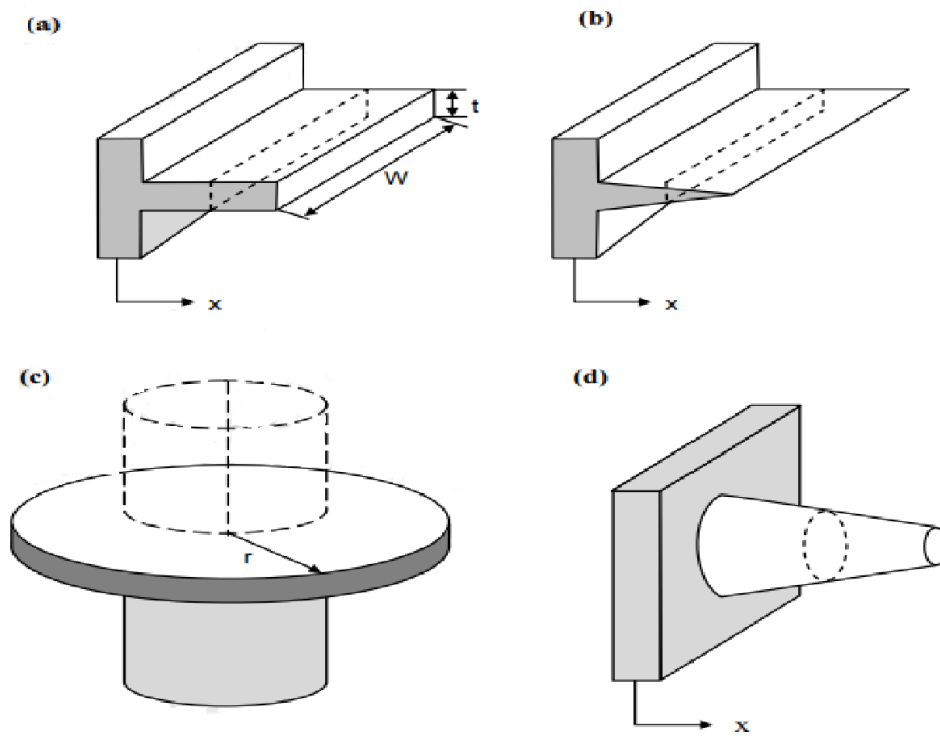


Figure 1.12 Configurations (a) Straight Fin of Uniform Cross Section, (b) Straight Fin of Non-Uniform Cross Section, (c) Annular Fin and (d) Pin Fin.

1.11.1 Heat Transfer from Finned Surfaces

A model configuration is shown in Figure 1.13, consider a volume element of a fin at location x having a length of Δx , cross sectional area of A_c , and a perimeter of p .

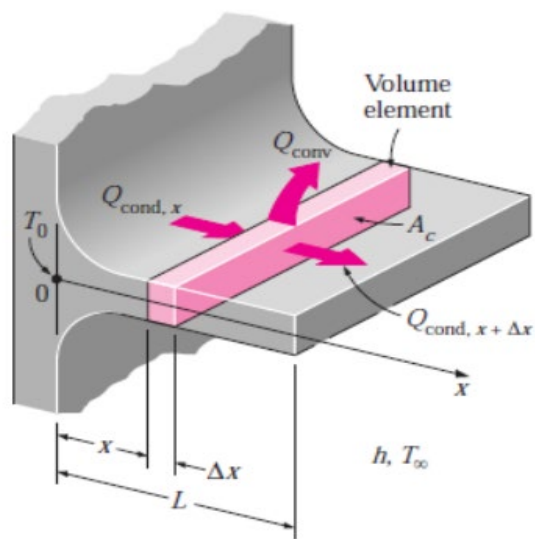


Figure 1.13 Volume element of a fin.

In the analysis of fins, we consider

- Steady operation with no heat generation in the fin
- The thermal conductivity k of the material to remain constant.
- The convection heat transfer coefficient h to be constant and uniform over the entire surface of the fin for convenience in the analysis.

Under steady conditions, the energy balance on this volume element can be expressed as:

$$Q_{cond, x} = Q_{cond, x+\Delta x} + Q_{conv} \quad (1.9)$$

Here,

$$Q_{conv} = h(p\Delta x)(T - T_{\infty}) \quad (1.10)$$

Dividing by Δx , we obtain:

$$\frac{Q_{cond, x+\Delta x} - Q_{cond, x}}{\Delta x} + hp(T - T_{\infty}) = 0 \quad (1.11)$$

As $\Delta x \rightarrow 0$,

$$\frac{dQ_{cond}}{dx} + hp(T - T_{\infty}) = 0 \quad (1.12)$$

Or,

$$\frac{d}{dx} \left(kA_c \frac{dT}{dx} \right) + hp(T - T_{\infty}) = 0 \quad (1.13)$$

The cross-sectional area A_c and the perimeter p of a fin vary with x , which makes this differential equation difficult to solve. In the special case of constant cross section and constant thermal conductivity, the differential equation (1.13) becomes:

$$\frac{d^2T}{dx^2} - \frac{hp}{kA_c}(T - T_{\infty}) = 0 \quad (1.14)$$

Or,

$$\frac{d^2\theta}{dx^2} - m^2\theta = 0 \quad (1.15)$$

Where,

$$m^2 = \frac{hp}{kA_c} \quad \text{and} \quad \theta = T - T_{\infty} \quad (1.16)$$

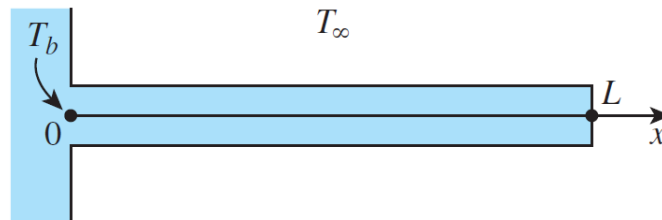
θ is the temperature excess. At the fin base we have $\theta_b = T_b - T_{\infty}$.

Equation (1.15) is a linear, homogeneous, second-order differential equation with constant coefficients. The solution functions of the differential equation above are the exponential functions e^{ax} or e^{-ax} or constant multiples of them. Therefore, the general solution of the differential equation is:

$$\theta(x) = C_1 e^{mx} + C_2 e^{-mx} \quad (1.17)$$

Where C_1 and C_2 are arbitrary constants, whose values are to be determined from the boundary conditions at the base and at the tip of the fin.

At the fin tip, we have several possibilities, including specified temperature, negligible heat loss (idealised as an insulated tip), convection (or combined convection and radiation) as shown in Figure 1.14 (In next sub-sections, we consider each case separately).



1. Infinitely long fin
2. Negligible heat loss (adiabatic tip)
3. Specified temperature
4. Convection

Figure 1.14 Boundary conditions at the fin base and the fin tip.

a) Infinitely Long Fin ($T_{fin-tip} = T_\infty$)

For a sufficiently long fin of uniform cross section (Ac is constant), the temperature of the fin at the fin tip will approach the environment temperature T_∞ and thus θ will approach zero. That is:

$$\text{Boundary condition at fin tip: } \theta(L) = T(L) - T_\infty = 0 \quad \text{as } L \rightarrow \infty$$

The general solution in this case will consist of a constant multiple of e^{-mx} , which its value can be determined from the requirement that at the fin base; where $x=0$, the value of θ is θ_b . The variation of temperature along the fin in this case can be expressed as:

$$\frac{T(x) - T_\infty}{T_b - T_\infty} = e^{-x\sqrt{\frac{hp}{kAc}}} \quad (1.18)$$

b) Negligible Heat Loss from the Fin Tip (Adiabatic fin tip, $Q_{fin\ tip} = 0$)

A more realistic situation is for heat transfer from the fin tip to be negligible since the heat transfer from the fin is proportional to its surface area, and the surface area of the fin tip is not likely to be so long. Then the fin tip can be assumed to be adiabatic, and the condition at the fin tip can be expressed as:

$$\text{Boundary condition at fin tip: } \left. \frac{d\theta}{dx} \right|_{x=L} = 0$$

The general solution requires that $\theta(0) = \theta_b = C_1 + C_2$ and $mC_1 e^{mL} - mC_2 e^{-mL} = 0$, respectively. The variation of temperature along the fin in this case can be expressed as:

$$\frac{T(x) - T_\infty}{T_b - T_\infty} = \frac{\cosh m(L - x)}{\cosh mL} \quad (1.19)$$

c) Specified Temperature ($T_{fin, tip} = T_L$)

In this case the temperature at the end of the fin (the fin tip) is fixed at a specified temperature T_L . This case could be considered as a generalization of the case of Infinitely Long Fin where the fin tip temperature was fixed at T_∞ . The condition at the fin tip for this case is

$$\text{Boundary condition at fin tip: } \theta(L) = \theta_L = T_L - T_\infty$$

The fin base boundary condition remains the same. The variation of temperature along the fin in this case can be expressed as:

$$\frac{T(x) - T_\infty}{T_b - T_\infty} = \frac{\left(\frac{T_L - T_\infty}{T_b - T_\infty}\right) \sinh mx + \sinh m(L - x)}{\sinh mL} \quad (1.20)$$

d) Convection from Fin Tip

Consider the case of convection only at the tip. The condition at the fin tip can be obtained from an energy balance at the fin tip ($Q_{cond} = Q_{conv}$), That is:

$$\text{Boundary condition at fin tip: } -kA_c \left. \frac{dT}{dx} \right|_{x=L} = hA_c(T(L) - T_\infty)$$

The boundary condition at the fin base is the same as the previous cases. The variation of temperature along the fin in this case can be expressed as:

$$\frac{T(x) - T_\infty}{T_b - T_\infty} = \frac{\cosh m(L - x) + \left(\frac{h}{mk}\right) \sinh m(L - x)}{\cosh mL + \left(\frac{h}{mk}\right) \sinh mL} \quad (1.21)$$

A practical way of accounting for the heat loss from the fin tip is to replace the fin length L in the relation for the insulated tip case by a corrected length defined as (see Figure 1.15).

$$\text{Corrected fin length: } L_c = L + \frac{A_c}{p}$$

Using the proper relations for A_c and p , the corrected lengths for rectangular and cylindrical fins are easily determined to be:

$$L_{c\text{-rectangular}} = L + \frac{t}{2} \quad \text{and} \quad L_{c\text{-cylindrical}} = L + \frac{D}{4}$$

Where t is the thickness of the rectangular fins and D is the diameter of the cylindrical fins.

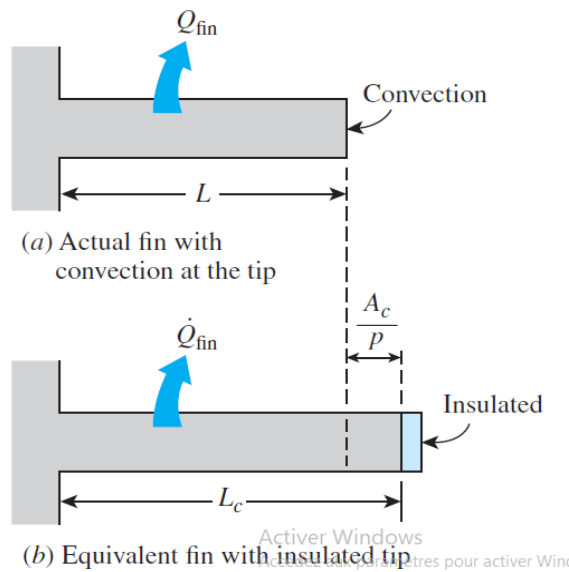


Figure 1.15 Actual fin convection at the tip (a) and equivalent fin with insulated tip (b).

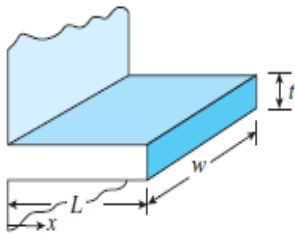
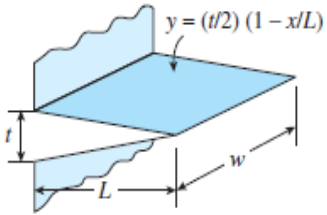
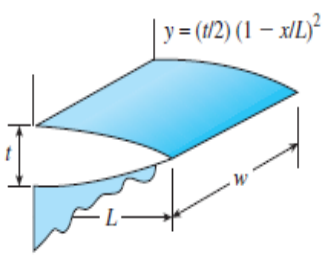
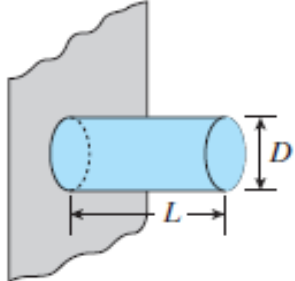
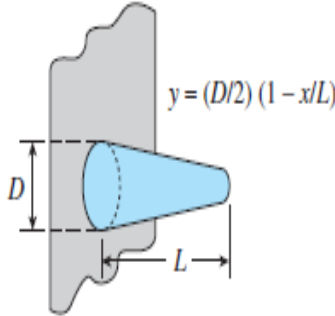
1.11.2 Fin Efficiency

In reality, the temperature of the fin will drop along the fin, and thus the heat transfer from the fin will be less because of the decreasing temperature difference $T_x - T_\infty$ toward the fin tip. To account for the effect of this decrease in temperature on heat transfer, we define a fin efficiency as:

$$\eta_{fin} = \frac{Q_{fin}}{Q_{fin_max}} = \frac{\text{Actual heat transfer rate from the fin}}{\text{Ideal heat transfer rate from the fin if the entire fin were at base temperature}} \quad (1.22)$$

Table (1.8) presents efficiency and parameters of common fin configurations.

Table 1.8 Efficiency and parameters of common fin configurations.

Fin efficiency	Parameters	Fin configurations
Straight rectangular fins $\eta_{fin} = \frac{\tan mL_c}{mL_c}$	$m = \sqrt{2h/kt}$ $L_c = L + t/2$ $A_{fin} = 2wL_c$	
Straight triangular fins $\eta_{fin} = \frac{1}{mL} \frac{I_1(2mL)}{I_1(2mL)}$	$m = \sqrt{2h/kt}$ $A_{fin} = 2w\sqrt{L^2 + (t/2)^2}$	
Circular fins of rectangular profile $\eta_{fin} = \frac{2}{1 + \sqrt{(2mL)^2 + 1}}$	$m = \sqrt{2h/kt}$ $A_{fin} = wL[C_1 + (L/t)\ln(t/L + C_1)]$ $C_1 = \sqrt{1 + (t/L)^2}$	
Pin fins of rectangular profile $\eta_{fin} = \frac{\tanh mL_c}{mL_c}$	$m = \sqrt{4h/kD}$ $L_c = L + D/4$ $A_{fin} = \pi DL_c$	
Pin fins of parabolic profile $\eta_{fin} = \frac{3}{2mL} \frac{I_2(4mL/3)}{I_0(4mL/3)}$	$m = \sqrt{4h/kD}$ $A_{fin} = \frac{\pi D^4}{96L^2} \{ [16(L/D)^2 + 1]^{3/2} - 1 \}$	

1.12 Solar Radiation

1.12.1 Source of Solar Energy

The source of solar energy is the Sun. The Sun is a sphere of intensely hot gaseous matter with a diameter of 1.39×10^9 m and is, on the average, 1.5×10^{11} m away from the Earth [7]. Due to sunlight travels with the speed of light in vacuum (about 300,000 km/s), after leaving the Sun, solar energy reaches the Earth in 8 min and 20 s.

The Sun has an effective blackbody temperature of 5760 K. The temperature in the central region is much higher, approximately $(8 \text{ to } 40) \times 10^6$ K and the density is estimated to be about 100 times that of water. In effect, the Sun is a continuous fusion reactor in which hydrogen is turned into helium. The Sun's total energy output is 3.8×10^{20} MW, which is equal to 63 MW/m² of the Sun's surface. This energy radiates outward in all directions. The Earth obtains only a small fraction of the total radiation emitted, equal to 1.7×10^{14} kW; however, even with this small fraction, it is estimated that 84 min of solar radiation falling on Earth is equal to the world energy demand for one year.

Solar energy from the Sun can be classified as a heat (electromagnetic waves) and light (photons), respectively. Basically, the Sun is responsible to produce directly most of the renewable energy sources. It is also responsible for providing indirect sustenance for non-renewable sources such as fossil fuels.

Knowledge of the sun's path through the sky is necessary to calculate the solar radiation falling on a surface, the solar heat gain, the proper orientation of solar collectors, the placement of collectors to avoid shading, and many more factors.

1.12.2 Solar Constant

Figure 1.16 shows schematically the geometry of the Sun/Earth relationships. The eccentricity of the earth's orbit is such that the distance between the Sun and the Earth varies by 1.7%. At a distance of one astronomical unit, 1.496×10^{11} m, the mean Earth-Sun distance, the Sun subtends an angle of 32'. The radiation emitted by the Sun and its spatial relationship to the Earth result in a nearly fixed intensity of solar radiation outside of the Earth's atmosphere.

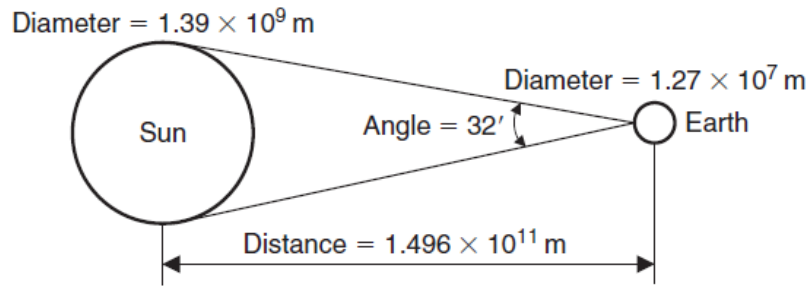


Figure 1.16 Sun-Earth relationships [8].

The solar constant is the energy from the sun per unit time received on a unit area of surface perpendicular to the direction of propagation of the radiation at mean Earth-Sun distance outside the atmosphere. The solar intensity on a plane perpendicular to the direction of solar radiation is given by:

$$I_{ext} = I_{sc} \left[1 + 0.033 \cos\left(\frac{360 \times Nd}{365}\right) \right] \quad (1.23)$$

Where I_{sc} is the solar constant defined as the radiant solar flux received in the extraterrestrial region on a plane of unit area kept perpendicular to the solar radiation at the mean Sun–Earth distance. The value of solar constant is about 1367 W/m^2 . Nd is day number during year (see Figure 1.17).

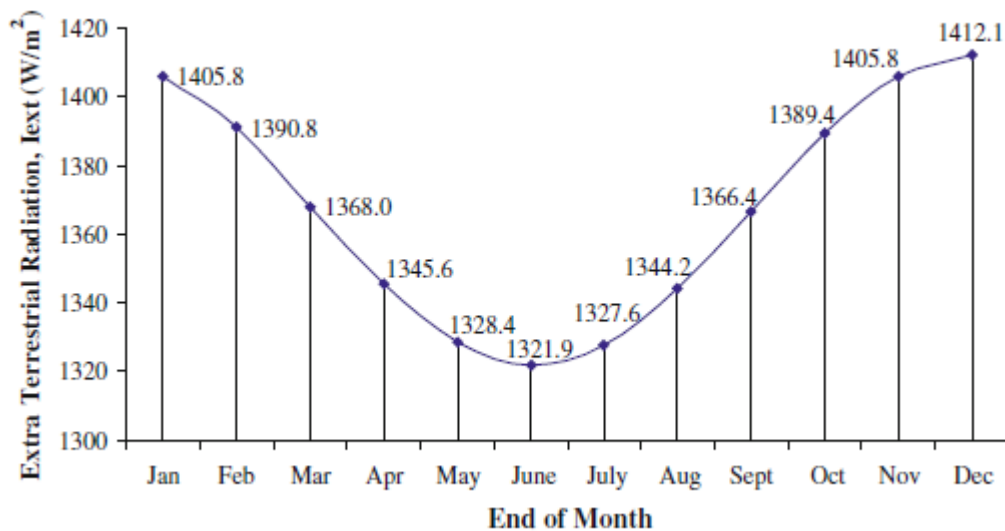


Figure 1.17 Variation of I_{ext} with month of the year.

1.12.3 1.2 Sun–Earth Angles

A better understanding of Sun–Earth angles is crucial for estimating solar intensity throughout year for any surface at any location with a desired inclination and orientation. These Sun–Earth angles are defined below:

Latitude (ϕ): The latitude of an observer (location) on the Earth’s surface is the angle made between the radial line joining the observer (location) with the centre of the Earth, and its projection on the equatorial plane as shown in Figure 1.18. For an observer in the northern hemisphere, latitude is positive, whereas for the southern hemisphere it is negative.

Declination (δ): Declination is defined as the angle between the line joining the centres of the Sun and the Earth, which also determines the direction of the direct rays coming from the Sun and their projection on the equatorial plane as shown in Figure 1.18. Declination is due to the rotation of the Earth around an axis, which makes an angle of either 66:5' with the plane or 23:5' with normal rotation around the Sun. The declination is calculated by the following relation:

$$\delta = 23,45 \sin \left(360 \times \frac{(284 + Nd)}{365} \right) \quad (1.24)$$

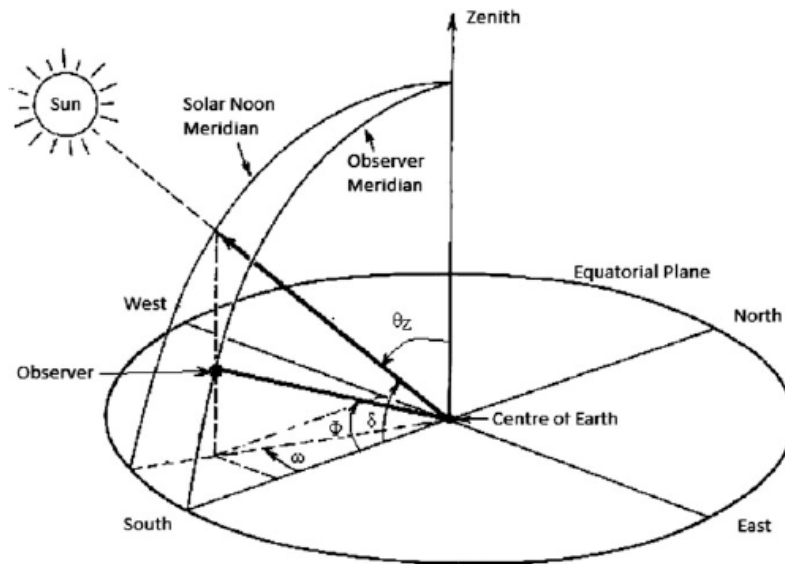


Figure 1.18 View of different Sun–Earth angles [9].

The declination angle variation with the number of days is shown in Figure 1.19. The maximum value of δ is 23.45° (June 21), and minimum value of δ is -23.45° (December 21).

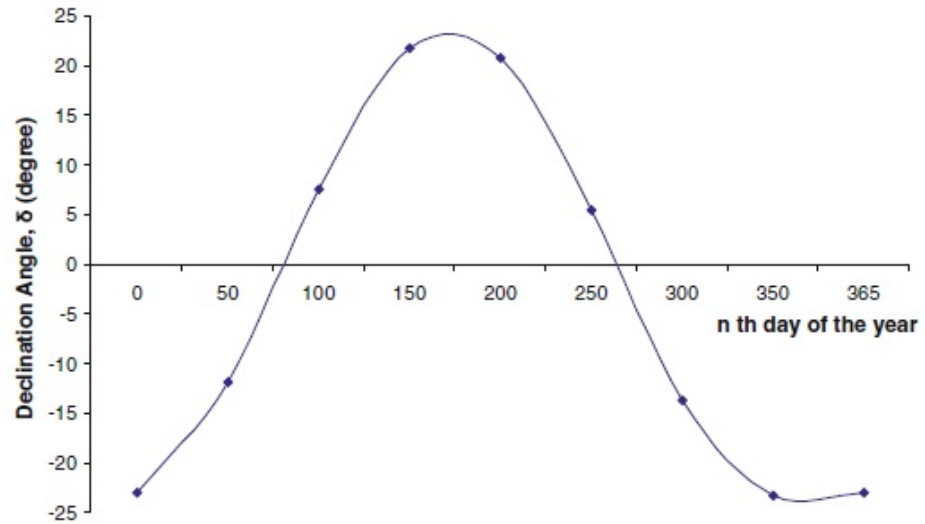


Figure 1.19 Variation of declination angle with n^{th} day of the year.

Table 1.9 shows the recommended average days for months and values of n by months.[6]

Table 1.9 Recommended average days for months and values of n by months [10].

Month	Number for i^{th} Day of Month	For Average Day of Month		
		Date	n	δ
January	i	17	17	-20.9
February	$31 + i$	16	47	-13.0
March	$59 + i$	16	75	-2.4
April	$90 + i$	15	105	9.4
May	$120 + i$	15	135	18.8
June	$151 + i$	11	162	23.1
July	$181 + i$	17	198	21.2
August	$212 + i$	16	228	13.5
September	$243 + i$	15	258	2.2
October	$273 + i$	15	288	-9.6
November	$304 + i$	14	318	-18.9
December	$334 + i$	10	344	-23.0

Hour angle (ω): This is the angle between projections of the Sun's rays (solar meridian) and the line running south–north through centre. The south–north line is also referred to as the “line due south”. The hour angle is defined as the angular displacement of the Sun from the local meridian because of the Earth's rotation around its own axis. The hour angle corresponding to 1 h is 15° . Expression for the hour angle is given by:

$$\omega = (ST - 12) \times 15^\circ \quad (1.25)$$

Where ST is the local solar time.

The total hour angle from sunrise to sunset is 2ω . The $\pm\omega$ correspond to an hour angle with reference to sunrise and sunset, respectively.

Zenith (θ_z): The angle between Sun's rays; the line perpendicular to a horizontal plane is known as the “zenith angle”, see Figure 1.18.

Altitude (α): The angle made between a horizontal plane and the Sun's rays is known as the “altitude angle.” Referring to Figure 1.18.

$$\alpha = 90 - \theta_z \quad (1.26)$$

Slope (β): This is the angle between the plane surface under consideration and the horizontal surface (tangential plane at observer). Its numerical value is considered positive for slope toward the south and negative for slope toward the north.

Surface azimuth angle (γ): The angle made between the line due south and the projection of normal to the inclined surface on the horizontal plane (tangential plane at observer on the surface of the Earth). In the northern hemisphere, conventionally γ is negative (positive for the southern hemisphere) for projections in east of south and positive (negative for southern hemisphere) for projections falling west of south.

Solar azimuth angle (γ_s): The angle made between the projection of beam radiation on the horizontal plane and the line due south. The sign convention of the solar azimuth angle is the same as the sign convention of the surface azimuth angle.

Sunshine hour (N): The total duration in hours of the Sun's movement from sunrise to sunset. It is defined in terms of the hour angle as:

$$N = \frac{2\omega}{15} \quad (1.27)$$

Here 1h = 15° .

Angle of incidence (θ_i): The angle made between normal to the inclined surface and the solar beam radiation falling on the inclined. In general, the angle of incidence can be expressed as:

$$\begin{aligned} \cos \theta_i = & (\cos \varphi \cos \beta + \sin \varphi \sin \beta \cos \gamma) \cos \delta \cos \omega + \cos \delta \sin \omega \sin \beta \sin \gamma \\ & + \sin \delta (\sin \varphi \cos \beta - \cos \varphi \sin \beta \cos \gamma) \end{aligned} \quad (1.28)$$

For a horizontal plane facing due south, $\gamma = 0$; $\beta = 0$; $\theta_i = \theta_z$ (zenith angle).

$$\cos \theta_z = \cos \varphi \cos \delta \cos \omega + \sin \delta \sin \varphi \quad (1.29)$$

1.12.4 Solar Radiation Calculation

Solar radiation, while passing from the extraterrestrial region to the terrestrial region through the Earth's atmosphere, suffers scattering losses and atmospheric absorption. After absorption by the atmosphere, the rate of normal solar flux (normal solar radiation/irradiance) reaching the Earth's surface is determined by:

$$I_N = I_{\text{ext}} \times \exp [-(m \cdot \varepsilon \cdot T_R + \alpha)] \quad (1.30)$$

where m is the air mass. T_R is the turbidity factor, which is defined as the cloudiness/haziness factor for the lumped atmosphere.

Beam radiation (I_b): This is a normal component of solar radiation (normal irradiance) in W/m^2 propagating along the line joining the receiving surface and the Sun on a horizontal/inclined surface. It has a direction and also termed "direct radiation".

Diffuse radiation (I_d): This is the solar radiation (in W/m^2) scattered by aerosols and other particulates; diffuse radiation does not have any definite direction.

The total radiation (I): This is the sum of the beam (direct) and diffuse radiation in W/m^2 . It is also known as "global radiation".

1.13 Application

Renewable energy resources should be considered in heating systems to minimise the use of fossil fuels. Furthermore, solar energy is one of the most promising and available energy sources all over the world that can be integrated into numerous applications in the form of thermal energy and electrical energy. The solar thermal technology can be applied in many sectors such as food industries, chemical and pharmaceutical industries, textile industries, paper industries...etc.

Due to its simple working principle, easy installation and low cost and maintenance, the flat plate solar collector is the most favourable thermal collector that can be employed for heating applications. However, this type of collector suffers from low thermal performance, therefore it requires further improvement to cover a wide range of applications [11].

Table 1.10 Typical temperature ranges of industrial processes.

Industry	processes	temperature range [°C]
Food and beverages	Cooking	120–190
	Drying	120–180
	Washing	60–80
	Pasteurizing	80–130
	Boiling	95–105
	Sterilizing	100–150
	Drying 60–125	Drying 60–125
Chemical	Dissolving, distillation	85–170
	Thickening, leaching	85–170
	Preheating water	60–90
	Processing heat	120–18
Textile	Washing	40–80
	Bleaching, dyeing	60–90
	Drying, degreasing	60–135
	Pressing	80–100
Pulp and paper	Kraft pulping	185
	Kraft bleaching	140
	Drying	180
Timber	Thermo-diffusion beams	80–100
	Preheating water	60–90

	Drying	60–100
Air conditioning	Absorption cooling	60–180
Stone, glass, and clay	Brick curing	75–180
	Gypsum curing	300
	Gypsum calcining	160
	Glass fiber drying	100–180

1.14 Conclusion

The flat plate thermal solar collector is a special type of non-concentrating collector. This heating system typically operates and attains the maximum thermal efficiency within the temperature range from 50 °C up to 100 °C. Depending on the fluid circulation mode, two main types are distinguished; namely, the passive circulation and the active circulation. In order to ameliorate the thermal performance of such collector, the parameters characterising the operation mode should be optimised. Thus, in the next chapter, the influence of some external and internal parameters on the thermal performance of a solar collector is presented.

Chapter 2: Literature Review

The preceding chapter identifies the internal and external parameters that have important impact on the thermal performance of a flat plate solar collector. In this chapter, a detailed literature review is concentrated on performance enhancement techniques such as geometrical and material modifications, heat transfer fluids, selective coating and spacing insulation, in order to identify the research gap on improving the thermal performance of a flat plate solar water collector.

2.1 History and Utilisation of Solar Heating Systems

In the past, to heat water for daily usage, people had been exploiting different fossil fuels, for instance, coal, wood ...etc. The advancement of technology promotes people to exploit natural gas for the same goal [12]. Despite applying fossil fuel and natural gas as heat sources have proven to be efficient, but they are unfriendly and non-renewable sources. In addition, the coal and natural gas have to go through various refinements to make them useable, which makes them very expensive. Instead, the demand for other available energy sources, which are relatively renewable energy, friendly, less expensive and safer to use, has increased.

One of the most important alternative sources is solar energy, that can be used to heat water by solar water heating systems [13]. Indeed, humans have always exploited solar irradiation to gather their thermal energy needs. Furthermore, solar energy has become gradually popular in recent years. The technology of thermal solar systems was principally accepted by the market and small units about 2m² were installed to overcome the domestic needs of a household.

The primely design of thermal solar collector consisted a black painted metal tank full of water [14]. The tank was placed outside and exposed directly to the sun to absorb the solar energy. After a certain period of time, the hot water inside the tank can be used for domestic applications. The disadvantage of this solar heating system was that even on clear hot days it typically took long period for the water to be heated, sometimes a whole day. Besides, there were no thermal insulations in the system to preserve thermal energy that gained by water for a long period, in which the gained heat dissipated rapidly. In 1891, Clarence Kemp adds to this old design a metal plate sheet under the tank, as illustrated in Figure 2.1, in order to enhance the thermal efficiency of the solar tank system [15]. Over the past decades, tremendous progress has been made in the development of this kind of solar heaters. Thus, in the ensuing paragraphs we will mention the most essential performance enhancement techniques.



Figure 2.1 Prototype of the primely solar water collector [16].

2.2 Performance Enhancement Techniques.

The performance of a flat plate solar collector is essentially characterised by its thermal efficiency. Indeed, this efficiency is a function of the useful energy rate that we are constantly seeking to improve:

- By increasing the amount of absorbed solar energy received by the absorber sheet.
- By ameliorating the heat transfer fluid features.
- By reducing heat loss from the front side of the collector (between the absorber and the environment) and from the back side of the collector (non-receiving areas).

The performance enhancement methods aim to ameliorate the overall thermal performance of flat plate solar collectors.

In this respect, through the literature, many methods and techniques have been investigated by researchers which make it possible to develop high-efficient thermal solar collectors [17]. These methods include geometrical and material modifications, using heat transfer fluids, applying selective coatings and the improvement of spacing and insulation [18]. Figure 2.2 shows various performance enhancement techniques, and the advancement of these techniques is discussed in subsequent sub-sections. High thermal efficiency, low cost, and reliable operation under extreme weather conditions are the basic requirements of an ideal collector [19].

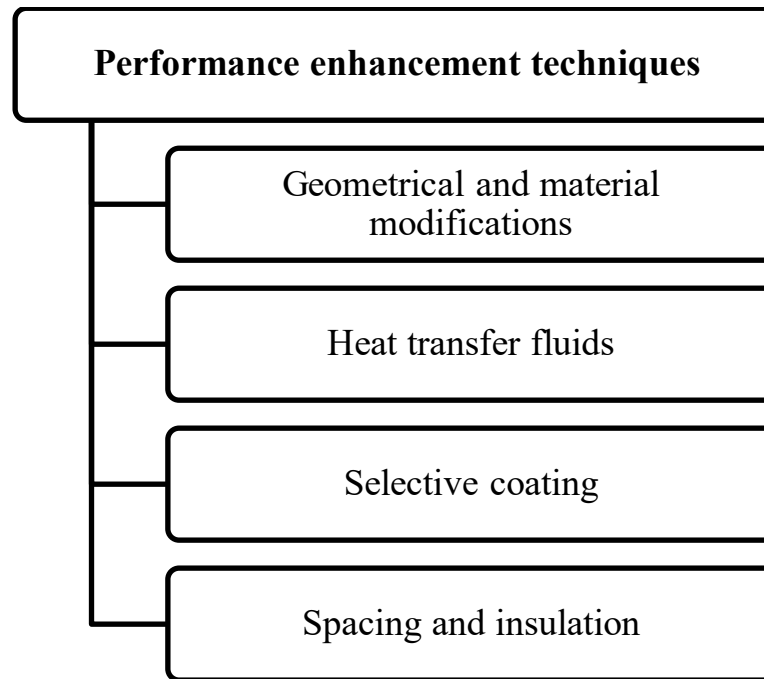


Figure 2.2 The most used performance enhancement techniques in flat plate solar collectors

2.2.1 Geometrical and Material Modifications

Transparent cover

The top transparent cover shape, material, number, thickness, transmittance, reflectance, absorptance and emittance coefficients are the effective parameters to get optimum performance of a flat plate solar collector. The features of the top cover impact the thermal conductive and convective heat loss from the collector top side. Dondapati et al. [20] investigated the effect of top transparent cover characteristics such as material selection (Polycarbonate, Polyethylene, Polyvinyl fluoride, Polystyrene and Polyester) and transmissivity coefficient varies between 0.81 and 0.89 on the performance of flat plate solar collector. Polyvinyl Fluoride material showed a positive effect on the collector efficiency due to its relatively high transmissivity coefficient (about 0.89) compared to the other materials selected for the investigation. Ramadhani et al. [21] experimentally studied four flat plate solar collectors with different glass cover thicknesses. Low iron (extra clear) glass cover of thicknesses 3mm, 4mm, 5mm, and 6mm was used as top transparent cover material. The result presented that the collector with 4mm glass thick exhibits the best thermal efficiency compared to 3mm, 5mm, and 6mm glass thicknesses. Shaik et al. [22] evaluated the optical transmission properties of different transparent cover materials such as acrylic, low- iron glass, medium- iron glass, and high-iron glass. Low iron glass (LiG with 6mm thickness) observed to be the best transparent cover due to its highest optical efficiency (75.65%) and thus high thermal efficiency (63.2%) among the glass cover materials considered in the

study. Hellstrom et al. [23] analysed an antireflection treatment of the top transparent cover. The antireflection treated glass cover, with 4% higher transmittance coefficient than an untreated one, increased the annual output heat energy with 6.5% at 50 °C. Agbo and Okoroigwe [24] assessed the impact of the number of the top transparent covers on the thermal losses within the solar collector. Double glassing cover diminished the overall heat loss coefficient by 44%, therefore resulting in better overall system performance, compared to single glassing cover.

Multi-channels absorber and heat pipes

Usually, heat transfer can be improved by enlarging the heat transfer surface of the receiver and upgrading the shape of the absorber sheets and pipes as well as the contact area between them. In this regard, a wide variety of absorber sheets and pipes designs were investigated by several researchers. Fan et al. [25] designed a new V-corrugated absorber with multi-channels. The thermal performance of this proposed configuration was modelled and compared with that of flat sheet-and-tube configuration. They concluded that the thermal efficiency and optical efficiency was 69.4% and 84.9%, respectively, which is higher than a conventional flat plate solar collector. Armenta-Déu [26] experimentally tested a semi spherical solar collector with spirally rolled up cylindrical absorber. He also developed new expressions for the equivalent temperature to predict the thermal performance of the semi spherical absorber collector. The modified expressions considering the heat loss coefficients and optical efficiency has been corrected. Poongavanam et al. [27] experimentally proved that the shot peened absorber plate and pipes can improve the thermal efficiency of a conventional flat plate solar collector to achieved more than 54%. This high efficiency was reached through the enhanced heat transfer characteristics by the roughness created. An experimental investigation of an innovative flat plate solar collector using micro channel heat pipe array was presented by Deng et al. [28]. Their results were compared with 15 samples (regrouped into 6 categories) coming either from literature or commercial products. The comparisons showed that the maximum thermal efficiency of the tested new design exceeded 25% over the average level of those nominated samples. Oyinlola et al. [29] theoretical and experimental analysed the temperature distribution for compact (thin and light-weight) solar thermal collector equipped with a micro-channel absorber plate. It was found that the axial conduction could significantly alter the microchannel absorber temperature. In addition, Oyinlola et al. [30] investigated the impact of different microchannel dimensions on the thermal and hydraulic performance of flat plate solar collector. Comparatively, a higher Nusselt number was attained when the aspect ratio of the microchannel closed unity. Arvanitisa et al. [31] experimentally evaluated and compared two conceptually

different flat plate absorbers, based on: a) a plate with straight rectangular multichannel and b) a serpentine tube-on-plate configuration with composite U-bends. The thermal efficiency of absorber with rectangular multichannel was found to be up to 18% higher than the serpentine tube-on-plate configuration. An optimum pumping power for a flat plate solar collector using microchannel absorber is presented by Moss et al. [32]. They concluded that the pumping power requirement could augment rapidly with the passage length, thus pumping power requirements may be reduced by relating multiple collectors in parallel rather than in series. Their results for the conceptual system revealed that the optimum pumping power lied in the range 0.01W/m^2 to 1.6W/m^2 for a collector area of 4m^2 .

2.2.2 Heat Transfer Fluids

Porous medium

Better thermal efficiency of the heat transfer fluid can be achieved by using porous foam materials. The performance of the porous medium is also subject to the inclination of the collector. Jouybari et al. [33] experimentally investigated the thermal performance of a flat plate solar collector with fully filled copper porous foam (porosity of 0.93). Employing the porous medium minimised the heat losses in the lower values of Reynolds number caused by enhancing the potential of solar energy absorption by working fluid. Anirudh and Dhinakaran [34] numerically studied the performance improvement of a flat plate solar collector filled with fully saturated porous metal foam. The insertion of the porous metal foam ameliorated the thermal efficiency due to better thermal mixing, along with buoyancy characteristics. Saedodin et al. [35] experimentally and numerically studied the influence of porous metal foam on the performance of a flat plate solar collector. The results have showed that exploiting the porous medium incremented Nusselt number and the thermal efficiency up to 82% and 18.5%, respectively. Ameri and Eshaghi [36] enhanced a flat plate solar collector performance by employing porous foam material of 0.8 porosity. The heat losses reduced by 3.149 times and thus the thermal efficiency reached 83.97%. Furthermore, Nusselt number was raised by 1.3 times when compared to the conventional system with laminar flow.

Nanofluids

Nanofluids are the mixture of nano-sized particles (1nm -100nm) and base heat transfer fluid such as water and oil. Nanofluids can improve thermal conductivity, thermal diffusivity and coefficient of convective heat transfer of the working fluid. The use of titanium dioxide-water (TiO_2 -water) nanofluid as an absorbing medium for flat plate solar collector was experimentally studied by Kiliç et al. [37]. They concluded that using TiO_2 -water nanofluid could provide better

thermal efficiency than that of pure water. Thermal efficiency of 48.67% was attained with the nanofluid compared to the thermal efficiency of 36.20% with pure water as heat transfer fluid. For reasons that this nanofluid had high specific heat capacity along with the increased contact surface of working fluid. Yousefi et al. [38] experimentally investigated the impact of using Al_2O_3 -Water nanofluid with particles size of 15nm, as working fluid, on the thermal efficiency of a flat plate solar collector. The results exhibited that, in comparison with water as working fluid, exploiting Al_2O_3 nanofluid enhanced the thermal efficiency by 28.3%. Moghadam et al. [39] examined the employment of CuO–water nanofluid with mean particle dimension of 40nm, as an absorbing medium, on the thermal efficiency of a flat plate solar collector. They found that the collector efficiency improved by 21.8%. Otanicar et al. [40] analysed three different groups of nanofluids (Graphite sphere-based of 30nm diameter, carbon nanotube-based of 6-20nm diameter, and silver sphere-based of 20-40nm diameter), with water as transfer working fluid. The results showed that mixing these nanoparticles in a liquid augmented the thermal efficiency by 5%. The influence of pH variation on nanofluids characteristics was experimentally studied by Goudarzi et al. [41]. The results revealed that, with the pH variation of nanofluids far from isoelectric point of nanoparticles (as the nanofluids become more acidic), thermal efficiency of the collector is augmented. Consequently, at the acidic condition of pH= 3, CuO nanofluid improved thermal collector efficiency by around 52% compared with that of pH= 10.5.

2.2.3 Selective Coatings

The use of selective coatings on flat plat solar collectors helps to harvest maximum solar energy. The selective coatings have different emissivity coefficient and absorptivity coefficient for different wavelengths due to their optical properties that depend on solar spectral range. The basic necessity of selective coating on the absorber plate is to reduce the emissivity with maximum absorptivity, thus maximum absorbed energy can be gained. Sivakumar et al. [42] developed and evaluated the thermal performance of a flat plate solar collector using nanoparticles cupric oxide (CuO) coating an aluminium absorber. The thermal efficiency of the collector using an absorber coated with CuO enhanced by 4% compared to a collector using black painted absorber. An experimental investigation on the thermal performance of three flat plate solar collectors with black chrome coated absorber, carbon coated absorber and black painted absorber was carried out by Sakhaei and Valipour [43]. Using field-emission scanning electron microscope images, the selective surface of the carbon coating showed high absorption due to light trapping and avoidance of light reflection. Therefore, the collector with carbon coated absorber had the maximum efficiency of 69.4%. The thermal efficiency of collector with

black chrome coated absorber and carbon coated absorber respectively enhanced by about 11.3% and 13% compared to the collector with black painted absorber. Senthil et al. [44] experimentally studied the effect of a mixed coating of graphene and black paint on the performance of flat plate solar collector. This mixed coating provided approximately 6.25% thermal efficiency more than that of the black paint coating due to higher thermal conductivity of graphene particles. Nazari et al. [45] analysed the impact of cuprous absorber coated with copper oxide nanoparticles (CuO NSs) on thermal exergy of a flat plate solar collector and compared its results with collector using black painted copper absorber and uncoated copper absorber. They concluded that the thermal exergy of a collector using copper absorber coated with CuO NSs enhanced by 18.8% and 35.8% compared to that of a collector with black painted absorber and uncoated absorber, respectively. By embedding cupric oxide nanoparticle (CuO) and carbon nanotubes (CNTs) into the black paint, an innovative selective coating with high solar absorptance of 0.964 and low emittance of 0.124 was fabricated by Abdelkadera et al. [46]. The results demonstrated that thermal efficiency improved by about 24.4%.

2.2.4 Spacing and Insulation

The spacing and insulation between top and back covers should be optimised to maintain lower heat losses from the flat sheets of collector to the ambient. The convective, conductive and radiative heat transfer coefficients highly depend with dimensions, material and characteristics of the spacing and insulator.

Transparent Insulation Materials

The heat losses from front side of flat plate solar collectors can be reduced using Transparent Insulation Materials (TIM). Garcia et al. [47] evaluated the influence of inserting equally spaced convective transparent barriers inside the air gap located between the absorber sheets and the front glass cover. Results showed that when two, three and four transparent barriers are added, the changes in heat loss are -2.2%, -5.3% and 2.9%, respectively. Rommel and Wagner [48] discussed the thermal and optical properties of the integration of a transparent honeycomb polycarbonate material with respect to the design of enhanced flat plate solar collector. Collectors containing this material exhibit good thermal performance while maintaining high solar transmittance and achieving high efficiencies especially for system temperatures above 80°C, but not exceeding 140°C as honeycombs begin to melt at 120°C which cause material problems. Ammar et al. [49] examined the potential enhancements in the thermal performance of flat plate solar collector using parallel transparent slats. They found that, for a 30° tilted collector, six parallel slats placed at a negative angle -45° improved the thermal

efficiency by 30% compared to the collector without slats. Kessentini et al. [50] experimentally and numerically investigated flat plate collector with plastic transparent insulation materials. The results allowed to propose a promising design of a stagnation proof collector with plastic transparent insulation material able to work at an operating temperature of more than 100°C with good thermal efficiency.

Gas insert

The main advantage of replacing the air between the absorber plate and the top glass cover using some other gases is to reduce the heat transfer rate and, at the same time, limit humidity. Vestlund et al. [51] investigated the influence of different inert gases on the thermal losses in a flat plate collector. Their results exhibited that the overall heat loss can be minimised up to 20% when air is replaced with inert gas. Bennour and Mzad [52] examined the effect of trapped gases such as argon, xenon, krypton, and SF₆ within a double glazing and between the absorber plate and the inner glass on thermal efficiency of flat plate solar collector. They found that Xenon showed the best thermal performances followed by Krypton and Argon, compared to air. Respectively, the thermal efficiencies were 51.8%, 50.6%, 48.8% and 45.8% for Xenon, Krypton, Argon and air.

Vacuum insulation

Flat plate solar collectors suffer from high thermal losses through its front glass cover, which leads to a low thermal efficiency and low operating temperatures. This issue could be overcome by creating a vacuum environment around the absorber plate, which allows to prevent conductive and convective heat losses due to the high insulating characteristics of vacuum environment. One important topic of research in solar heating systems seeks to integrate the advantages of the vacuum insulation, which is commonly used in evacuated tube solar collector, for improving the thermal performance of flat plate solar collector. Eaton and Blum [53] suggested and theoretically studied the use of moderate vacuum environment ($\sim 1.5 \cdot 10^2$ Pa <Pressure < $\sim 3.5 \cdot 10^3$ Pa) between the absorber plate and the transparent cover. They concluded that this process could eliminate the natural conductive and convective heat losses in the air gap allowing the collector thermal efficiency to operate at more than 40% and produce temperatures up to 150°C. Robert [54] analysed the heat losses of flat plate absorbers completely surrounded by evacuated glass tubes and investigated the effect of the low thermal conductivity of gas on convective heat loss under different values of pressure. Beikircher et al. [55] experimentally and numerically studied the employing of air and argon as filling gas under pressure range from 10^{-3} to 10^4 Pa. The results indicated that at moderate internal pressures of 10^3 Pa, gas conduction was

decreased by 30%, as diminishing the internal pressure, this reduction was even greater. While at the pressure of 10^{-1} Pa the gas conduction was nearly totally suppressed. Benz et al. [56] examined the effect of the interior pressure varying from 10^3 to 10^4 Pa on the gas conduction of air, krypton and nanostructured aerogel. In another experiment [57], they constructed a prototype of vacuum flat plate solar collector filled by a low-pressure krypton gas. The collector achieved an efficiency of about 45% at elevated temperature of 150°C .

Recently, a group of researchers has successfully investigated and built a prototype of vacuum flat plate solar collector. Where, Henshall et al. [58] proposed the design of the evacuated enclosure. The absorber plate was fully housed by a thin layer of a high vacuum environment and covered by two parallel tempered glasses separated by metal support pillars. They expected that flat plate solar collector's thermal performance could be enhanced if the enclosure could be evacuated and they suggested that, with specified design parameters, this vacuum enclosure would be able to provide a vacuum flat plate solar collector of high thermal efficiency. Then, Arya et al. [59] presented detailed experimental investigation including a new hermetic sealing method that could maintain vacuum insulation in the evacuated collector. Next, Moss et al. [60] (2018) studied and tested two different absorber designs under a solar simulator (indoor testing) under a range of $200\text{--}1000\text{ W/m}^2$. They succeeded to reduce the heat loss coefficient by $3.7\text{ W/m}^2\text{K}$ and to raise the collector efficiency from 30% to 60%. After that, in a two-part work, Arya et al. [61] investigated two vacuum enclosures and tested them under three different conditions of internal pressure (2.1×10^{-3} Pa, 8.4 Pa and 1.013×10^5 Pa). The first part included the fabrication process and the construction techniques for manufacturing evacuated enclosures. They found that the high vacuum enclosure (2.1×10^{-3} Pa) had an overall heat loss coefficient of $1.35\text{ W/m}^2\text{ K}$ and indicated that this value could be minimised to $0.82\text{ W/m}^2\text{ K}$, in which the support pillars were made by low thermal conductivity materials such as glass. In the second part of the study [62], they tested the enclosure having a copper plate under a solar simulator. The absorber plate achieved maximum temperatures of 122.8°C , 104.2°C and 103.6°C at pressure conditions of high vacuum, low vacuum and no vacuum, respectively. Radwan et al. [63] analysed and investigated a new designed vacuum flat plate solar collector with top glass of high transmittance ($\tau = 0.92$) and a serpentine flow filed heat sink. Their results showed an improvement of 26.6% and 8% in thermal efficiency and exergy efficiency of collector, respectively. An optimised flat plate solar collector based on vacuum insulation with a new piping arrangement and cover glass of anti-reflection coating was presented by Gao et al. [64]. The optimised collector attained an average thermal efficiency and exergy efficiency of 55% and

8.5%, respectively. De Maio et al. [65] evaluated the impact of applying new multilayers selective coating with emissivity of 0.045 on vacuum flat plate solar collector performance. The absorber multilayers can be 8% more efficient than the commercial coating at operating temperatures under 250°C.

2.3 Conclusion

A deep analysis and a good understanding of aforementioned studies allows us to take a general idea about the most important parameters that significantly affect the thermal performance of a flat plate solar collector, and to identify the knowledge gap. For more understanding of this work, a combination of numerical and experimental investigations was carried out. The following chapter will provide a detailed description of the theoretical model adopted in this study.

Chapter 3: Theoretical Model and Computational Algorithm

Theoretical modelling is an important tool used for studying thermal performance of solar collectors. In any solar energy application, it would be desirable to theoretically analyse the given system as intensively as possible before proceeding to the experimental work. In this chapter, in order to predict the thermal behaviour of a flat plate solar collector exposed to solar radiation at a specified geographical position and a given period of time, it is necessary to establish mathematical equations that includes the evaluation of heat losses, collector factors and energy balance equations which govern the thermal phenomena of the flat plate solar collector.

3.1 Heat Transfer in Collector

In order to simulate the thermal behaviour of a flat plate solar collector exposed to solar radiation at a specific geographical position and a given period, it is necessary to understand the heat transfer in the collector and then to establish a mathematical model and balance equations that govern these thermal phenomena. Heat transfer inside a flat plate collector is in unsteady state conditions, which does not mathematically facilitate the modelling of the heat transfer phenomena, due to the permanent variation in incident solar radiation and surrounding conditions.

To model the thermal performance of a collector, the theoretical approach has been made based on simplifying assumptions without obfuscate the basic physical circumstance. These assumptions are as follows:

1. Thermal performance is in steady state conditions.
2. Heat flow through the collector components is one dimensional.
3. The horizontal headers provide uniform flow to riser tubes.
4. The covers are opaque to infrared radiation.
5. The sky is considered as a blackbody for long-wavelength radiation at an equivalent sky temperature.
6. Material properties are independent of temperature variations.
7. Losses through front side and back side are to the same ambient temperature.
8. Shading and dust on the collector are not considered.
9. Wind speed on the collector face is assumed to be constant.

The solar collectors' theories are well described and can be found in fundamental literatures [66] [67] [8].

The thermal balance of a flat plate collector is written in the following form:

$$Q_{ab} = Q_u + Q_p \quad (3.1)$$

Where, Q_{ab} is the absorbed energy rate, which can be calculated as:

$$Q_{ab} = A(\tau\alpha)_c G^* \quad (3.2)$$

A is the collector absorber area.

$(\tau\alpha)_c$ is the absorptance-transmittance product.

G^* is the incident global solar irradiation.

While, Q_p represent the energy heat loss, which can be calculated as:

$$Q_p = AU_L(T_p - T_a) \quad (3.3)$$

U_L is the overall heat loss coefficient.

T_a and T_p are ambient and absorber plate temperature respectively.

Using equations (3.2) and (3.3), the useful energy rate can be represented as:

$$Qu = A[(\tau\alpha)_c G^* - U_L(T_p - T_a)] \quad (3.4)$$

The problem with equation (3.4) is that the mean temperature of the absorber plate is difficult to calculate and to measure, since it is a function of incident solar radiation, surrounding conditions, circulating fluid conditions and collector design parameters. Consequently, there is a need to reformulate the useful energy rate in terms of the inlet fluid temperature and a coefficient named the collector heat removal factor rather than the mean absorber plate temperature. Indeed, this coefficient can be evaluated analytically from basic collector's principles which will be described in details later.

3.2 Collector Heat Losses Evaluation

The heat loss to the exterior environment is a substantial parameter for studying the performance of solar collector, since the latter is always subject to heat losses. Part of the absorbed energy is transferred to the surrounding in the form of thermal energy mainly by convection, conduction and radiation heat transfer due to the temperature difference between the different components of the collector as well as with the ambient environment. Heat loss in a solar collector comprises of front heat loss through the top side and back heat loss through the rear side. To evaluate these losses, an electrical analogy related to the thermal resistances is carried out on the different elements of collector. The equivalent thermal-circuit diagram for a flat plate solar collector is shown in figure (3.1).

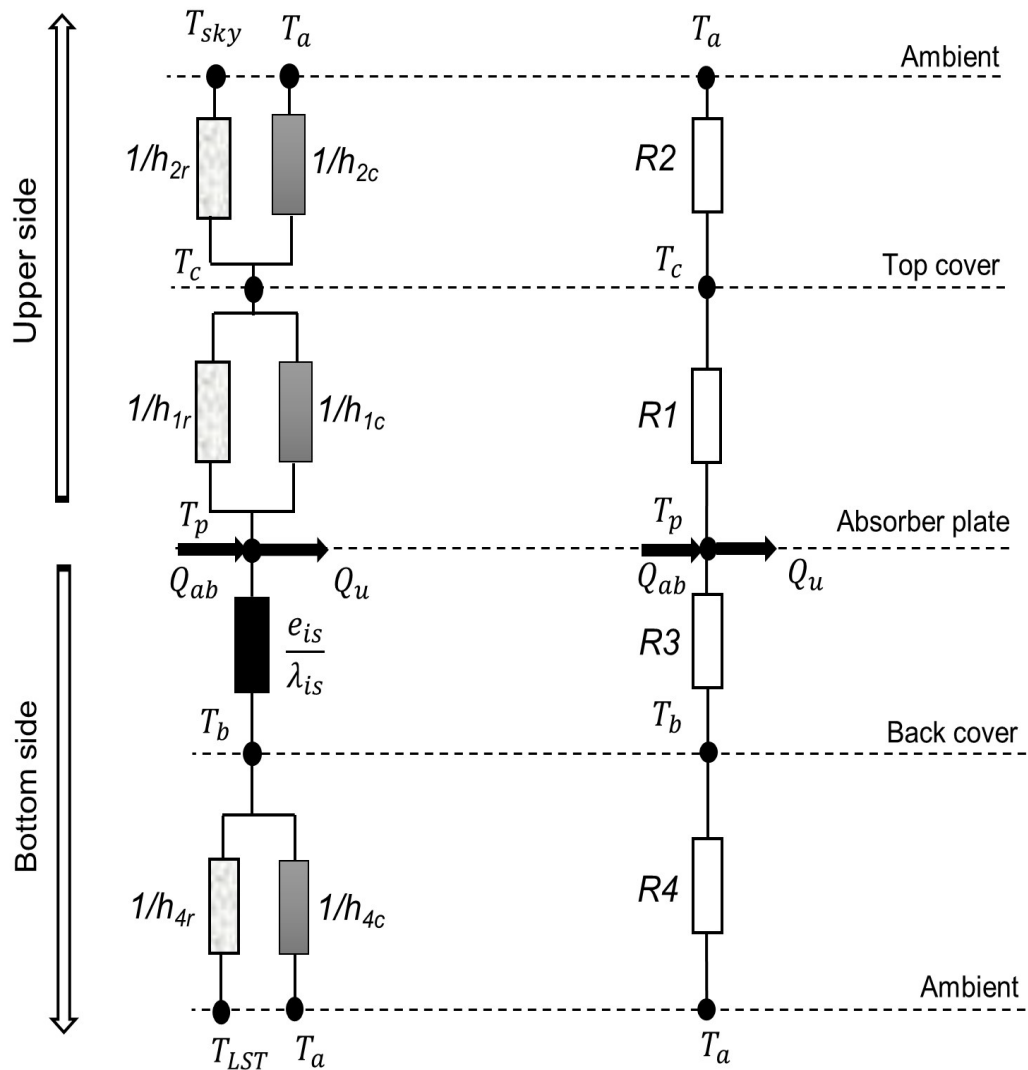


Figure 3.1 Equivalent thermal-circuit diagram for a flat plate solar collector.

From the equivalent thermal-circuit diagram for a solar collector, it can be defined:

- **R1:** Thermal resistance between the absorber plate and the front cover.
- **R2:** Thermal resistance between the front cover and ambient.
- **R3:** Thermal resistance between the absorber plate and the rear cover.
- **R4:** Thermal resistance between the rear cover and ambient.

3.2.1 Top Heat Loss Coefficient

The heat loss rate through the front side can be presented as:

$$Qp_{top} = AU_t(T_p - T_a) \quad (3.5)$$

U_t is the top heat loss coefficient.

In order to calculate the top heat loss coefficient U_t , the upper side is divided into two parts as follows:

a) *Heat loss between the absorber plate and the front cover*

The heat loss rate between the absorber plate and the front cover depends greatly on the front insulation proprieties.

$$Qp_{top-1} = A(h_{1c} + h_{1r})(T_p - T_c) = \frac{A(T_p - T_c)}{R_1} \quad (3.6)$$

h_{1c} is the heat transfer coefficient by convection from the absorber plate to the front cover.

h_{1r} is the heat transfer coefficient by radiation from the absorber p late to the front cover.

T_c is the front cover temperature.

The heat transfer coefficient by convection from the absorber plate to the front cover h_{1c} can be calculated as follows:

$$h_{1c} = N_u \frac{K_g}{L_g} \quad (3.7)$$

N_u is the Nusselt number.

K_g and L_g are respectively the thermal conductivity and the spacing between absorber plate and transparent cove.

Heat transfer by natural convection in a closed cavity between two parallel plates inclined with some angle from the horizon is of significant importance in the study of collector thermal performance. In natural convection, the Nusselt number depends on the Rayleigh number which is a function of Grashof number and Prandtl number. The calculation of the Nusselt number for natural convection in an inclined collector has been the subject of various experimental and numerical studies. Several correlations have been proposed and validated under specific conditions. Among these correlations, the expression of Hollands et al. [68] is practically the most widely used. It deals with natural convection of an inclined cavity heated from below. This

correlation is a valid expression for a collector inclination angle β varies between $0^\circ \leq \beta \leq 75^\circ$.

$$Nu = 1 + 1.44 \left[1 - \frac{1708(\sin 1.8\beta)^{1.6}}{Ra \cos(\beta)} \right] \left[1 - \frac{1708}{Ra \cos(\beta)} \right]^+ + \left[\left(\frac{Ra \cos(\beta)}{5830} \right)^{1/3} - 1 \right]^+ \quad (3.8)$$

It is worth to mention that the superscript symbol + in equation (3.8) implies only the positive values of the terms in the square brackets that should be used (i.e., use zero when the term is negative).

Table 3.1 summarises some of the Nusselt number correlations used for the natural convection calculation in a closed cavity.

Table 3.1 Selected correlations of Nusselt number used for the natural convection calculation in a closed cavity.

Author	Formula	Ra	β																
Buchberg [69]	$Nu = 1 + 1.446 \left(1 - \frac{1708}{Ra \cos(\beta)} \right)^+$ $Nu = 0.229(Ra \cos(\beta))^{0.252}$ $Nu = 0.157(Ra \cos(\beta))^{0.285}$	$1708 < Ra \cos(\beta) < 5900$ $5900 < Ra \cos(\beta) < 9.2 \times 10^4$ $9.2 \times 10^4 < Ra \cos(\beta) < 10^6$	$0^\circ - 60^\circ$																
Yin [70]	$Nu = 0.210 Gr_L^{0.269} \left(\frac{H}{L} \right)^{-0.131}$	$1.5 \times 10^3 < Gr < 7 \times 10^6$	90°																
Randall [71]	$Nu = 0.118(Ra \cos^2(\beta - 45))^{0.29}$	$2.8 \times 10^3 < Ra < 2.2 \times 10^5$	$45^\circ - 90^\circ$																
Schinkel [72]	$Nu = a(\beta) (Ra)^{\frac{1}{3}}$ <table border="1" style="margin-left: 20px;"> <thead> <tr> <th>β</th> <th>$a(\beta)$</th> </tr> </thead> <tbody> <tr> <td>0°</td> <td>0.080</td> </tr> <tr> <td>10°</td> <td>0.079</td> </tr> <tr> <td>20°</td> <td>0.075</td> </tr> <tr> <td>30°</td> <td>0.074</td> </tr> <tr> <td>40°</td> <td>0.074</td> </tr> <tr> <td>50°</td> <td>0.074</td> </tr> <tr> <td>60°</td> <td>0.072</td> </tr> </tbody> </table>	β	$a(\beta)$	0°	0.080	10°	0.079	20°	0.075	30°	0.074	40°	0.074	50°	0.074	60°	0.072	$10^5 < Ra < 4 \times 10^6$	$0^\circ - 90^\circ$
β	$a(\beta)$																		
0°	0.080																		
10°	0.079																		
20°	0.075																		
30°	0.074																		
40°	0.074																		
50°	0.074																		
60°	0.072																		

	<table border="1"> <tr> <td>70°</td> <td>0.069</td> </tr> <tr> <td>80°</td> <td>0.068</td> </tr> <tr> <td>90°</td> <td>0.062</td> </tr> </table>	70°	0.069	80°	0.068	90°	0.062												
70°	0.069																		
80°	0.068																		
90°	0.062																		
Niemann [73]	$Nu = 1 + \frac{m(Ra)^k}{Ra + n}$ <table border="1"> <thead> <tr> <th>β</th> <th>m</th> <th>n</th> <th>k</th> </tr> </thead> <tbody> <tr> <td>0</td> <td>0.07</td> <td>0.32 x10⁴</td> <td>1.33</td> </tr> <tr> <td>45</td> <td>0.043</td> <td>0.41 x10⁴</td> <td>1.36</td> </tr> <tr> <td>90</td> <td>0.0236</td> <td>1.01 x10⁴</td> <td>1.393</td> </tr> </tbody> </table>	β	m	n	k	0	0.07	0.32 x10 ⁴	1.33	45	0.043	0.41 x10 ⁴	1.36	90	0.0236	1.01 x10 ⁴	1.393	$10^2 < Ra < 10^8$	/
β	m	n	k																
0	0.07	0.32 x10 ⁴	1.33																
45	0.043	0.41 x10 ⁴	1.36																
90	0.0236	1.01 x10 ⁴	1.393																

The Rayleigh number is defined as follows:

$$Ra = \frac{g\beta'\Delta T L_g^3}{\vartheta_a \alpha} \quad (3.9)$$

g is the gravitational constant.

β' is the volumetric coefficient of expansion (for an ideal gas, $\beta' = \frac{1}{T}$).

ΔT is the temperature difference between parallel plates.

ϑ_a is the kinematic viscosity.

α is the thermal diffusivity.

The heat transfer coefficient by radiation from the absorber plate to the front cover h_{1r} can be calculated as follows:

$$h_{1r} = \frac{\sigma(T_p^2 + T_c^2)(T_p + T_c)}{\frac{1 - \varepsilon_p}{\varepsilon_p} + \frac{(1 - \varepsilon_c)A}{\varepsilon_c A_g} + 1} \quad (3.10)$$

σ is Stefan-Boltzmann constant.

ε_p and ε_c are the absorber plate and the top cover emissivity, respectively.

A and A_g are the absorber plate and top cover area, respectively.

The equivalent thermal resistance between the absorber plate and the top cover R_1 is given by:

$$R_1 = \frac{1}{h_{1c} + h_{1r}} \quad (3.11)$$

b) Heat loss between the front cover and ambient

The upper face of the front cover is exposed to convective exchange with the ambient air as well as radiative exchange with the sky.

$$Qp_{top-2} = (h_{2c} + h_{2r})(T_c - T_a) = \frac{(T_c - T_a)}{R_2} \quad (3.12)$$

h_{2c} is the heat transfer coefficient by convection from the front cover to ambient.

h_{2r} is the heat transfer coefficient by radiation from the front cover to ambient.

The convective heat loss coefficient from the front cover to the surrounding h_w is usually estimated using a linear function related to the wind speed v_{wind} . Most of these correlations are of the form:

$$h_{2c} = a + b \times v_{wind}^n \quad (3.13)$$

The correlation which has been widely used to study flat solar collectors is that suggested by Jurges [74] for a surface of $0.5 \times 0.5 \text{ m}^2$ and referenced by McAdams [75], Duffie and Beckman [67] and others.

$$h_{2c} = 5.7 + 3.8v_{wind} \quad (3.14)$$

According to Duffie and Beckman, the equation (3.14) is not suitable for collector length greater than 0.5 m. Despite this, it is frequently applied to study collectors of more than 0.5 m length, due to the absence of an alternative reliable equation. Watmuff [76] assumed that in this relation (3.14), the effect of radiation is included, for this reason they proposed the following expression, which was also commonly used for solar collectors' performance investigation:

$$h_{2c} = 2.8 + 3v_{wind} \quad (3.15)$$

It is worth mentioning that in real conditions, the instantaneous wind speed and the direction of the air currents vary rapidly, thus, these correlations are imprecise but remain widely used.

There are numerous expressions that suggested to quantify the heat exchange by convection with the surrounding, table (3.2) shows an overview of some of these correlations.

Table 3.2 Selected correlations for the external natural convection calculation on the top cover.

Author	Formula	Wind speed [m/s]
McAdams [75]	$h_{2c} = 5.7 + 3.8v_{wind}$ $h_{2c} = 6.47v_{wind}^{0.78}$	$v_{wind} < 5$ $v_{wind} > 5$
Watmuff [76]	$h_{2c} = 2.8 + 3v_{wind}$ $h_{2c} = 2.3 + 3v_{wind}$	$v_{wind} \leq 5$ $5 < v_{wind} < 7$
Sparrow [77]	$h_{2c} = \frac{0.86\rho C_p v_{wind}}{Pr^{2/3} Re^{1/2}}$	$4.5 < v_{wind} < 24$
Kumar [78]	$h_{2c} = 10.03 + 4.687v_{wind}$	$0 < v_{wind} < 4$
Sharples [79]	$h_{2c} = 8.3 + 2.2v_{wind}$ $h_{2c} = 6.5 + 3.3v_{wind}$	$0.8 < v_{wind} < 6.5$

The heat transfer coefficient by radiation from the front cover to ambient h_{2r} is given as a function of sky temperature T_{sky} and the outside cover face temperature T_c .

$$h_{2r} = \frac{\sigma \varepsilon_c (T_c^4 - T_{sky}^4)}{T_c - T_a} \quad (3.16)$$

The sky temperature is mostly given as a function of the ambient temperature (T_a). Several expressions are investigated to estimate the sky temperature, the largely used correlation is that given by Swinbank [80] as follows:

$$T_{sky} = T_a - 6 \quad (3.17)$$

Swinbank calculates the sky temperature using only ambient temperature (T_a), however Berdahl et al. [81] and Bliss [82] incorporate the dew-point temperature (T_{dp}) in their formulae. Brunt [83] and Aubinet [84] use the water vapor pressure parameter (p_d) and the sky clarity index K_0 ($K_0 = \frac{G}{G_0}$; which is the ratio between the global horizontal solar irradiation (G) and incident solar irradiation (G_0)). The formula provided by EN 6946 [85] helps to estimate the sky temperature in case of cloudy sky. These correlations are summarised in Table (3.3).

Table 3.3 Selected equations for equivalent sky temperature calculation.

Author	Formula	Condition
Swinbak [80]	$T_{sky} = 0.0522(T_a)^{1.5}$ $T_{sky} = 0.037536(T_a)^{1.5} + 0.32T_a$	Clear sky
Berdahl et al. [81]	$T_{sky} = T_a(0.711 + 0.0056T_{dp} + 0.0000737T_{dp}^2)^{1/4}$	Clear sky and T_{dp}
EN 6946 [85]	$T_{sky} = T_a$	cloudy sky
Bliss [82]	$T_{sky} = T_a(0.8004 + 0.00396T_{dp})^{1/4}$	T_{dp}
Aubinet [84]	$T_{sky} = 94 + 12.6\ln(p_d) - 13K_0 + 0.341T_a$	p_d and K_0 index
Brunt [83]	$T_{sky} = (0.564 + 0.059\sqrt{p_d})^{1/4}$ $T_{sky} = (0.527 + 0.065\sqrt{p_d})^{1/4}$	p_d

The equivalent thermal resistance between the top cover and the ambient R_2 is then given by:

$$R_2 = \frac{1}{h_{2c} + h_{2r}} \quad (3.18)$$

The top heat loss coefficient U_t from the front face of the absorber plate to the exterior environment depends greatly on the front insulation proprieties. For conventional flat plate collector, the conduction/convection heat losses through the air gap between absorber and front cover as well as the radiative heat losses, are presented as follows:

$$U_t = \left(\frac{1}{h_{1c} + h_{1r}} + \frac{1}{h_{2c} + h_{2r}} \right)^{-1} = \frac{1}{R_1 + R_2} \quad (3.19)$$

However, in case of evacuated air of the gap between absorber and front cover, the vacuum environment will prevent the heat losses by conduction/convection. And for a perfect suppression of this mode of heat transfer ($h_{1c} \approx 0$), a low pressure of less than 10^{-5} mbar is required [86]. Therefore, the top heat loss coefficient can be defined as follows:

$$U_t = \left(\frac{1}{h_{1r}} + \frac{1}{h_{2c} + h_{2r}} \right)^{-1} = \frac{1}{R_1 + R_2} \quad (3.20)$$

Duffie and Beckman developed an expression based on an empirical correlation proposed by Kelvin for the calculation of the top heat loss coefficient. This correlation is expressed as follows:

$$U_t = \left[\frac{N}{\frac{c}{T_p} \left[\frac{(T_p - T_a)}{(N + f)} \right]^e} + \frac{1}{h_{2c}} \right]^{-1} + \frac{\sigma(T_p + T_a)(T_p^2 + T_a^2)}{(\varepsilon_p + 0.00591 N h_{2c})^{-1} + \frac{2N + f - 1 + 0.133\varepsilon_p}{\varepsilon_c} - N} \quad (3.21)$$

N is the number of top covers.

Where, the coefficients c , f and e can be calculated as follow:

$$c = 520(1 - 0,000051(\beta^2)) \quad \text{for } \begin{cases} 0^\circ < \beta < 70^\circ \\ 70^\circ < \beta < 90^\circ \rightarrow \beta = 70^\circ \end{cases} \quad (3.22)$$

$$f = (1 + 0,089 h_w - 0,1166 h_w \varepsilon_p) \times (1 + 0,07866N) \quad (3.23)$$

$$e = 0.43 \left(1 - \frac{100}{T_p} \right) \quad (3.24)$$

3.2.2 Back Heat Loss Coefficient

The heat loss rate through the back side can be expressed as follows:

$$Qp_{back} = AU_b(T_p - T_a) \quad (3.25)$$

U_b is the back heat loss coefficient.

To calculate the back heat loss coefficient, the bottom side is divided into two parts as follows:

a) Heat loss between the absorber plate and the back cover

The back heat loss rate from the rear face of the absorber plate to the surroundings can be given by the conduction, convection and radiation thermal resistance that depends mainly on back insulation characterises. In typical flat plate collector, only the conduction heat loss is counted and the radiation heat loss is restricted by using an opaque insulation material (such as Rockwool material).

$$Qp_{back-3} = A \left(\frac{\lambda_{is}}{e_{is}} \right) (T_p - T_b) = \frac{A(T_p - T_b)}{R_3} \quad (3.26)$$

e_{is} and λ_{is} are thickness and thermal conductivity of the back insulation, respectively.

Where, the equivalent thermal resistance between the absorber plate and the rear cover R_3 can be represented as:

$$R_3 = \left(\frac{\lambda_{is}}{e_{is}} \right)^{-1} \quad (3.27)$$

b) Heat loss between the back cover and ambient

The back cover is exposed to convective heat exchange and radiative heat exchange with the surrounding.

$$Qp_{back-4} = A(h_{4c} + h_{4r})(T_b - T_a) = \frac{A(T_b - T_a)}{R_4} \quad (3.28)$$

T_b is the back cover temperature.

h_{4c} and h_{4r} are respectively the convective heat loss coefficient and the radiative heat loss coefficient from the rear cover to the ambient. These two coefficients can be calculated in the same processes as heat loss coefficients of the front side.

The equivalent thermal resistance between the back cover and the ambient R_4 is given by:

$$R_4 = \frac{1}{h_{4c} + h_{4r}} \quad (3.29)$$

Therefore, the back heat loss coefficient can be defined as follows:

$$U_b = \left(\frac{e_{is}}{\lambda_{is}} + \frac{1}{h_{4c} + h_{4r}} \right)^{-1} = \frac{1}{R_3 + R_4} \quad (3.30)$$

3.2.3 Overall Heat Loss Coefficient

We suppose that all heat losses occur to a common ambient temperature T_a , thus, the collector overall heat loss coefficient U_L is the summation of the front and back heat loss coefficients, and it is given by:

$$U_L = U_t + U_b = \frac{1}{R_1 + R_2} + \frac{1}{R_3 + R_4} \quad (3.31)$$

3.3 Heat Transfer from Sheets to Tubes

3.3.1 Absorber plate temperature distribution

The useful heat energy is influenced by the mean absorber plate temperature as expressed in equation (3.4). The temperature distribution of the absorber plate between tubes is based on the amount of energy flow through the sheets. Hence, in this section, the heat transfer from sheets to tubes is analysed.

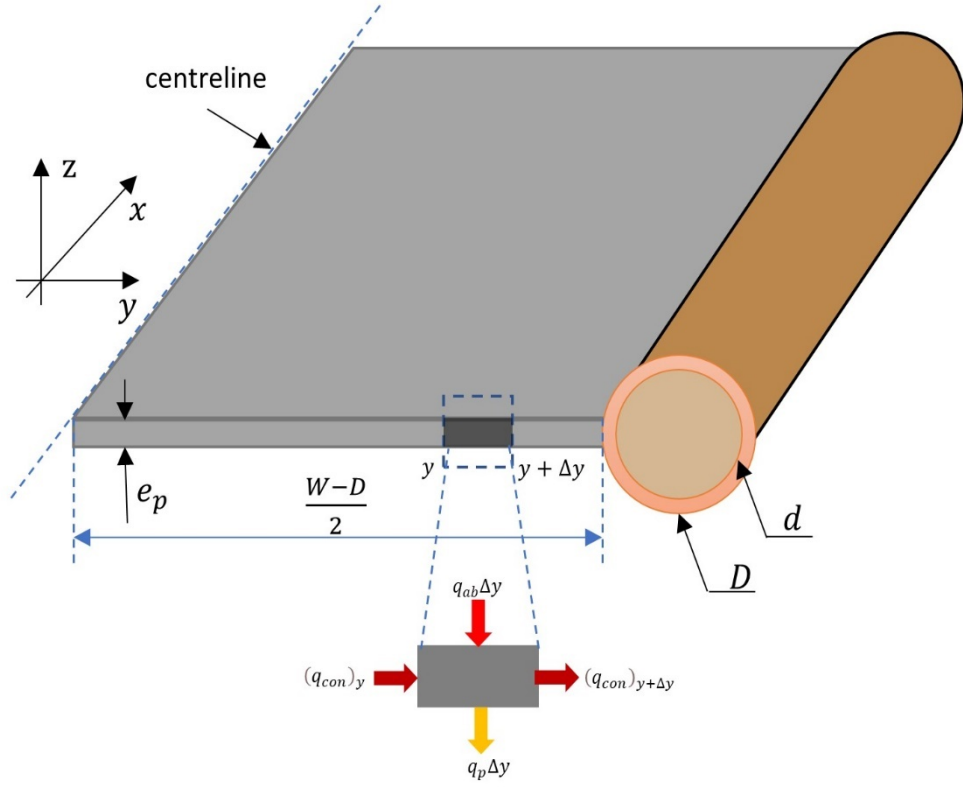


Figure 3.2 The heat transfer from sheet to tube.

As shown in Figure 3.2, the distance between tubes is W , the tube diameter is D , and the thickness of absorber sheet is e_p . It is known from the knowledge of heat transfer that the heat flux at the sheets' centrelines between tubes is considered zero. Accordingly, the section from the centreline to the tube centre is chosen for the analysis. The energy balance equation and the distribution of temperatures between the tubes in the perpendicular fluid direction can be determined as the following procedures:

$$q_{ab}\Delta y + (q_{con})_y = (q_{con})_{y+\Delta y} + q_p\Delta y \quad (3.32)$$

Or

$$q_{ab}\Delta y - \lambda_p e_p \left(\frac{dT}{dy} \right)_y = -\lambda_p e_p \left(\frac{dT}{dy} \right)_{y+\Delta y} + U_L (T_p - T_a) \Delta y \quad (3.33)$$

Dividing throughout by Δy and using the limit as $\Delta y \rightarrow 0$, the equation (3.33) can be simplified as:

$$\frac{d^2 T_p}{dy^2} = \frac{U_L}{\lambda_p e_p} \left(T_p - T_a - \frac{q_{ab}}{U_L} \right) \quad (3.34)$$

To solve this second-order differential equation, two boundary condition are supposed as follows:

$$\left. \frac{dT_p}{dy} \right|_{y=0} = 0 \quad \text{and} \quad T_p \Big|_{y=\left(\frac{W-D}{2}\right)} = T_{tb} \quad (3.35)$$

We can define two variables, $\overline{T_p}$ and m as follows:

$$\overline{T_p} = T_p - T_a - \frac{q_{ab}}{U_L} \quad (3.36)$$

$$m^2 = \frac{U_L}{\lambda_p e_p} \quad (3.37)$$

Equation (3.34) becomes as follows:

$$\frac{d^2 \overline{T_p}}{dy^2} - m^2 \overline{T_p} = 0 \quad (3.38)$$

The above equation (3.38) has the following general solution:

$$\overline{T_p}(y) = C_1 \sinh(my) + C_2 \cosh(my) \quad (3.39)$$

Two boundary conditions are required to solve the differential equation. These are as follows:

For $y = 0$:

$$\left. \frac{dT_p}{dy} \right|_{y=0} = mC_1 \cosh(0) + mC_2 \sinh(0) = 0 \quad \Rightarrow \quad C_1 = 0 \quad (3.40)$$

And for $y = \frac{W-D}{2}$:

$$T_{tb} - T_a - \frac{q_{ab}}{U_L} = C_2 \cosh\left(m \frac{W-D}{2}\right) \quad \Rightarrow \quad C_2 = \frac{T_{tb} - T_a - \frac{q_{ab}}{U_L}}{\cosh\left[m \left(\frac{W-D}{2}\right)\right]} \quad (3.41)$$

Therefore,

$$\frac{T_p(y) - T_a - \frac{q_{ab}}{U_L}}{T_{tb} - T_a - \frac{q_{ab}}{U_L}} = \frac{\cosh(m(y))}{\cosh\left[m \left(\frac{W-D}{2}\right)\right]} \quad (3.42)$$

In general

$$T_p(y) = \left[T_{tb} - T_a - \frac{q_{ab}}{U_L} \right] \frac{\cosh(m(y))}{\cosh\left[m \left(\frac{W-D}{2}\right)\right]} + T_a + \frac{q_{ab}}{U_L} \quad (3.43)$$

The thermal energy transferred to the section of the tube per unit of length in the flow direction can be defined by evaluating Fourier's law at the fin base.

$$q_{at} = -\lambda_p e_p \left. \frac{dT_p}{dy} \right|_{y=\frac{W-D}{2}} = -\frac{U_L}{m} \left[T_{tb} - T_a - \frac{q_{ab}}{U_L} \right] \tanh \left[m \left(\frac{W-D}{2} \right) \right] \quad (3.44)$$

The part of the absorber plate between $y = 0$ and $y = \frac{W-D}{2}$ acts as a heating sheet. If this sheet is at a uniform temperature, the flow transferred from the sheet to the tube would be written as:

$$q_{at_max} = [q_{ab} - U_L(T_{tb} - T_a)] \frac{W-D}{2} \quad (3.45)$$

We can define the sheet efficiency F as follows:

$$F = \frac{q_{at}}{q_{at_max}} = \frac{\tanh \left[m \left(\frac{W-D}{2} \right) \right]}{m \left(\frac{W-D}{2} \right)} \quad (3.46)$$

3.3.2 Collector Efficiency Factor

To evaluate the collector efficiency factor, it is important to calculate the equivalent thermal resistances from the sheet to the fluid inside tube, see Figure 3.3.

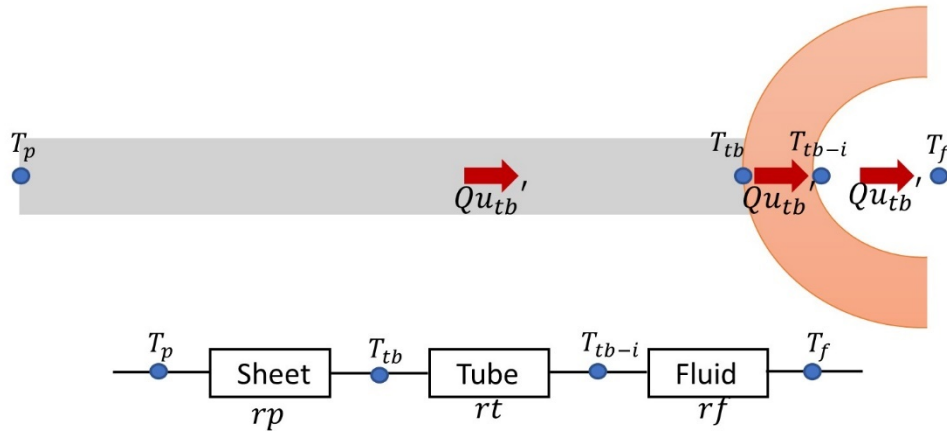


Figure 3.3 The equivalent thermal-circuit diagram of heat transfer from the sheet to the fluid inside tube.

The collector efficiency factor F' represents the ratio of actual useful heat energy gain Qu_{tb}' to the rate of the useful energy gain when the collector absorber plate temperature is at the inlet fluid temperature $Qu_{tb}'|_{T_p=T_f}$. It is defined as follows:

$$F' = \frac{Qu_{tb}'}{Qu_{tb}'|_{T_p=T_f}} = \frac{Qu_{tb}'}{WL_{tb}U_L \left[\frac{q_{ab}}{U_L} - (T_f - T_a) \right]} \quad (3.47)$$

The collected useful energy gain by sheets surfaces and appeared tube areas can be represented as follows:

$$Qu_{tb}' = U_L \left[\frac{q_{ab}}{U_L} - (T_{tb} - T_a) \right] [(W - D)F + D] = U_L \left[\frac{q_{ab}}{U_L} - (T_{tb} - T_a) \right] / rp \quad (3.48)$$

This gained useful energy from equation (3.48) must be transferred to the fluid through the tube, which can be expressed as follows:

$$Qu_{tb}' = \frac{(T_{tb} - T_{tb-i})\pi A_{mw}}{\frac{e_t}{\lambda_t}} = (T_{tb} - T_{tb-i}) / rt \quad (3.49)$$

Where, the mean wall area A_{mw} is given as follows:

$$A_{mw} = \frac{D - d}{\ln(D/d)} \quad (3.50)$$

The useful energy gain by the fluid is expressed as follow:

$$Qu_{tb}' = \frac{(T_{tb-i} - T_f)\pi di}{\frac{1}{h_f}} = (T_{tb-i} - T_f) / rf \quad (3.51)$$

To determine the film heat-transfer coefficient h_f between the fluid inside tube and the inner tube wall, the Nusselt number Nu is given as follows:

$$Nu = \frac{U_h D}{K_w} = C Re^m Pr^n K_R \quad (3.52)$$

The thermal conductance from the inner wall of the heat exchanger to the cold water U_c , as well as the thermal conductance from the hot water to the outer wall of the heat exchanger U_h , can be evaluated by the following equations:

For laminar flow and a long tube, we can suppose $m = n = 0$, $K_R = 1$ and $C = 3.66$. On substituting the values, we get the following equation:

$$U_h = 3.66 \frac{K_w}{D} \quad \text{and similarly} \quad U_c = 3.66 \frac{K_w}{d} \quad (3.53)$$

The total thermal conductance U_k from the water to the walls is given as

$$(U_k)^{-1} = \frac{1}{U_h} + \frac{1}{U_c} \quad (3.54)$$

Then, h_f can be written as follows:

$$h_f = \frac{U_k}{L_{tb}} \quad (3.55)$$

The equations (3.48), (3.49) and (3.51) can be rewritten as follows:

$$Qu_{tb}' = \left[\frac{q_{ab}}{U_L} - (T_t - T_a) \right] / r_p = (T_t - T_{ti}) / r_t = (T_{ti} - T_f) / r_f \quad (3.56)$$

As result

$$Qu_{tb}' = \frac{\left[\frac{q_{ab}}{U_L} - (T_t - T_a) \right]}{r_p + r_t + r_f} \quad (3.57)$$

Thus

$$Qu_{tb}' = WF'U_L \left[\frac{q_{ab}}{U_L} - (T_f - T_a) \right] \quad (3.58)$$

Where

$$F' = \frac{1}{WU_L \left[\frac{1}{[(W - D)F + D]U_L} + \frac{e_t}{\pi A_{mw} \lambda_t} + \frac{1}{\pi d i h_f} \right]} \quad (3.59)$$

Table 3.4 formulae of F' and F for various configurations of collector.

	Formula	Collector configuration
pipe lower bond model	$F' = \frac{1}{\frac{WU_L}{\pi D h} + \frac{WU_L}{C_{bond}} + D + (W - D)F}$ $F = \frac{\tanh [m(W - D)]/2}{[m(W - D)]/2}$	

pipe upper bond model	$F' = \frac{1}{\frac{WU_L}{\pi D h} + \frac{D}{W} + \frac{1}{\left(\frac{WU_L}{c_{\text{bond}}}\right)} + \frac{W}{(W-D)F}}$ $F = \frac{\tanh [m(W-D)]/2}{[m(W-D)]/2}$	
pipe side bond model	$F' = \frac{1}{\frac{WU_L}{\pi d i h_f} + \frac{W}{D} + (W-D)F}$ $F = \frac{\tanh [m(W-D)]/2}{[m(W-D)]/2}$	

3.4 Fluid Temperature Distribution in Flow Direction

It is necessary to calculate the mean outlet fluid temperature in order to determine the useful heat energy gain. Thus, in this section, the fluid temperature distribution in flow direction is analysed. As illustrated in Figure 3.4, the energy gain obtained by a single tube is ultimately transferred to the fluid flowing through it.

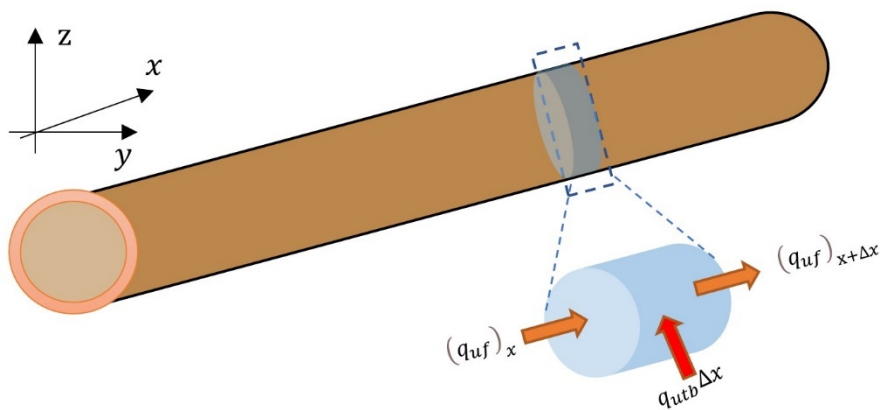


Figure 3.4 The energy flow through fluid.

The thermal balance of the fluid between the distances (x) and ($x + \Delta x$) can be written as follows:

$$\frac{\dot{m}_f}{n} c_f T_f|_x + qu_{tb} \Delta x = \frac{\dot{m}_f}{n} c_f T_f|_{x+\Delta x} \quad (3.60)$$

The simplification of equation (3.60) is given as follows:

$$\frac{\dot{m}_f}{n} c_f \frac{dT_f}{dx} = F'WU_L \left[\frac{q_{ab}}{U_L} - (T_f - T_a) \right] dx \quad (3.61)$$

$$\frac{dT_f}{dx} + \frac{n}{\dot{m}_f c_f} F'WU_L \left[-\frac{q_{ab}}{U_L} + T_f - T_a \right] = 0 \quad (3.62)$$

We can state two variables, \bar{T}_f and m' :

$$\bar{T}_f = T_f - T_a - \frac{q_{ab}}{U_L} \quad \text{and} \quad m' = \frac{nF'WU_L}{\dot{m}_f c_f} \quad (3.63)$$

Equation (3.62) can be rearranged as follows:

$$\frac{d\bar{T}_f}{dx} + m' \bar{T}_f = 0 \quad (3.64)$$

The differential equation (3.64) has the following solution:

$$\bar{T}_f(x) = C_1 \exp(-m'x) \quad (3.65)$$

Two boundary conditions are used to solve the differential equation. These are as follows:

For $x = 0$:

$$T_f|_{x=0} = T_{fi} \rightarrow \bar{T}_f = C_1 \exp(0) \Rightarrow T_{fi} - T_a - \frac{q_{ab}}{U_L} = C_1 \quad (3.66)$$

And for $y = \frac{W-D}{2}$:

$$\begin{aligned} T_f|_{x=L_{tb}} = T_{fo} \rightarrow \bar{T}_f = C_1 \exp(-m'L_{tb}) \Rightarrow \\ T_{fo} - T_a - \frac{q_{ab}}{U_L} = \left[T_{fi} - T_a - \frac{q_{ab}}{U_L} \right] \exp\left(-\frac{nF'WU_L}{\dot{m}_f c_f} (L_{tb})\right) \end{aligned} \quad (3.67)$$

Therefore,

$$\frac{T_f(x) - T_a - \frac{q_{ab}}{U_L}}{T_{fi} - T_a - \frac{q_{ab}}{U_L}} = \exp\left(-\frac{nF'WU_L}{\dot{m}_f c_f} (x)\right) \quad (3.68)$$

The maximum outlet fluid temperature at the end of tube can be expressed as follows:

$$T_{fo} = \left[T_{fi} - T_a - \frac{q_{ab}}{U_L} \right] \exp \left(- \frac{nF'WU_L}{\dot{m}_f c_f} (L_{tb}) \right) + T_a + \frac{q_{ab}}{U_L} \quad (3.69)$$

In general

$$T_f(x) = \left[T_{fi} - T_a - \frac{q_{ab}}{U_L} \right] \exp \left(- \frac{nF'WU_L}{\dot{m}_f c_f} (x) \right) + T_a + \frac{q_{ab}}{U_L} \quad (3.70)$$

After the determination of outlet fluid temperature, we can rewrite the useful energy rate as follows:

$$Qu = \dot{m}_f c_f (T_{fo} - T_{fi}) = \dot{m}_f c_f \left(\left[T_{fi} - T_a - \frac{q_{ab}}{U_L} \right] \exp \left(- \frac{nF'WU_L}{\dot{m}_f c_f} (L_{tb}) \right) + \left[\frac{q_{ab}}{U_L} + T_a \right] - T_{fi} \right) \quad (3.71)$$

$$Qu = \dot{m}_f c_f \left(- \left[\frac{q_{ab}}{U_L} - (T_{fi} - T_a) \right] \exp \left(- \frac{nF'WU_L}{\dot{m}_f c_f} (L_{tb}) \right) + \left[\frac{q_{ab}}{U_L} - (T_{fi} - T_a) \right] \right) \quad (3.72)$$

$$Qu = \dot{m}_f c_f \left(- \left[\frac{q_{ab}}{U_L} - (T_{fi} - T_a) \right] \exp \left(- \frac{nF'WU_L}{\dot{m}_f c_f} (L_{tb}) \right) + 1 \right) \quad (3.73)$$

$$Qu = \dot{m}_f c_f \left[\frac{q_{ab}}{U_L} - (T_{fi} - T_a) \right] \left\{ 1 - \exp \left(- \frac{nF'WU_L}{\dot{m}_f c_f} (L_{tb}) \right) \right\} \quad (3.74)$$

3.4.1 Collector Heat Removal Factor

The collector heat removal factor F_R is defined as the ratio of the actual useful heat energy gain to the maximum useful energy gain. The latter can be attained when the collector is at the inlet fluid temperature, for the reason that the heat loss to the surroundings is then at a minimum. The maximum useful energy gain is expressed as follows:

$$Qu|_{T_p=T_f} = AU_L \left[\frac{q_{ab}}{U_L} - (T_{fi} - T_a) \right] \quad (3.75)$$

Thus, the collector heat removal factor is defined as follows:

$$F_R = \frac{Qu}{Qu|_{T_p=T_f}} = \frac{\dot{m}_f c_f}{AU_L} \left(1 - \exp \left(- \frac{nF'WL_{tb}U_L}{\dot{m}_f c_f} \right) \right) \quad (3.76)$$

The collector heat removal factor times this maximum possible useful energy gain is equal to the actual useful energy gain, which can be rewritten as follows:

$$Qu = AU_L F_R \left[\frac{q_{ab}}{U_L} - (T_{fi} - T_a) \right] \quad (3.77)$$

The equation (3.77) is extremely useful in the evaluation of thermal solar collectors' performance. With it, the useful heat energy gain can be calculated as a function of the inlet fluid temperature. Since the inlet fluid temperature is usually known and easily measured, and the overall heat loss coefficient can be calculated as described above, hence, this is a convenient representation when analysing thermal solar systems.

After calculating the heat removal factor and the useful heat energy rate, the mean temperature of absorber plate can be determined as follows:

$$T_p = T_{fi} + \frac{Qu}{AF_R U_L} (1 - F_R) \quad (3.78)$$

The instantaneous thermal efficiency of the collector can be calculated as follows:

$$\eta_{th} = F_R \left(\tau\alpha - U_L \frac{(T_{fi} - T_a)}{G^*} \right) \quad (3.79)$$

3.5 Computational Programming Methodology

For the application of solar energy, it would be desirable to carry out a theoretical analysis of the given heating system as extensively as possible before proceeding with the experimental work. This is an important step that may save time, budget and efforts. There are numerous software tools and computer programmes that help to accurately predict the thermal performance of the investigated system.

3.5.1 Calculation Programme Principle

The equations described in the sections above should be presented in a manner that is convenient for solving by computer programmes in structured languages such as FORTRAN, PYTHON, MATLAB...etc. Typically, this means that the requested equations are simplified, and iterative solutions are required. It is only mandatory to write the equations in an appropriate form and let the calculation programme organize the solution.

The method used by Hottel, Willliier and Bliss to evaluate the thermal performance of a solar collector has been adopted. A method that assumes, in permanent mode, that the average temperatures of all components of the collector are constant and uniform, while neglecting transient effects. This method can be shipped in an algorithm that allows to take into consideration the thermo-physical, optical and geometric parameters, which include all the governing equations of solar thermal collector. The calculation model of the developed algorithm

is based on an iterative resolution of the energy balance equations of the solar thermal collector that takes into account the associated boundary conditions.

The mathematical equations are restructured in an algorithm. The latter is transferred to a computational program under MATLAB environment to simulate the thermal performances of the investigated flat plate thermal solar collector. As shown in Figure 3.5, the optical, thermal and geometrical properties of the heating system and the weather conditions are considered as constant parameters for a given period. At time $t_{i=0}$, reasonable initial estimated value of top transparent cover and absorber plate temperatures are set to be related to the inlet fluid temperature (for the cover $T_{c_{i=0}} = T_{fi_{i=0}} + 10^{\circ}\text{C}$ and for the absorber plate $T_{p_{i=0}} = T_{fi_{i=0}} + 20^{\circ}\text{C}$). Using the climatic data and the required parameters as inputs to calculate U_L , F_R and Qu . A novel value of T_p is gained and applied to recalculate U_L , F_R and Qu . An iterative calculation is required if the difference between the new calculated value and the previous one is exceeding an absolute error value of ξ , $|(T_p)_{j+1} - (T_p)_j| < \xi^{\circ}\text{C}$. This operation is repeated again for an additional time step of Δt minutes, $t_{i=i+1} = t_i + \Delta t$ minutes, until the programmed end time. Basic outputs of the calculation model are all heat loss coefficients, mean absorber temperature and thermal efficiency. Other outputs such as outlet fluid temperature, absorber energy rate and useful energy rate can also be supplemented by the model. The computational program can be modified to be suitable for investigating several types of collectors.

3.5.2 Calculation Programme Steps

The calculation programme is based on the following steps:

First step:

Enter the different characteristics of the collector and climatic data.

Weather data:

Solar radiation; Wind speed; Ambient temperature...etc.

Thermophysical parameters:

Thermal conductivity of elements; Working fluid mass flow rate; Viscosity...etc.

Optical parameters:

Transmittance coefficient; Absorptance coefficient; Emissivity...etc.

Geometric parameters:

Lengths, widths and thicknesses of components; Tubes diameters...etc.

Second step:

Assume the initial temperatures of different elements as follows:

For transparent cover temperature $T_{c_i=0} = T_{fi_i=0} + 10^{\circ}\text{C}$.

For absorber plate temperature $T_{p_i=0} = T_{fi_i=0} + 20^{\circ}\text{C}$.

Third step:

Calculate the different heat losses coefficients such as:

Heat transfer coefficients by conduction, convection and radiation; Front, back and overall heat transfer coefficients.

Forth step:

Calculate and verify the cover temperature initially assumed.

Compare the calculated/ recalculated value to the starting/ previously recalculated value.

If the difference exceeds a convergence criterion of ξ , $|(T_c)_{j+1} - (T_c)_j| < \xi = 0.01^{\circ}\text{C}$, the calculation loop is repeated by taking the recalculated value as initial value.

Otherwise, the calculation is stopped by retaining the results of the last loop, and going to the next step.

Fifth step:

Calculate the different collector factors such as:

Sheet efficiency, collector efficiency factor, collector heat removal factor.

Sixth step:

Calculate and verify the absorber plate temperature initially assumed.

Compare the calculated/ recalculated value to the starting/ previously recalculated value.

If the difference exceeds a convergence criterion of ξ , $|(T_p)_{j+1} - (T_p)_j| < \xi = 0.01^{\circ}\text{C}$, the calculation loop is repeated by taking the recalculated value as initial value.

Otherwise, the calculation is stopped by retaining the results of the last loop, and going to the next step.

Seventh step:

Calculate:

The outlet fluid temperature and instantaneous thermal efficiency.

Eighth step:

Repeat the same process for an additional time until the ending programmed time.

Nineth step:

Print the outputs.

3.5.3 Calculation Programme Organigram

The different steps mentioned above are represented in the following flowchart as follows:

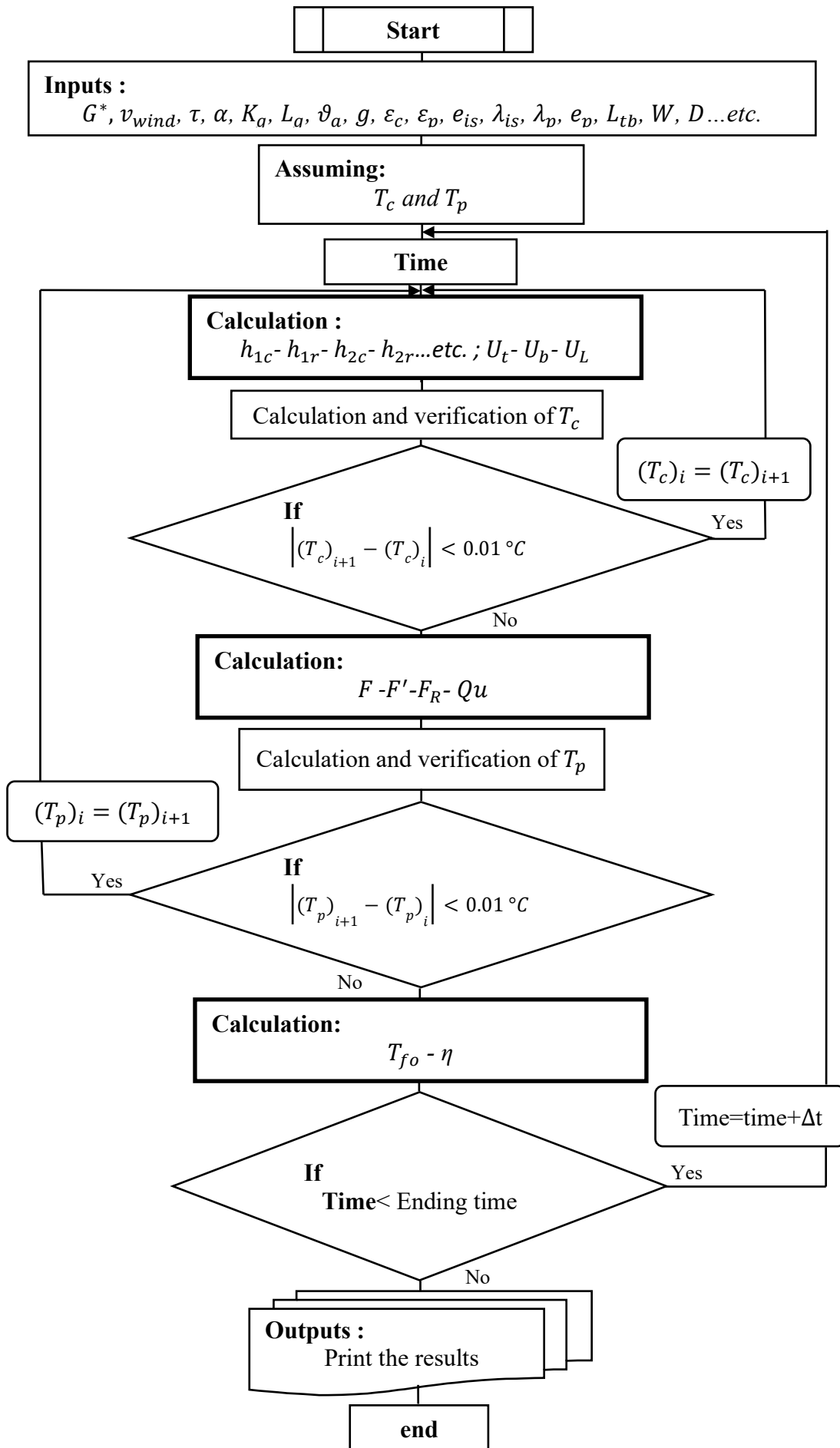


Figure 3.5 Calculation programme organigram.

3.6 Conclusion

A detailed theoretical approach of a flat plate solar thermal collector is presented. The equations describing this approach are restructured into an algorithm and then solved using a computational program under MATLAB environment to simulate the thermal performance of the studied collector. The predicted results obtained from the calculation program are validated using the results of the experimental work that carried out on a typical thermosyphon flat plate solar water collector, which will be described in the next chapter.

Chapter 4: Experiments Carried Out on Flat Plate Solar Water Collector

In this part, a general description of the experimental bench as well as the different measuring devices used and the procedure followed for the conduct of the tests, are presented. We consider a typical flat plate solar water collector that installed at Renewable Energy Applied Research Unit (URAER). Moreover, the chapter also includes the instrumentation calibration procedure and the instruments accuracy of measuring devices.

4.1 Site Characteristics

The experimental apparatus is placed at Renewable Energy Applied Research Unit (URAER), see Figure 4.1, located at Gart Taam Z.I daïra Bounoura wilaya of Ghardaïa, Algeria. The geographic coordinates of the site are $32^{\circ} 23'$ north latitude, $3^{\circ} 46'$ east longitude and 467m altitude [87]. Given its geographical position and its distance from the Mediterranean coast (about 750km), the weather conditions of Ghardaïa benefit from an arid and dry climate, characterised by exceptional sunshine duration and solar radiation intensity. In general, it has eminent potential of solar radiation intensity, where the annual average of the global solar irradiation measured on a horizontal plane surpasses 6000Wh/m^2 . In addition, its sunshine duration is more than 3000 hours/year, which favours the application of solar energy systems for various fields.



Figure 4.1 Location of URAER [88].

4.2 Measurement Station Features

The application of solar energy requires a complete and detailed knowledge of climatic data of the site. This can be easy when the site is equipped with a measurement station. To evaluate thermal solar conversion systems, a radiation database is essential. The installation of

the measurement station at the URAER site comes within this context, which makes it possible to better characterise the site. The meteorological station of the site is equipped with reliable sensitive sensors to ensure the measurements of the solar irradiation components (global, direct and diffuse) on a horizontal plane, normal plane and inclined plane to the latitude of the place. Moreover, the station is equipped with advanced tools to measure ancillary meteorological parameters such as humidity, atmospheric pressure, wind speed and ambient temperature. The recording of these parameters is done daily for 24 hours throughout the year.

4.3 Experimental Heating System Description

The heating system used for the experimental work is a conventional flat plate thermal solar collector based on thermosiphon working fluid circulation. This heating device is a one-piece assembly consisting of a flat plate panel of 2.60m² connected to a storage tank of 155L located in the upper part of the assembly; to ensure the closed loop thermosiphon fluid movement. To facilitate the displacement, the orientation and the inclination of the assembly, a mobile support adapted to the test conditions was exploited. The support is fixed on an angle of inclination that corresponds to the latitude of the place (Ghardaïa, 32°) and oriented toward south.



Figure 4.2 Photograph of the experimented flat plate thermal solar collector.

4.3.1 Heating System Components

The tested thermosyphon flat plate thermal solar system incorporates various elements. In the following paragraphs, a detailed description of the elements used during the experiment is provided.

The characteristics of the main components of the heating system are:

Casing

Dimensions (L/W/H)	2050 / 1270 / 91 mm
Material of the frame	PVC-aluminium profiles
Inclination	32°

Top transparent cover

Dimensions (L/W/H)	1950 / 1180 / 4 mm
Material of the cover	ordinary glass
Shape of cover	flat plate sheet
Number of covers	1

Absorber sheets

Dimensions (L/W/H)	1800 / 100 / 1 mm
Material of sheets	aluminium
Shape of sheets	flat plate sheets
Number of sheets	10
Coating of sheets	black paint

Tubes (risers)

Dimensions (L/D/d)	1800 / 10 / 8 mm
Material of tubes	copper
Number of tubes	10

Back isolation

Dimensions (L/W/H)	1900 / 1100 / 50 mm
Material of insulation	Rockwool

Sealing system

Material of sealing black gasket and transparent silicone

4.4 Instruments of Measurement

4.4.1 Measurement of Temperature

The temperatures of different heating system components, such as transparent cover, absorber plate, storage tank, ambient...etc, are measured using Nickel-Chromium/Nickel-Aluminium thermocouples type K (see Figure 4.3). These thermocouples, with a diameter of 0.5 mm, have good accuracy and large temperature rang.

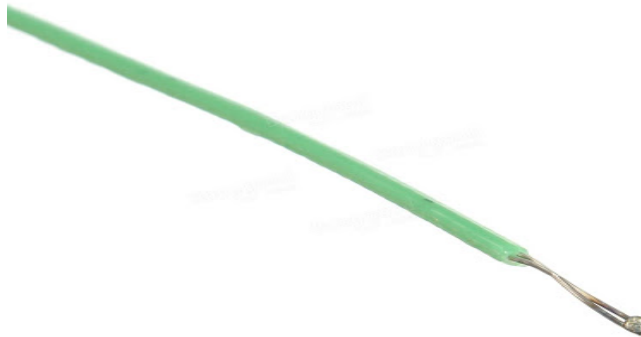


Figure 4.3 Photograph of the thermocouple used for measurement.

In our experiment, we used several thermocouples for different locations on heating system as follows:

01 thermocouple is installed on the front transparent cover.

01 thermocouple is installed on the absorber plate.

01 thermocouple is installed on the back insulator.

01 shaded thermocouple for ambient temperature.

02 thermocouples are installed into the collector inlet and outlet fluid side.

02 thermocouples are installed into the storage tank inlet and outlet fluid side.

4.4.2 Measurement of Solar Irradiation

The measurement of the incident solar irradiation is carried out using a Pyranometer Kipp-Zonen type. The latter is mounted on a metal support equipped with Solys2 solar tracker and sun sensor in order to measure the solar radiation at any inclination and orientation angles, see Figure

4.4. All these instruments are mounted on Solys2 solar tracker with sun sensor. A data logger type Campbell Scientific CR1000 is used to record the data daily for one minute and ten minutes averages.



Figure 4.4 Photograph of the pyranometers used for measurement.

The pyranometer can directly measure the beam solar radiation and diffuse solar radiation if the sensing element is shaded from the beam radiation. For this purpose, a shadow band is mounted with its axis tilted at an angle equal to the latitude of the location plus the declination for the day of measurement (see Figure 4.4). Since the shadow band hides a considerable portion of the sky, the measurements require corrections for that part of diffuse radiation obstructed by the band.

4.4.3 Data Acquisition

A data logger type AGILENT-34970A connected to a computer is used for data acquisition which permits the recording of different temperatures and other useful parameters, see Figure 4.5. Besides, an Agilent Benchlink data acquisition software is installed in the computer system, this program also has graphic capabilities to visualise the internal data. The registration of temperatures is done daily with five-minute step.



Figure 4.5 Photograph of the data logger and the computer.

4.5 Instruments Accuracy

In this part, we are focusing on the accuracy of instruments used during measurements. This analysis allows to estimate the measurement uncertainty relating to the measured parameters taken during the experimental work.

Depending on the devices used in our experiment, the potential errors of instruments that should be considered are:

- Accuracy of pyranometers.
- Accuracy of thermocouples.

For the estimation of the error, noting for example ΔT the standard deviation between the measured value and the true value, an uncertainty is therefore given in the form $\pm\Delta T$.

4.5.1 Accuracy of pyranometers

The pyranometers installed at the URAER measurement unit are of Kipp-Zonen type. These devices are widely used due to their reliability and high sensitivity. They have an accuracy of about $\pm 3\%$ for the measurement of solar radiation intensity.

4.5.2 Accuracy of Thermocouples

The thermocouples fixed on the heating system are of type K, according to the manufacturer's instructions, they have an accuracy of $\pm 2\%$ for temperature measurements.

4.5.3 Thermocouple Calibration

All thermocouples used in this experiment are calibrated by a professional engineer. The tools employed for the calibration of thermocouples are:

- Thermometer
- Glass kettle
- Power supply

The steps of thermocouples calibration are:

- Fill the glass kettle with water and heat it up to the boiling point.
- Put both thermocouples and thermometer inside the glass kettle.
- Connect thermocouples to the data logger and then to the computer.
- Register the results from both thermocouples and thermometer.
- Repeat these steps several time (at least 3 times).
- Take the average value from both thermocouples and thermometer.

4.6 Experiment Procedure

4.6.1 Experiment Schematic Diagram

The schematic diagram of the whole experimental test rig setup with the location of the instruments (measuring tools and recording devices), is illustrated in Figure 4.6. The numbers show elements and instruments used for this experiment, for example, 1 represents the flat plat heating panel system, 2 represents the storage tank. 3, 4, 5 and 6 represent the location of the thermocouples for the absorber plat, front glass cover, inlet fluid and outlet fluid, respectively. Also, 7 and 8 are thermocouples that measure the temperatures of the fluid at the inlet and outlet of storage tank respectively. 9 is data acquisition system, 10 is meteorological data system and 11 is a computer.

The thermocouples (3, 4, 5, 6, 7 and 8) that represented in Figure 4.6 are related to the data acquisition system (9). The latter is connected with a computer (11) in order to save and

display results. In addition, meteorological data collection system (10) is used to record the solar radiation during the experiment.

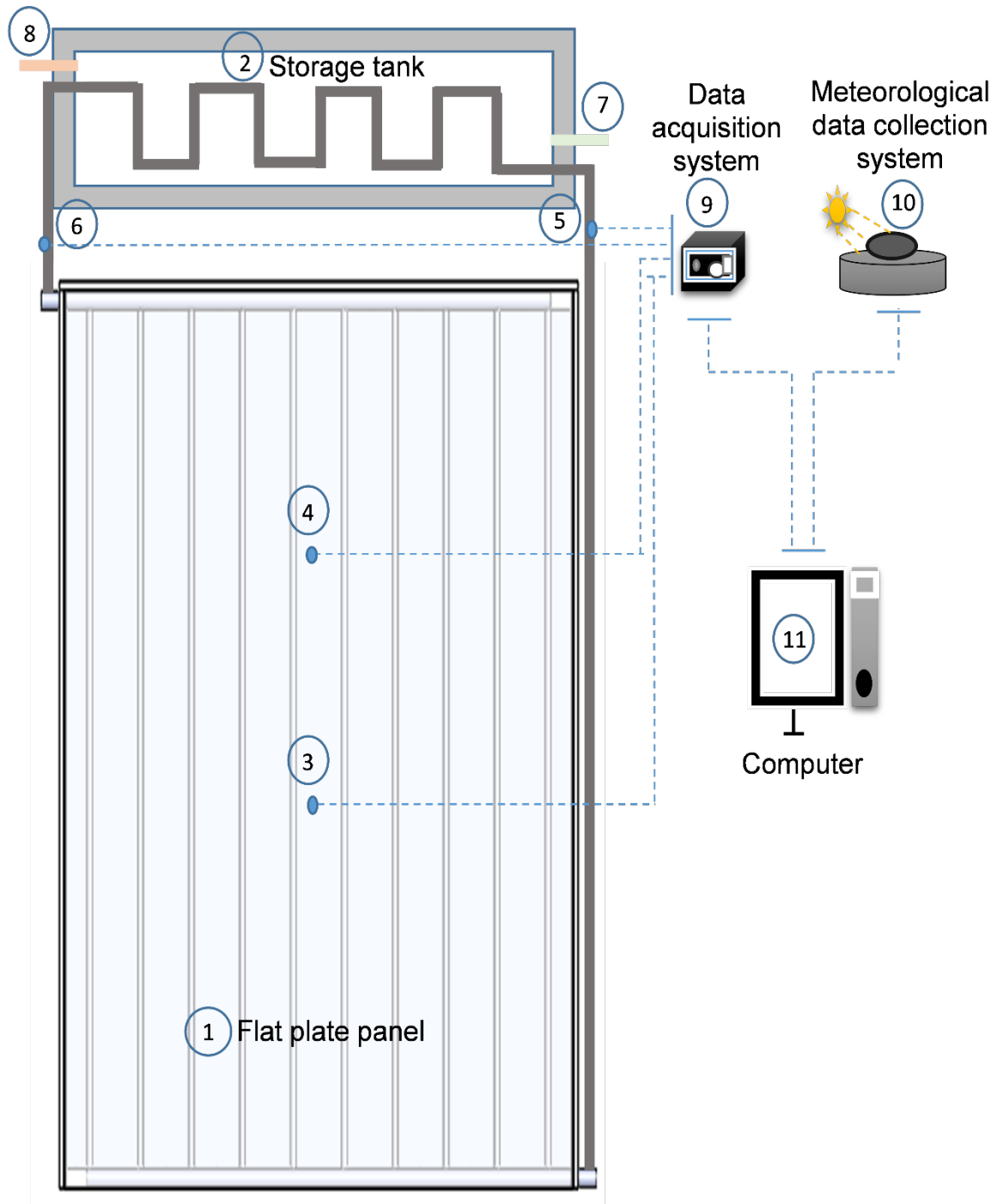


Figure 4.6 Schematic diagram of the experiment.

4.6.2 Procedure of the Experimental Work

The procedure of the experimental work was carried out as mentioned below:

- Open the inlet valve to fill the storage tank with water.
- Replenish the closed thermosyphon loop with working fluid and check if it is completely filled.
- Fix the thermocouples in their appropriate positions.
- Prepare data acquisition system and computer to register the data.
- Relate thermocouples with data acquisition system and then connect the data acquisition system to the computer.
- Instal data acquisition system software in computer system.
- Put data acquisition system and computer inside a cupboard to protect them from risk of wind, rain, dust...etc.
- Start the tests.

4.6.3 Recommendations Before Starting Tests

Before commencing the tests on our heating system, the following conditions must be respected for the smooth running of the experiment:

- ✓ Make sure that there are no leaks or damage in the heating system components.
- ✓ Make sure that the closed thermosyphon circulation and storage tank are fully filled.
- ✓ Make sure that the front transparent cover is well cleaned.
- ✓ Ensure that there are no external disturbances (external heat source, shadow effect, dust...etc.).
- ✓ Ensure that all measuring devices are in proper condition and well installed.
- ✓ Ensure that the orientation and inclination of the heating system panel are at optimum angles for maximum solar capture.
- ✓ The heating system should be exposed to natural conditions of clear sky and ambient temperature (outdoor test) for real evaluation of thermal performance.

The respect of these recommendations is paramount to ensure reliable results and to achieve better performance of the solar heating system.

4.7 Conclusion

The experimental setup of a typical thermosyphon solar water collector is presented in this chapter. There are two main aims from the experimental work, the first aim is to experimentally investigate this kind of heating system in order to better understand it. The second aim is to validate the theoretical thermosyphon model predictions by comparing the results obtained from experimental tests with the calculation programme results.

Chapter 5: Results and discussions

After describing the theoretical model, the computational programme and the experimental work carried out on the flat plate solar water collector. We present in this chapter the results of the calculation and experiment as well as the model validation. In addition, this chapter includes a comparison between the three different configurations of solar collector (the new proposed configuration and two other traditional configurations). An investigation is conducted to identify the influence of insulation technique, selective coating and the number of tubes on the thermal performance of the studied solar collectors. Furthermore, the cost evaluation of each collector is discussed.

5.1 Experimental Results and Model Validation

In order to study the thermal behaviour of a solar collector, a detailed theoretical analysis of each part of the collector is required and a computational calculation program should be executed. The experimental data such as solar irradiation and measured temperatures (ambient, inlet fluid, absorber plate temperatures...etc) are mandatory for both calculation inputs and the validation of obtained results.

5.1.1 Solar Radiation Measurement

The term solar irradiation means the power coming from the sun that attains a surface per unit area over a specific period of time. Direct solar irradiation is the part that directly reaches a surface; diffused solar irradiation is the part that is scattered by the atmosphere; and global solar irradiation is the sum of both direct and diffused components achieving the same surface.

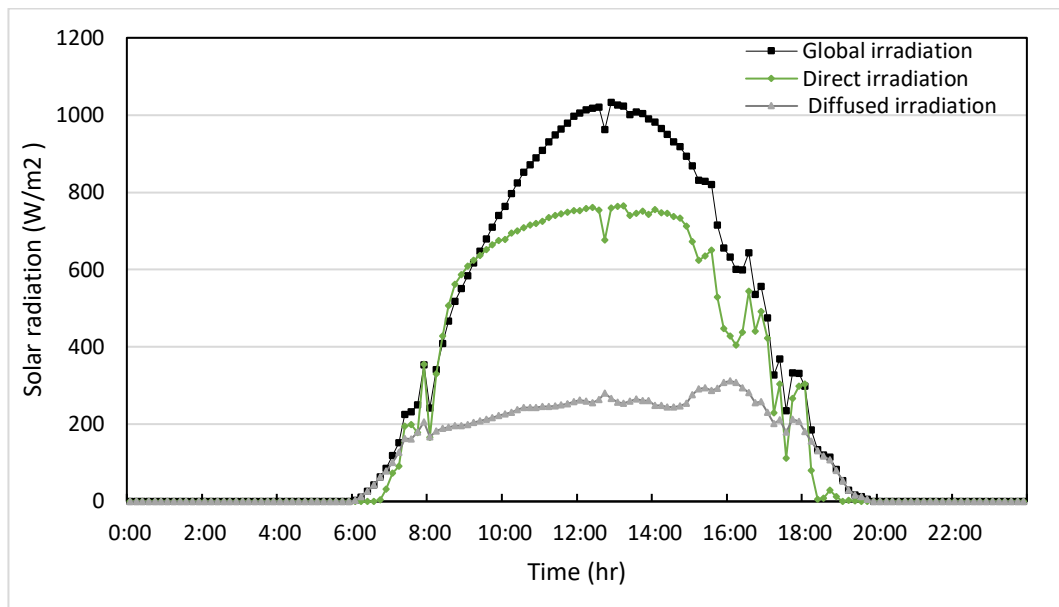


Figure 5.1 Evolution of diffused, direct and global solar irradiation as a function of local time during 22nd May.

In our study, the thermal performance of the investigated solar water collector system is evaluated considering the climatic data of Renewable Energy Applied Research Unit (URAER), located at Ghardaïa, Algeria during 22nd May. The solar irradiation data of the presented day, see Figure 5.1, consists of hourly solar irradiation and shows the evolution of the global, direct and diffused solar irradiation as a function of the local time. A regular evolution of solar irradiation is observed over day time. This is a typical day for the researchers which follows the theoretical pattern with a small margin of error. However, perturbations are remarked starting in the

afternoon. These perturbations are caused by the presence of some clouds that reflect the observed oscillation.

5.1.2 Temperatures Measurement

The measured temperatures such as ambient, absorber and inlet fluid temperature as well as the geometric parameters of the thermal solar collector presented in chapter 4 are introduced as input data to the developed program, in order to validate this latter.

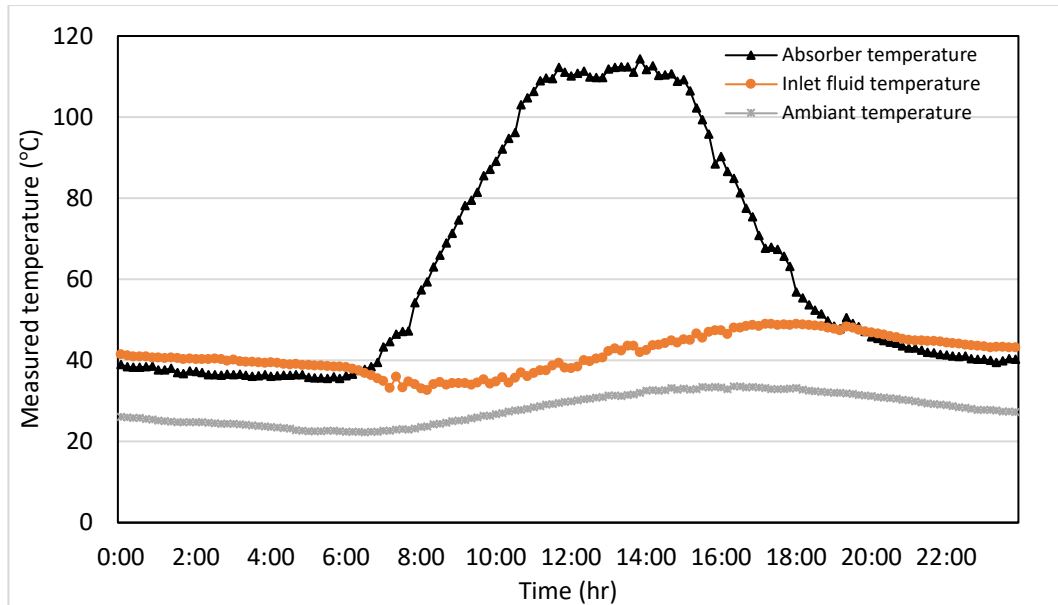


Figure 5.2 Evolution of absorber plate temperature, ambient air temperature and inlet fluid temperature as a function of local time during 22nd May.

Figure 5.2 illustrates the variation of absorber plate temperature, ambient air temperature and inlet fluid temperature as a function of local time during 22nd May. As shown in Figure 5.2, in the morning, when solar radiation starts to hit the flat plate of the collector, the plate absorbs this radiation and begins to heat up. As a result, the temperature of the plate rises steadily until it reaches its maximum value around noon when solar radiation is at its peak. At this point, the flat plate is absorbing solar energy at its maximum rate. However, as the day progresses past noon, the intensity of solar radiation starts to decrease. Since the flat plate is no longer receiving as much energy from the sun, its temperature begins to decrease as well. This decline continues until sunset, when solar radiation is no longer present to heat the plate. On the other hand, the temperature of the inlet fluid (which circulates through the risers' tubes to absorb heat) increases from morning until sunset due to the continuous circulation of the fluid through the collector system. Even though the flat plate temperature decreases after reaching its peak at noon, there is still heat accumulated within the storage tank fluid. The latter is well insulated against heat

losses. As the working fluid flows through the tubes, it absorbs this stored heat, causing its temperature to continue rising throughout the day until sunset. The ambient temperature varies from 22.28°C -minimum value- at 6:30 to 33.55°C -maximum value- at 16:30. Its average temperature is 27.97°C. It is worth to mention that the heating system is working under natural closed-loop fluid flow circulation (thermosyphon effect). Consequently, the average value for inlet fluid temperature is about 41.49°C. The minimum and the maximum values of inlet fluid temperature are 32.67°C at 8:10 and 48.94°C at 17:20, respectively, as shown in Figure 5.2.

5.1.3 Model Validation

The theoretical model presented in chapter 3 is developed and coded using MATLAB software. This model contained geometrical and thermo-physical properties of the examined thermal solar collector, see Table 5.1 . The results obtained using our computational program are validated by experimental data in terms of the absorber plate temperature. Validation of the theoretical model is shown in Figure 5.3.

Table 5.1 Characteristics of the examined flat plate solar collector.

Parameters	Characteristics
Number of covers	1
Cover transmittance	0.88
Cover thickness	4 mm
Fluid in front gap	Air
Absorber material	Aluminium
Absorber thermal conductivity	286 W/m K
Absorber absorptance	0.95
Absorber emissivity	0.95
Absorber thickness	1 mm
Absorber width	100 mm
Tube material	Copper
Tubes thermal conductivity	380 W/m K
Number of tubes	10
Tube inner/outer diameter	8/10 mm
Tube length	1800 mm
Working fluid	Water

Mass flow rate	0.01 kg/s
Insulator material	Rook wool
Insulation thickness	50 mm

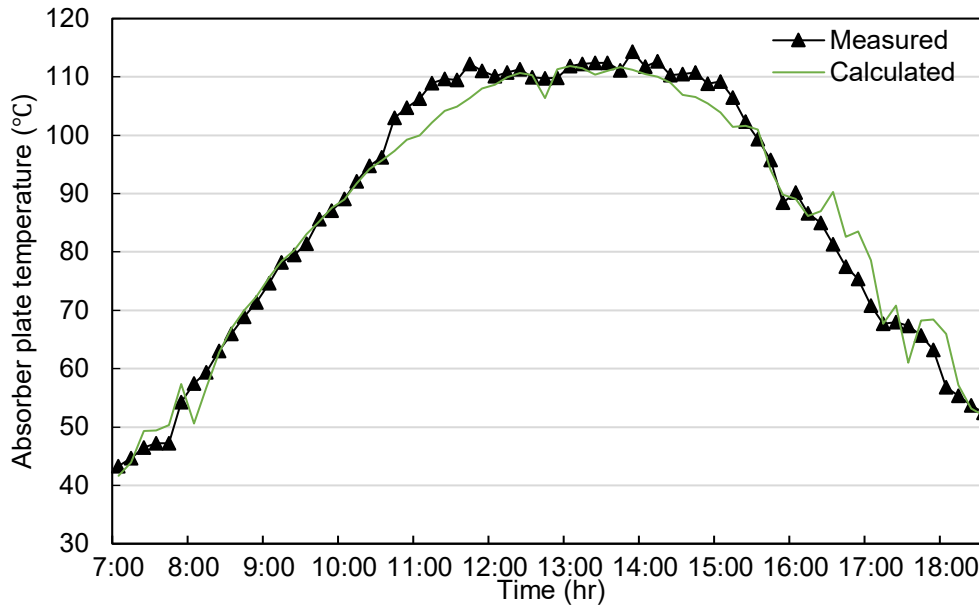


Figure 5.3 Evolution of measured and calculated absorber plate temperatures as a function of local time during 22nd May.

Figure 5.3 presents the comparison between measured and calculated absorber plate temperatures as a function of local time during 22nd May. As represented in this figure, experimental and numerical absorber plate temperatures simultaneously increase due to the regular augmentation of solar irradiation from early morning 7:00 until midday. After that, from noonday to 15:00, measured and predicted absorber plate temperatures remain nearly constant for the reason that the heating system reaches its maximum level. Then, both temperatures decrease according to the normal decline of solar irradiation. It is noticeably clear that the pattern and values of measured absorber plate temperatures have been closely predicted and followed by calculated results, except certain moments. For the reason that the calculated absorber plate temperature depends on the real time pyranometer solar irradiation measurement. The high precision of the pyranometer is recognised by a rapid response time and high sensitivity to solar irradiation fluctuations that is generated by intervening clouds through the solar beam path to the sensor. However, the absorber plate temperature is measured using a thermocouple fixed on the absorber sheet which represents a medium of high thermal energy storage and this delay the temperature change. Therefore, unlike the pyranometer, the thermocouple measurement cannot

immediately follow instantaneous temperature variations resulting from solar irradiation fluctuations. Therefore, this leads to a notable divergence between measured and calculated temperatures starting from 10:30, 14:00 and 16:30. As a conclusion, results exhibit a close agreement between measured and calculated absorber plate temperatures, where the value of mean absolute percentage error (MAPE) is about 3.3%, and R-squared (R^2) attains 0.97.

The MAPE expressed in percentage and associated with measured temperature and calculated temperature is presented as follows:

$$MAPE = \frac{1}{n} \sum_{i=1}^n \left| \frac{T_i - \hat{T}_i}{T_i} \right| \quad (5.1)$$

And R^2 is expressed as follows:

$$R^2 = 1 - \frac{\sum_{i=1}^n (T_i - \hat{T}_i)^2}{\sum_{i=1}^n (T_i - \bar{T})^2} \quad (5.2)$$

5.2 Contribution to Collector Performance Enhancement

As presented in chapter 2, there are numerous techniques to improve the performance of a thermal solar collector, which were deeply investigated and analysed by researchers. In this study, our contribution is to investigate a new technique of thermal insulation accompanied with a new configuration of solar collector in order to improve thermal performance of a flat plate solar collector. The investigated new configuration is characterised by a curved evacuated top glass cover and rear rock wool insulation.

5.2.1 Specifications of New Configuration

The proposed new configuration is based on a combination of two conventional heating systems; the flat plate solar collector (FPSC) and the evacuated tube solar collector (ETSC) [89]. The inspired design of the new vacuum flat plate solar collector (VFPSC) is structurally quite the same as the traditional flat plate solar collector, see Figure 1.6, except for the upper part of the collector, namely; the vacuum insulation in the inner gap between absorber plate and the top curved cover, as schematically shown in Figure 5.4. This inner space has no specific vacuuming in the traditional FPSC, while it is assumed to be evacuated to certain degrees in the proposed new VFPSC configuration. Indeed, the vacuum insulation used in evacuated tube solar collectors has proven to be the best insulation technique that can be used to prevent convective and conductive heat losses [90] [91]. This inspired us to evacuated the front side of the proposed configuration.

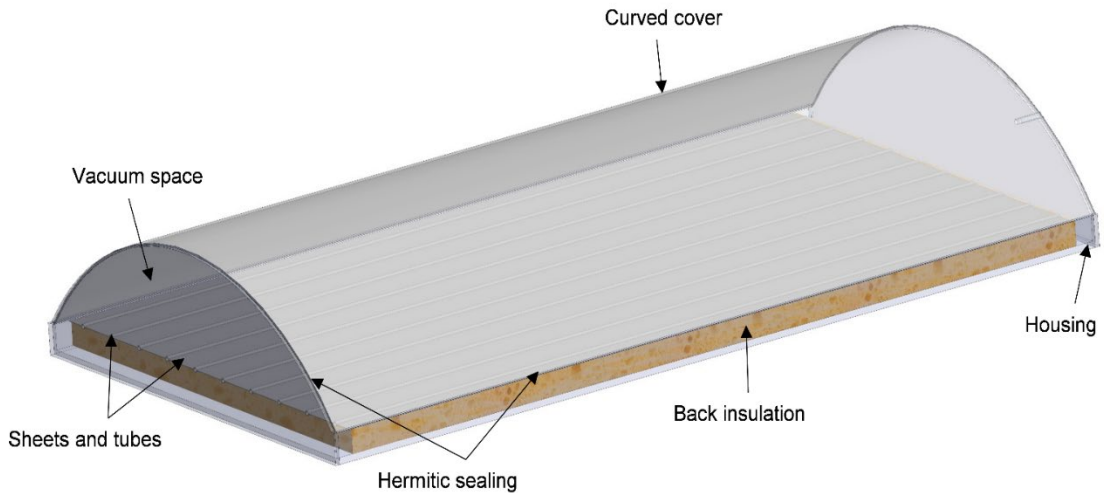


Figure 5.4 Isometric view of the proposed VFPC.

5.2.2 Insulation Technique Effect

In this analysis, we theoretically compare three types of solar collectors using different insulation techniques. It is worth to mention that the new VFPC and the both conventional FPSC / ETSC have similar characteristics of absorber sheets such as width, length, thickness, etc. and also the same tubes diameters, length and material. Details of standard collectors' parameters are presented in Table 5.1, except vacuum environment in the front gap of new VFPC.

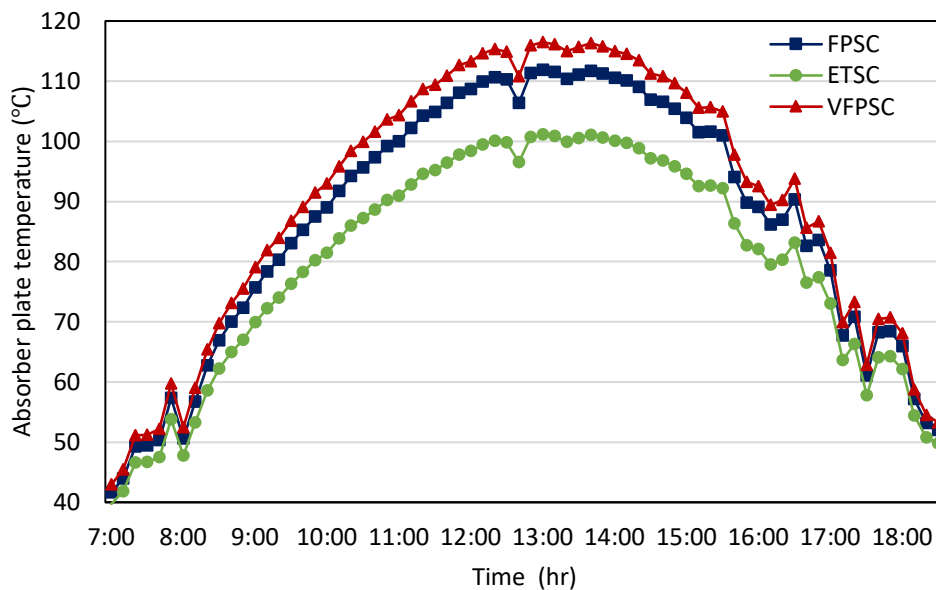


Figure 5.5 Evolution of absorber plate temperature of FPSC, ETSC and VFPC as a function of local time.

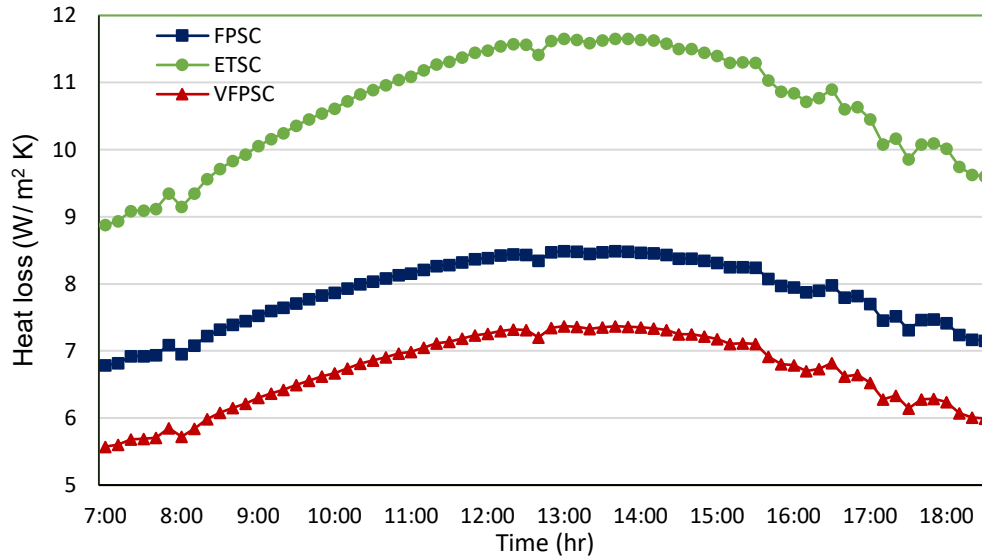


Figure 5.6 Evolution of overall heat loss of FPSC, ETSC and VFPSC as a function of local time.

Figures 5.5 and 5.6 respectively show the absorber plate temperature and the overall heat loss of FPSC, ETSC and VFPSC as a function of local time. As can be seen in Figure 5.5, the absorber plate temperature of VFPSC achieves the highest values during the whole day. For the reason that this new configuration has the best insulation against conductive/convective heat loss and thus lower overall heat loss compared to FPSC. Despite the ETSC and VFPSC have the same insulation technique from the front side, the back side of ETSC suffers from radiative heat loss. The latter is prevented by using rockwool insulator from the back side of VFPSC, which minimises its overall heat loss, see Figure 5.6. ETSC represents the worst results for the reason that this type of collector works efficiently by applying selective coating surfaces of low thermal emissivity, more details are given in the next subsection below.

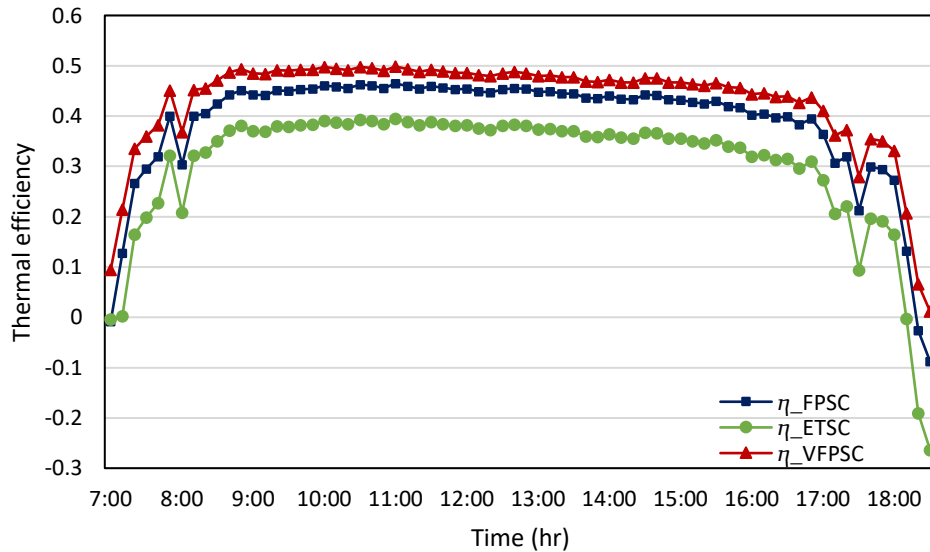


Figure 5.7 Evolution of thermal efficiency of FPSC, ETSC and VFPC as a function of local time.

Figure 5.7 shows the thermal efficiency of FPSC, ETSC and VFPC as a function of local time. As shown in Figure 5.7, FPSC, ETSC and VFPC attain overall thermal efficiency of 0.44, 0.37 and 0.48, respectively. As a result, the VFPC exhibits the highest absorber temperature and the lowest overall heat loss, therefore its thermal efficiency attains the best results among the studied collectors, see Figure 5.7.

5.2.3 Selective Coating Effect

The new VFPC and the conventional (FPSC and ETSC) are theoretically investigated for different range of absorber emissivity. At solar radiation of 1025.5 W/m^2 , a comparison between the different thermal solar collectors is done using the same parameters mentioned in the above subsection and Table 5.1. But only the absorber emissivity varies from 0.05 to 0.95 for all investigated collectors. The influence of the selective coatings on absorber plate temperature, overall heat loss, thermal efficiency is discussed.

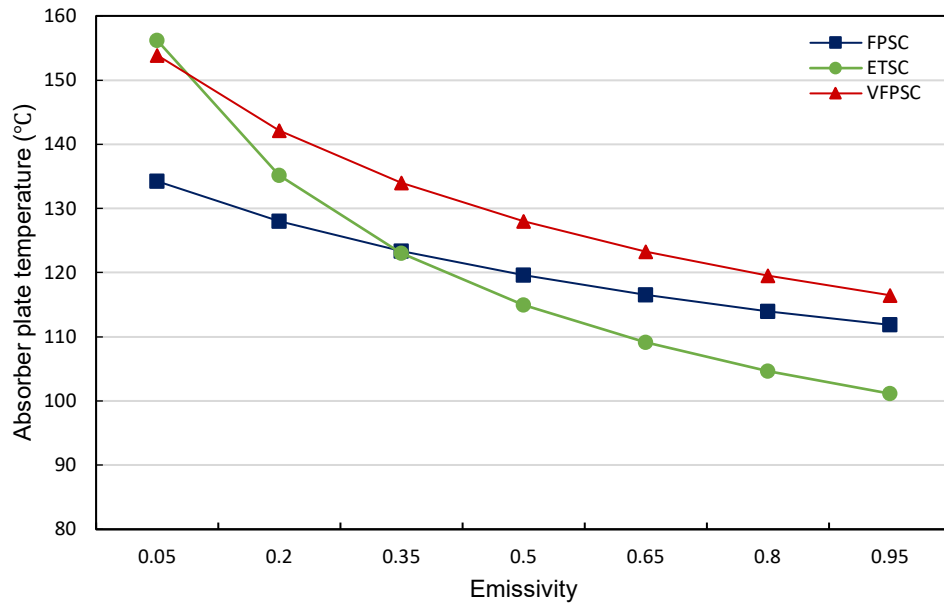


Figure 5.8 Absorber plate temperature of FPSC, ETSC and VFPC for different absorber emissivity.

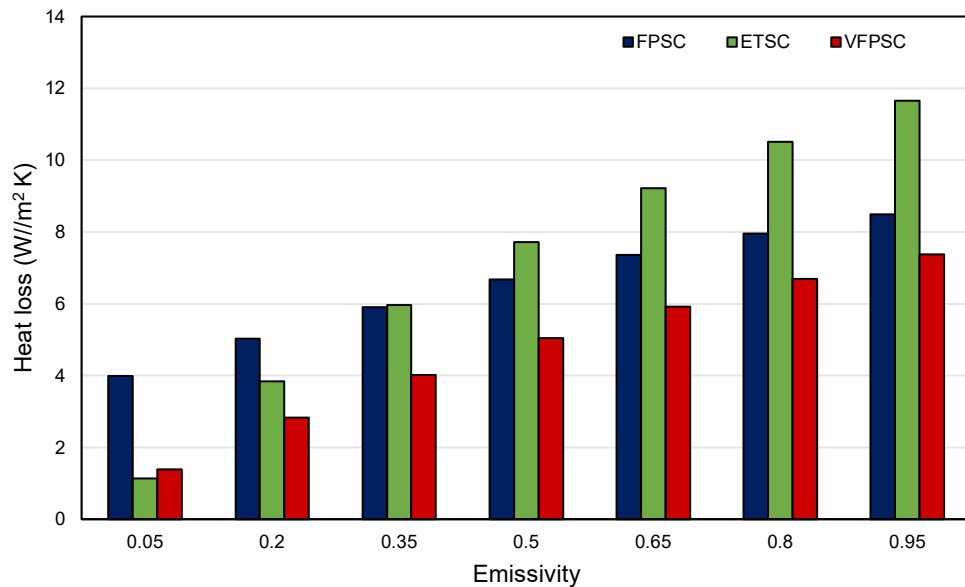


Figure 5.9 Overall heat loss of FPSC, ETSC and VFPC for different absorber emissivity.

Figures 5.8 and 5.9 respectively show the absorber plate temperature and the overall heat loss of new VFPC, FPSC and ETSC as a function of absorber emissivity within the range of 0.05 to 0.95. From Figure 5.8, as absorber emissivity augments, the absorber plate temperature declines in all thermal solar collectors because of the growth in the amount of overall heat loss, see Figure 5.9, specifically the radiative heat loss. The latter particularly concerns the ETSC since its absorber sheets exchange heat radiation from both front and back sides. Accordingly, its

absorber plate temperature diminishes and becomes even lower than that of the FPSC. When absorber emissivity is less than 0.35, the absorber plate temperatures for both new VFPC and ETSC are superior than FPSC due to the important reduction in overall heat loss resulting from the exploitation of vacuum insulation. However, when absorber emissivity exceeds 0.35, the absorber plate temperatures for both new VFPC and FPSC are superior than ETSC. For the reason that these two collectors have opaque thermal insulation (rockwool material) from their back sides which prevent conductive, convective and radiative heat loss and then reduce the overall heat loss. Regardless the absorber emissivity of 0.05, the new VFPC exhibits the highest absorber plate temperatures and the lowest overall heat losses for the whole range of absorber emissivity.

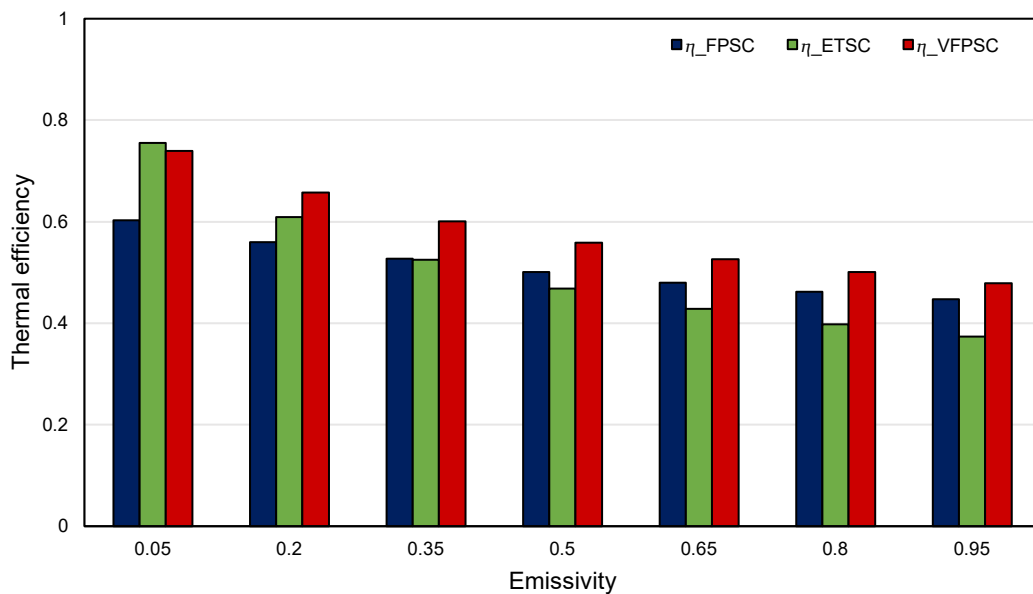


Figure 5.10 Thermal efficiency of FPSC, ETSC and VFPC for different values of absorber emissivity.

Figure 5.10 present the thermal efficiency of new VFPC, FPSC and ETSC as a function of absorber emissivity within the range of 0.05 to 0.95. From Figure 5.10, as the absorber emissivity augments from 0.05 to 0.95, the thermal efficiency of new VFPC, FPSC and ETSC decreases from 0.74, 0.6 and 0.75 to 0.48, 0.44 and 0.35, respectively. At absorber emissivity of 0.05, high thermal efficiency is achieved by ETSC and new VFPC because of the notable decrease of overall heat loss by using vacuum insulation, while FPSC has the lowest thermal efficiency. When absorber emissivity surpasses 0.05, the thermal efficiency of new VFPC shows the highest values and exceeds ETSC due to the limitation of back side radiation heat transfer by using opaque thermal insulation. Exceeding absorber emissivity of 0.35, the thermal

efficiency of FPSC becomes greater than ETSC since radiative heat loss becomes important as absorber emissivity increase. While in ETSC, only the conduction and convection heat transfer are restrained by using vacuum environment. The thermal efficiency of new VFPSM at absorber emissivity of 0.05 is greater than FPSC by about 22.77% and reaches almost the same value with ETSC, while, at absorber emissivity of 0.95, it is higher than that of FPSC and ETSC by about 7.13% and 28.32%, respectively.

As a result, the new VFPSM; that adopts the combined thermal insulation technique of vacuum insulation from the front side and opaque thermal insulation (Rockwool material) from the back side, presents good results in terms of absorber plate temperature, overall heat loss and thermal efficiency for the whole range of emissivity.

5.2.4 Optimum Number of Riser Tubes

The calculation is performed at solar radiation of 1025.5 W/m^2 , absorber emissivity of 0.05 and using the same parameters mentioned in the above subsection and Table 5.1. But only the number of tubes varies from 4 to 20 riser tubes for all studied collectors. Besides, the absorber plate area is kept constant (1.8 m^2), this means that when the number of tubes increase, the width of sheets will be narrowed. Figure 5.11 illustrates the parallel connection of inlet manifold and riser tubes. As presented in Figure 5.11, the mass flow rate of working fluid is divided in the inlet manifold to riser tubes connected in parallel. Therefore, as number of riser tubes augments, the mass flow rate passing through diminishes.

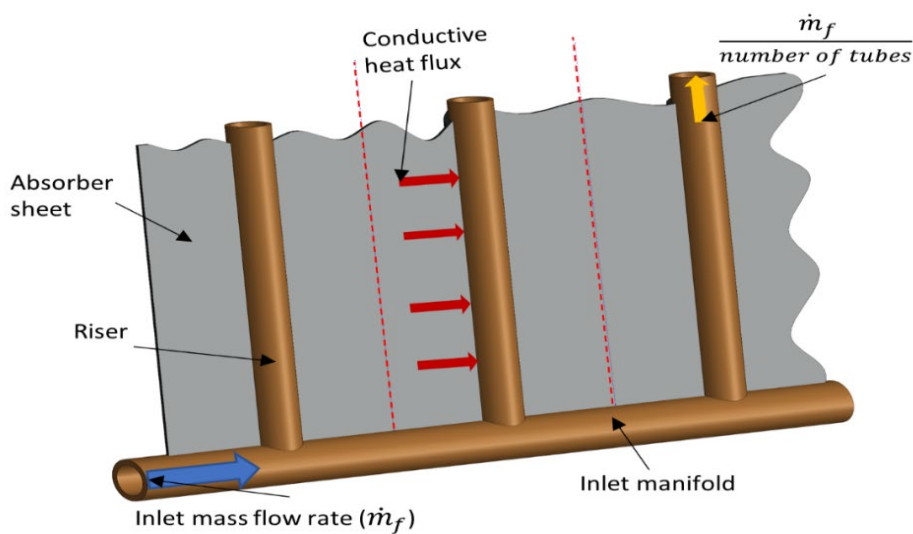


Figure 5.11 Inlet manifold and riser tubes connected in parallel.

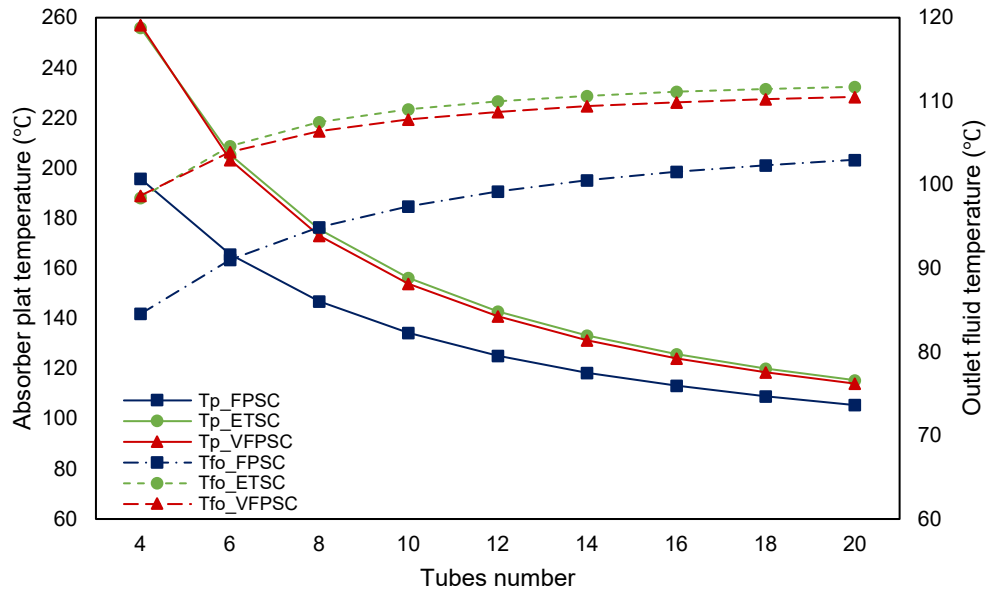


Figure 5.12 Outlet fluid (dashed line) and absorber plate (continuous line) temperatures of FPSC, ETSC and VFPC as a function of the tubes number.

Figure 5.12 presents absorber plate and outlet fluid temperature of new VFPC, FPSC and ETSC as a function of the number of tubes. As shown in Figure 5.12, in all solar collectors, for low number of riser tubes, the sheets of large absorbing area absorb great amount of solar irradiation, thus absorber plate temperatures attain the highest values. However, the energy absorbed by sheets is not efficiently transferred to the working fluid passing through tubes, that leads to a low sheet efficiency, see Equation 3.46. Furthermore, the thermosiphon solar collector is characterised by a low value of the fluid heat transfer coefficient. mass flow rate of the working fluid may not gain enough thermal energy from absorber sheets and hence, according to the theoretical result, the length of riser tubes should be elongated to a length of more than ten metres to get the appropriate outlet temperature the idea that is completely impractical.

It may be said that solar collectors of few riser tubes collect heat energy in absorber sheets and are accompanied by significant heat losses leading to a further reduction in outlet fluid temperatures and thermal efficiency. When number of riser tubes augments, the absorber plate temperature diminishes and the outlet fluid temperature rises. This occurs because the sheets width and mass flow rate of the working fluid passing through the riser tubes gradually decrease, allowing more conductive heat transfer to take place from sheets to the working fluid. It is noted that, when the number of riser tubes augments from 4 to 10, outlet fluid temperature of new VFPC, FPSC and ETSC rises by 9.12°C 12.89°C and 10.62°C respectively. As the number of riser tubes exceeds 10, a minor increase is remarked in outlet fluid temperature of about 2.69°C,

5.55°C and 2.68°C for new VFPC, FPSC and ETSC, respectively. In general, the increase attained from 4 to 10 riser tubes is much greater than that gained by changing from 10 to 20 riser tubes.

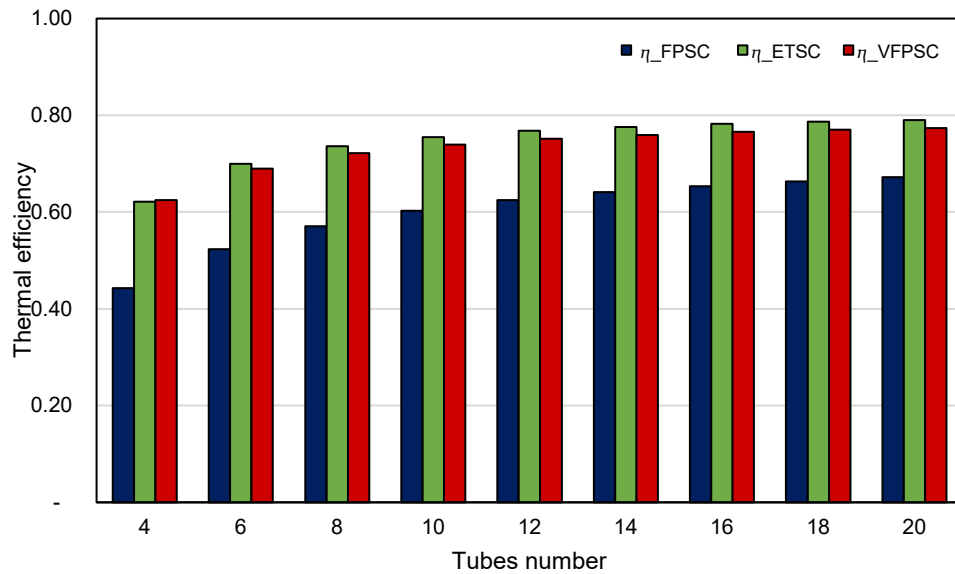


Figure 5.13 Thermal efficiency of FPSC, ETSC and VFPC as a function of the tubes number.

Figure 5.13 presents thermal efficiency of new VFPC, FPSC and ETSC for different number of tubes. As shown in Figure 5.13, the increase of the number of riser tubes from 4 to 10, leads to a rise in the thermal efficiency of all solar collectors. This augmentation is about 18.38%, 36.11% and 21.51% in new VFPC, FPSC and ETSC, respectively. However, a slight augmentation is noted when the number of riser tubes rises from 10 to 20, as 4.59%, 11.48% and 4.66% in new VFPC, FPSC and ETSC, respectively. Therefore, increasing the number of riser tubes over 10 is not worthy as it leads to an insignificant enhancement for the solar collectors' thermal efficiency and only conducts to a rise for solar collectors' cost, detail of the solar collectors cost is discussed in the following section. Overall, the number of 10 riser tubes is optimum since it allows to attain an acceptable thermal efficiency with a low cost.

5.3 Cost Evaluation

The total cost ($Cost_{Total}$) of thermal solar water system consists of three main parts: the manufacturing cost ($Cost_{manufacturing}$), the installation cost ($Cost_{installation}$) and the maintenance cost ($Cost_{maintenance}$), as shown in Equation 5.3 below:

$$Cost_{Total} = Cost_{manufacturing} + Cost_{installation} + Cost_{maintenance} \quad (5.3)$$

- The manufacturing cost consists of two parts: the thermal solar collector cost ($Cost_{collector}$) and tank cost ($Cost_{tank}$), as expressed in Equation 5.4 below:

$$Cost_{manufacturing} = Cost_{collector} + Cost_{tank} \quad (5.4)$$

- The installation cost depends on manpower cost and transportation cost.
- The maintenance cost depends on several conditions, for instance, environment circumstances (dust, hail, humidity...etc) and external devices (pump and electrical power source...etc).

5.3.1 Collector Parts Cost

As mentioned in chapter 1, the thermal solar collector mainly consists of; a top glassing cover, absorber plate coated by black paint (or selective surface), tubes and back insulation. The common working fluid within collector pipes is water and it is inexpensive. All these components are assembled in a proper encasement. Therefore, the cost of the elements can be written as follows:

a) Top glassing cover cost

The top cover cost can be estimated using Equation 5.5 below:

$$Cost_{Cover} = A_{cover} \times C_{cover} \quad (5.5)$$

where, A_{cover} and C_{cover} denote the total surface of top glassing cover and the cost of this cover per unit area, respectively.

b) Absorber plate cost

The absorber plate cost can be estimated by using the expression 5.6 below:

$$Cost_{Absorber\ plate} = n_{tb} \times L_{tb} \times (W - D) \times C_{sheet} \quad (5.6)$$

here, C_{sheet} is the cost of the absorber sheet per unit area.

c) Tubes cost

The tubes cost can be estimated by using the formula 5.7 below:

$$Cost_{Tubes} = n_{tb} \times L_{tb} \times C_{tube} \quad (5.7)$$

C_{tube} denotes the cost of the tube per unit length.

d) *Back insulation cost*

The back insulation cost can be estimated using the Equation 5.8 below, which is a function of insulation material volume.

$$Cost_{Insulation} = A_{insulation} \times e_{insulation} \times C_{insulation} \quad (5.8)$$

where, $A_{insulation}$, $e_{insulation}$ and $C_{insulation}$ are the total surface and the thickness of the back insulation and the cost of this insulation material per unit area, respectively.

5.3.2 Collectors Cost Comparison

The design of thermal solar collectors is concerned to obtain high thermal efficiency with low cost. In this evaluation, the total cost of each collector type is estimated for comparison purpose, see Table 5.2. The cost analysis is conducted based on the estimation of the main parts' prices of solar collectors that aforementioned in the subsection above. An additional cost C_{add} is considered to complete the total collector cost. Equation 5.9 below is used to determine the total collectors cost as following:

$$Cost_{collector} = Cost_{Cover} + Cost_{Absorber\ plate} + Cost_{Tubes} + Cost_{Coating} + Cost_{Insulator} + C_{add} \quad (5.9)$$

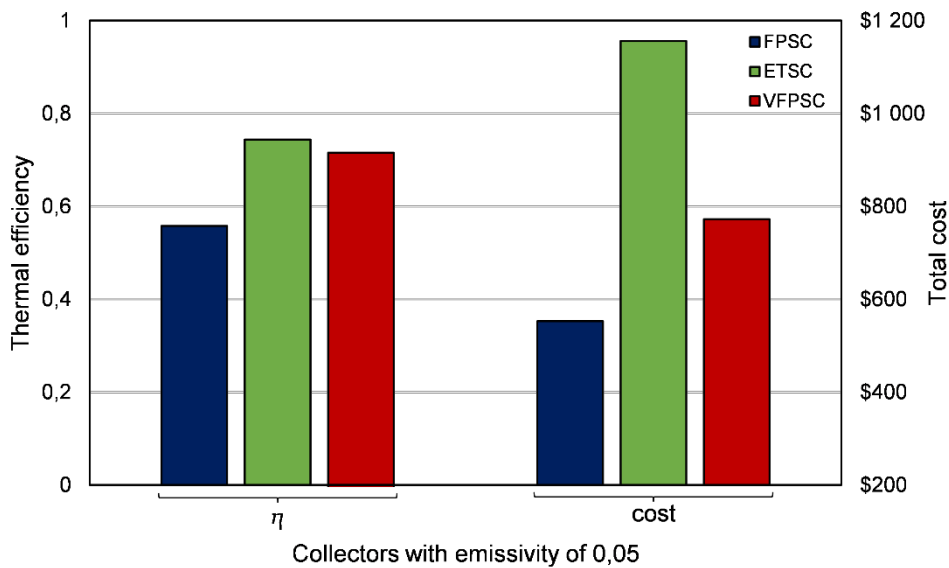


Figure 5.14 Thermal efficiency and total collector cost of FPSC, ETSC and new VFPS using absorber emissivity of 0,05.

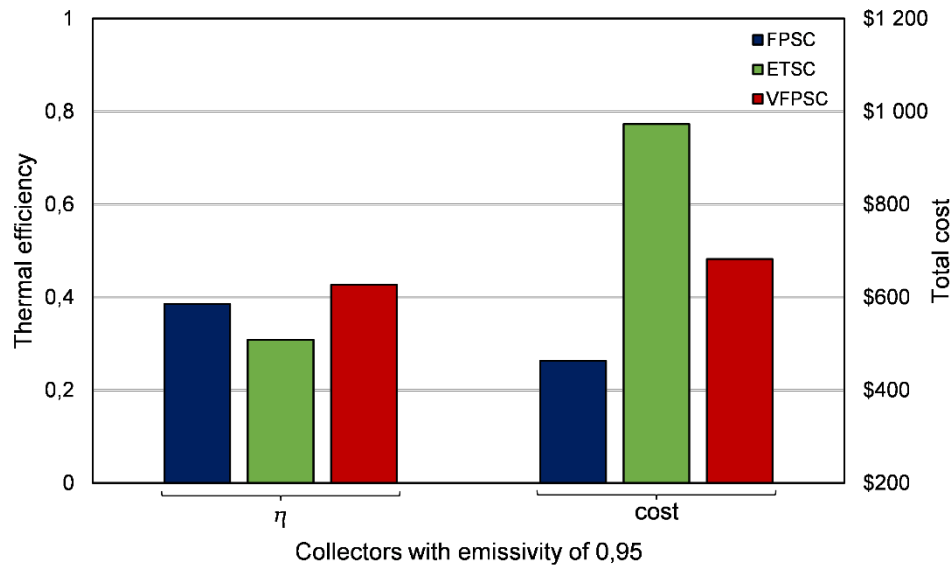


Figure 5.15 Thermal efficiency and total collector cost of FPSC, ETSC and new VFPC using absorber emissivity of 0,95

Figure 5.14 and 5.15 represent the thermal efficiency and the total collectors cost of FPSC, ETSC and VFPC at absorber emissivity of 0.05 and 0.95, respectively. As illustrated in Figure 5.14, at absorber emissivity of 0.05, new VFPC and ETSC reach almost the same high thermal efficiency and FPSC attains the lowest values. However, the total cost of ETSC is very significant compared to new VFPC and FPSC with the increase of about 49.62% and 109.04%, respectively.

From Figure 5.15, at emissivity of 0.95, the thermal efficiency of ETSC, VFPC and FPSC decreased by 58.52%, 40.33% and 30.88%, respectively, compared to the results of 0.05. While the total cost of ETSC remains the highest one and the cost augmentation is 42.59% and 110.21% with reference to the new VFPC and FPSC, respectively. It can be said that ETSC shows the lowest thermal efficiency and the highest cost.

It is worth to note that the evacuated solar collectors work effectively at selective surfaces of low absorber emissivity. However, selective coatings may suffer from rigorous operating conditions during their lifetime, for example, lack of corrosion resistance, ageing mechanisms, chemical interactions, humidity and thermal instability at high absorber temperatures, which influence their optical features and then necessitates supplementary maintenance cost [92]. Besides, complex techniques for the production of selective surfaces make their cost significant and lessen their price competitiveness. Hence, in the case of unavailability of selective surfaces

due to their limitations, the proposed new VFPSO reveals the possibility of obtaining thermal efficiency of about 50% with a modest cost.

Table 5.2 Main components prices and total cost of solar collectors

Components	Unit price	FPSC		ETSC		New VFPSO	
		Material	Cost \$	Material	Cost \$	Material	Cost \$
Transparent cover	31.51\$/m ² 60.5\$/m ²	Clear glass	56,7	Toughened glass	478,9	Toughened glass	126,2
Absorber plate	50.5\$/m ²	Copper	81.81	Copper	81.81	Copper	81.81
Tubes	6.1\$/m	Copper	109.8	Copper	109.8	Copper	109.8
Coating of emissivity 0.95	2.5\$/kg	Black paint	2.5	Black paint	2.5	Black paint	2.5
Coating of emissivity 0.05	51.5\$/m ²	Black chrome	92,7	Black chrome	185,4	Black chrome	92,7
Back insulation	6.7\$/m ²	Rock wool	12.06	-	-	Rock wool	12.06
Additional cost	-	-	200	-	300	-	350
Total cost (at emissivity 0.95)	-	-	462.88	-	973.07	-	682.39
Total cost (at emissivity 0.05)	-	-	553.08	--	1155.97	-	772.59

5.4 Conclusion

In conclusion, the proposed VFPSO that has a new insulation technique (vacuum insulation from front side and Rockwool material from the back side), shows great reduction in thermal losses, allowing this collector to function at elevated temperatures and high thermal efficiency with a competitive cost. Therefore, the proposed VFPSO offers high thermal performance advantages over both conventional flat plate and evacuated tube collectors. This new configuration may gradually replace both of these conventional alternatives if the manufacturing technique is available to build such a product.

Conclusion

In order to reduce dependency on fossil fuels, renewable energy has become an important research subject in recent years. Recently, climate change has reignited debates about the role of renewable energies, which remain clean sources and environmentally friendly to the environment. The current development in these sources helps to meet the requirements of minimising the greenhouse effect, preserving the environment from pollution, global warming, depletion of the ozone layer...etc. There are several available renewable energy sources, and solar energy is considered as an origin for all of them. Our country, Algeria, which is a developing country, is endowed with abundant and huge free solar energy potential. This makes it possible to exploit enormous capacities and to offer the appropriate energy solutions to the entire world if this sector gets the right attention. In our country, as all countries of the world, the requirement for hot water is produced usually through the use of electricity and natural gases. The application of solar thermal collectors can replace the conventional systems and may lessen the employment of the non-renewable energies sources for the same aim of heating water in domestic and industrial sectors.

As part of this thesis, a study on the thermal performance of a flat plate solar water collector under thermosyphon circulation has been presented. The main goal of the current study is to enhance the thermal performance of a flat plate thermal water solar collector. General introduction about renewable energies and thermal solar collectors is given. Then, literature review that summarise the previous studies in the same field is presented. A theoretical model that includes heat transfer and energy balance equations is demonstrated. Computational algorithm implemented in MATLAB program to calculate the required result is explained. The latter is validated with experimental result. The influence of various operational parameters on the thermal performance of the studied collector is investigated using the developed calculating program.

The flat plate thermal solar collector has many advantages such as its design simplicity, installation, cost and its long cycle life. However, the thermal performance of this system remains to be improved. Indeed, through theoretical analysis, heat losses on the collector sides are found very significant, and this cause a decrease in its thermal performance. Therefore, the enhancement of the thermal performance of a flat plate thermal water solar collector can be achieved by minimising heat losses from both the front and back sides of the collector using an

innovative insulating technique. For this reason, a comparative theoretical investigation is performed in order to present its benefits on heat losses, absorber temperatures and efficiency. As a result, the proposed new configuration exhibits better thermal performance as compared to other conventional configurations. It can be said that, the proposed new configuration shows a promising solution that can cover part of the energy needs while providing additional benefits. Besides, the presented study may improve the existing knowledge on solar thermal collectors and ameliorate their performance.

Bibliography

References

1. Islam, M.R., K. Sumathy, and S.U. Khan, *Solar water heating systems and their market trends*. Renewable and Sustainable Energy Reviews, 2013. **17**: p. 1-25.
2. Zahraoui, Y., et al., *Current status, scenario, and prospective of renewable energy in Algeria: a review*. Energies, 2021. **14**(9): p. 2354.
3. CEREFÉ. *Le Commissariat aux Energies Renouvelables et à l'Efficacité Energétique*. 2022; Available from: <https://www.cerefe.gov.dz/fr/accueil/>
4. Aoun, N. and K. Bouchouicha, *Estimating daily global solar radiation by day of the year in Algeria*. The European Physical Journal Plus, 2017. **132**(5): p. 1-12.
5. Stambouli, A.B. and H. Koinuma, *A primary study on a long-term vision and strategy for the realisation and the development of the Sahara Solar Breeder project in Algeria*. Renewable sustainable energy reviews, 2012. **16**(1): p. 591-598.
6. Çengel, Y.A. and A.J. Ghajar, *Heat and mass transfer : fundamentals & applications*. Fifth edition ed. 2015, New York, NY: McGraw Hill Education.
7. Falayi, E. and A.J.S.r. Rabiou, EB Babatunde, IntechOpen, *Solar radiation models and information for renewable energy applications*. 2012: p. 111-130.
8. Kalogirou, S.A., *Solar energy engineering: processes and systems*. 2013: Academic Press.
9. Tiwari, G. and A. Tiwari, *Handbook of solar energy*. 2017: Springer.
10. Duffie, J.A., W.A. Beckman, and W. Worek, *Solar engineering of thermal processes*. Vol. 3. 2013: Wiley Online Library.
11. Kedare, S.B. and N.B. Desai, *Solar Thermal Process Heat*. 2017.
12. Safari, A., et al., *Natural gas: A transition fuel for sustainable energy system transformation?* Energy Science Engineering, 2019. **7**(4): p. 1075-1094.
13. Ellabban, O., H. Abu-Rub, and F. Blaabjerg, *Renewable energy resources: Current status, future prospects and their enabling technology*. Renewable sustainable energy reviews, 2014. **39**: p. 748-764.
14. Smith, C., *Revisiting solar power's past*. Technology Review, 1995. **98**(5): p. 38-47.
15. Iordanou, G., *Flat-plate solar collectors for water heating with improved heat transfer for application in climatic conditions of the mediterranean region*. 2009, Durham University.
16. Fortuin, S. and G. Stryi-Hipp, *Solar Collectorssolar collector, Non-concentrationsolar collectornon-concentrating*, in *Solar Energy*, C. Richter, D. Lincot, and C.A. Gueymard, Editors. 2013, Springer New York: New York, NY. p. 378-398.
17. Suman, S., M.K. Khan, and M. Pathak, *Performance enhancement of solar collectors—A review*. Renewable Sustainable Energy Reviews, 2015. **49**: p. 192-210.
18. Vengadesan, E. and R. Senthil, *A review on recent development of thermal performance enhancement methods of flat plate solar water heater*. Solar Energy, 2020. **206**: p. 935-961.
19. Alam, T., et al., *Performance Augmentation of the Flat Plate Solar Thermal Collector: A Review*. Energies, 2021. **14**(19): p. 6203.

20. Dondapati, R.S., et al., *Effect of glazing materials on the performance of solar flat plate collectors for water heating applications*. Materials Today: Proceedings, 2018. **5**(14): p. 27680-27689.
21. Bakari, R., R.J. Minja, and K.N. Njau, *Effect of glass thickness on performance of flat plate solar collectors for fruits drying*. Journal of energy, 2014. **2014**.
22. Shaik, S., et al., *Evaluation of optical transmissivity of transparent materials on the performance of solar flat plate collectors*. Journal of Solar Energy Engineering, 2021. **143**(5).
23. Hellstrom, B., et al., *The impact of optical and thermal properties on the performance of flat plate solar collectors*. Renewable Energy, 2003. **28**(3): p. 331-344.
24. Agbo, S. and E. Okoroigwe, *Analysis of Thermal Losses in the Flat-Plate Collector of a Thermosyphon Solar Water Heater*. Research journal of Physics, 2007. **1**(1): p. 35-41.
25. Fan, M., et al., *A comparative study on the performance of liquid flat-plate solar collector with a new V-corrugated absorber*. Energy Conversion Management, 2019. **184**: p. 235-248.
26. Armenta-Deu, C., *Performance test in semispherical solar collectors with discontinuous absorber*. Renewable Energy, 2019. **143**: p. 950-957.
27. Poongavanam, G.K., et al., *Thermal performance augmentation of a solar flat plate collector using the shot peening technique*. Science Technology for the Built Environment, 2020. **26**(3): p. 437-445.
28. Deng, Y., et al., *Experimental investigation of performance for the novel flat plate solar collector with micro-channel heat pipe array (MHPA-FPC)*. Applied Thermal Engineering, 2013. **54**(2): p. 440-449.
29. Oyinlola, M.A., G.S. Shire, and R. Moss, *Thermal analysis of a solar collector absorber plate with microchannels*. Experimental Thermal Fluid Science, 2015. **67**: p. 102-109.
30. Oyinlola, M., G. Shire, and R. Moss, *Investigating the effects of geometry in solar thermal absorber plates with micro-channels*. International Journal of Heat Mass Transfer, 2015. **90**: p. 552-560.
31. Arvanitis, K.D., et al., *Experimental evaluation of flat-plate heat absorbers for medium-temperature linear-focus solar systems: Composite U-bends vs straight rectangular-multi-channels*. Applied Thermal Engineering, 2020. **175**: p. 115364.
32. Moss, R.W., et al., *Optimal passage size for solar collector microchannel and tube-on-plate absorbers*. Solar Energy, 2017. **153**: p. 718-731.
33. Jouybari, H.J., et al., *Experimental investigation of thermal performance and entropy generation of a flat-plate solar collector filled with porous media*. Applied Thermal Engineering, 2017. **127**: p. 1506-1517.
34. Anirudh, K. and S. Dhinakaran, *Numerical study on performance improvement of a flat-plate solar collector filled with porous foam*. Renewable Energy, 2020. **147**: p. 1704-1717.
35. Saedodin, S., et al., *Performance evaluation of a flat-plate solar collector filled with porous metal foam: Experimental and numerical analysis*. Energy Conversion Management, 2017. **153**: p. 278-287.
36. Ameri, M. and M.S. Eshaghi, *Exergy and thermal assessment of a Novel system utilizing flat plate collector with the application of nanofluid in porous media at a constant magnetic field*. Thermal Science Engineering Progress 2018. **8**: p. 223-235.
37. Kiliç, F., T. Menlik, and A. Sözen, *Effect of titanium dioxide/water nanofluid use on thermal performance of the flat plate solar collector*. Solar Energy, 2018. **164**: p. 101-108.

38. Yousefi, T., et al., *An experimental investigation on the effect of Al₂O₃-H₂O nanofluid on the efficiency of flat-plate solar collectors*. Renewable Energy, 2012. **39**(1): p. 293-298.
39. Moghadam, A.J., et al., *Effects of CuO/water nanofluid on the efficiency of a flat-plate solar collector*. Experimental Thermal Fluid Science, 2014. **58**: p. 9-14.
40. Otanicar, T.P., et al., *Nanofluid-based direct absorption solar collector*. Journal of renewable sustainable energy, 2010. **2**(3): p. 033102.
41. Goudarzi, K., et al., *Experimental study on the effect of pH variation of nanofluids on the thermal efficiency of a solar collector with helical tube*. Experimental Thermal Fluid Science, 2015. **60**: p. 20-27.
42. Sivakumar, S., et al., *Effect of nano cupric oxide coating on the forced convection performance of a mixed-mode flat plate solar dryer*. Renewable Energy, 2020. **155**: p. 1165-1172.
43. Sakhaei, S.A. and M.S. Valipour, *Investigation on the effect of different coated absorber plates on the thermal efficiency of the flat-plate solar collector*. Journal of Thermal Analysis Calorimetry, 2020. **140**(3): p. 1597-1610.
44. Senthil, R., et al., *Enhancement of absorptance of absorber surfaces of a flat plate solar collector using black coating with graphene*. Energy Sources, Part A: Recovery, Utilization, Environmental Effects, 2021. **43**(20): p. 2595-2608.
45. Nazari, M., S. Jafarmadar, and S. Khalilarya, *Exergy and thermoeconomic analyses of serpentine tube flat-plate solar water heaters coated with CuO nanostructures*. Case Studies in Thermal Engineering, 2022. **35**: p. 102072.
46. Abdelkader, T.K., et al., *Energy and exergy analysis of a flat-plate solar air heater coated with carbon nanotubes and cupric oxide nanoparticles embedded in black paint*. Journal of Cleaner Production, 2020. **250**: p. 119501.
47. Garcia, R.P., S. del Rio Oliveira, and V.L. Scalon, *Thermal efficiency experimental evaluation of solar flat plate collectors when introducing convective barriers*. Solar Energy, 2019. **182**: p. 278-285.
48. Rommel, M. and A. Wagner, *Application of transparent insulation materials in improved flat-plate collectors and integrated collector storages*. Solar Energy, 1992. **49**(5): p. 371-380.
49. Ammar, M., et al., *Performance optimization of flat plate solar collector through the integration of different slats arrangements made of transparent insulation material*. Sustainable Energy Technologies Assessments, 2021. **46**: p. 101237.
50. Kessentini, H., et al., *Development of flat plate collector with plastic transparent insulation and low-cost overheating protection system*. Applied Energy, 2014. **133**: p. 206-223.
51. Vestlund, J., M. Rönnelid, and J.-O. Dalenbäck, *Thermal performance of gas-filled flat plate solar collectors*. Solar Energy, 2009. **83**(6): p. 896-904.
52. Bennour, F. and H. Mzad, *Effects of Optimized Gas Filled Spaces on the Performance of the Double Glazed Solar Air Heater*. SSRN 3961282, 2021.
53. Eaton, C. and H. Blum, *The use of moderate vacuum environments as a means of increasing the collection efficiencies and operating temperatures of flat-plate solar collectors*. Solar Energy, 1975. **17**(3): p. 151-158.
54. Roberts, G., *Heat loss characteristics of an evacuated plate-in-tube collector*. Solar Energy, 1979. **22**(2): p. 137-140.
55. Beikircher, T., N. Benz, and W. Spirkl, *Gas heat conduction in evacuated flat-plate solar collectors: analysis and reduction*. Solar energy, 1995.

56. Benz, N., T. Beikircher, and B. Aghazadeh, *Aerogel and krypton insulated evacuated flat-plate collector for process heat production*. Solar energy, 1996. **58**(1-3): p. 45-48.
57. Benz, N. and T. Beikircher, *High efficiency evacuated flat-plate solar collector for process steam production*. Solar energy, 1999. **65**(2): p. 111-118.
58. Henshall, P., et al., *Constant temperature induced stresses in evacuated enclosures for high performance flat plate solar thermal collectors*. Solar Energy, 2016. **127**: p. 250-261.
59. Arya, F., et al., *Current developments in flat-plate vacuum solar thermal collectors*. International Journal of Energy Power Engineering, 2016. **10**(6): p. 688-692.
60. Moss, R.W., et al., *Simulator testing of evacuated flat plate solar collectors for industrial heat and building integration*. Solar Energy, 2018. **164**: p. 109-118.
61. Arya, F., et al., *Vacuum enclosures for solar thermal panels Part 1: Fabrication and hot-box testing*. Solar Energy, 2018. **174**: p. 1212-1223.
62. Arya, F., et al., *Vacuum enclosures for solar thermal panels Part 2: Transient testing with an uncooled absorber plate*. Solar Energy, 2018. **174**: p. 1224-1236.
63. Radwan, A., et al., *Development of a new vacuum-based photovoltaic/thermal collector, and its thermal and exergy analyses*. Sustainable Energy Fuels, 2020. **4**(12): p. 6251-6273.
64. Gao, D., et al., *Experimental and numerical analysis of an efficiently optimized evacuated flat plate solar collector under medium temperature*. Applied Energy, 2020. **269**: p. 115129.
65. De Maio, D., et al., *Efficiency of selective solar absorber in high vacuum flat solar thermal panels: The role of emissivity*. 2020.
66. Tiwari, G. and A. Tiwari, *Handbook of solar energy*. Vol. 498. 2016: Springer.
67. Duffie, J.A., W.A. Beckman, and N. Blair, *Solar engineering of thermal processes, photovoltaics and wind*. 2020: John Wiley & Sons.
68. Hollands, K., et al., *Free convective heat transfer across inclined air layers*. 1976.
69. Buchberg, H., I. Catton, and D. Edwards, *Natural convection in enclosed spaces—a review of application to solar energy collection*. 1976.
70. Yin, S., et al., *Natural convection in an air layer enclosed within rectangular cavities*. International Journal of Heat Mass Transfer, 1978. **21**(3): p. 307-315.
71. Randall, K., J. Mitchell, and M. El-Wakil, *Natural convection heat transfer characteristics of flat plate enclosures*. 1979.
72. Schinkel, W.M., *Natural convection in inclined air-filled enclosures*. 1980.
73. Niemann, M. and J. Fröhlich, *Buoyancy-affected backward-facing step flow with heat transfer at low Prandtl number*. International Journal of Heat Mass Transfer, 2016. **101**: p. 1237-1250.
74. Jürges, W., *The heat transfer at a flat wall (Der Wärmeübergang an einer ebenen Wand), Beihefte zum Gesundh. Ing*, 1924. **1**: p. 19.
75. Mcadams, W.H., *Heat Transmission: 3d Ed*. 1954: McGraw-Hill.
76. Watmuff, J., W. Charters, and D. Proctor, *Solar and wind induced external coefficients-solar collectors*. Cooperation Mediterranee pour l'Energie Solaire, 1977: p. 56.
77. Sparrow, E. and S. Lau, *Effect of adiabatic co-planar extension surfaces on wind-related solar-collector heat transfer coefficients*. 1981.
78. Kumar, S., et al., *Wind induced heat losses from outer cover of solar collectors*. Renewable Energy, 1997. **10**(4): p. 613-616.
79. Sharples, S. and P. Charlesworth, *Full-scale measurements of wind-induced convective heat transfer from a roof-mounted flat plate solar collector*. Solar Energy, 1998. **62**(2): p. 69-77.

80. Swinbank, W.C., *Long-wave radiation from clear skies*. Journal of the Royal Meteorological Society, 1963. **89**(381): p. 339-348.
81. Berdahl, P. and M. Martin, *Emittance of clear skies*. Solar energy, 1984. **32**(5): p. 663-664.
82. Bliss Jr, R.W., *Atmospheric radiation near the surface of the ground: a summary for engineers*. Solar energy, 1961. **5**(3): p. 103-120.
83. Brunt, D., *Notes on radiation in the atmosphere. I*. Journal of the Royal Meteorological Society, 1932. **58**(247): p. 389-420.
84. Aubinet, M., *Longwave sky radiation parametrizations*. Solar Energy, 1994. **53**(2): p. 147-154.
85. ISO , N., *Building components and building elements-thermal resistance and thermal transmittance-calculation method*. 2007, International Organization for Standardization Geneva, CH.
86. Badar, A.W., R. Buchholz, and F. Ziegler, *Experimental and theoretical evaluation of the overall heat loss coefficient of vacuum tubes of a solar collector*. Solar Energy, 2011. **85**(7): p. 1447-1456.
87. Gairaa, K. and Y. Bakelli, *Solar energy potential assessment in the Algerian south area: Case of Ghardaïa region*. Journal of Renewable Energy, 2013. **2013**.
88. Gairaa, K. and Y. Bakelli, *Solar Energy Potential Assessment in the Algerian South Area: Case of Ghardaïa Region*. Journal of Renewable Energy, 2013. **2013**: p. 496348.
89. Seddaoui, A., M.Z.D. Ramdane, and R. Noureddine, *Performance investigation of a new designed vacuum flat plate solar water collector: A comparative theoretical study*. Solar Energy, 2022. **231**: p. 936-948.
90. Saikia, S.S., S. Nath, and D. Bhanja, *Effect of vacuum deterioration on thermal performance of coaxial evacuated tube solar collector considering single and two phase flow modelling: A numerical study*. Solar Energy, 2019. **177**: p. 127-143.
91. Ibrahim, N.I., F.A. Al-Sulaiman, and F.N. Ani, *Performance characteristics of a solar driven lithium bromide-water absorption chiller integrated with absorption energy storage*. Energy Conversion Management, 2017. **150**: p. 188-200.
92. Zhang, K., et al., *A review on thermal stability and high temperature induced ageing mechanisms of solar absorber coatings*. Renewable Sustainable Energy Reviews, 2017. **67**: p. 1282-1299.